TABLE OF CONTENTS

Page

LIST OF TABLES

Page

LIST OF FIGURES

Page

LIST OF ABREVIATIONS

ASE	Aggregate spectral efficiency
BFS	Brillouin frequency shift
BGS	Brillouin gain spectra
BOTDA	Brillouin optical time domain analysis
BOTDR	Brillouin optical time domain reflectometer
CCD	Charged coupled device
CVB	Cylindrical vector beam
CW	Continuous wave
DBG	Dynamic Brillouin grating
DMD	Differential modal delay
EDFA	Erbium doped fiber amplifier
ERI	Effective refractive index
ESA	Electrical spectrum analyzer
FBG	Fiber Bragg grating
FL	Fourier lens
FMF	Few mode fiber
HCF	Hollow core fiber
HWP	Half-wave plate
IPGIF	Inverse parabolic graded index fiber
LP	Linearly polarized
LPFG	Long period fiber grating

MDM	Mode division multiplexing
MC	Mode converter
MCF	Multicore fiber
MIMO	Multiple input multiple output
MMF	Multimode fiber
MS	Mode stripper
MUX/DEMUX	Multiplexing/demultiplexing
OAM	Orbital angular momentum
OC	Optical circulator
PBS	Polarization beam splitter
PC	Polarization controller
PCVB	Perfect cylindrical vector beam
PDL	Polarization dependent loss
QWP	Quarter wave plate
RIP	Refractive index profile
SBS	Stimulated Brillouin scattering
TDM	Time division multiplexing
SDM	Space division multiplexing
SLM	Spatial light modulator
SMF	Single-mode fiber
SPP	Spiral phase plate
WDM	Wavelength division multiplexing
WP	Wollaston prism

LIST OF SYMBOLS

n_{eff}	Effective refractive index
Δn_{eff}	Effective refractive index difference
l	Topological charge
ϕ	Azimuthal angle, phase offset
λ	Wavelength
Λ	Grating pitch
λ_{res}	Resonance wavelength
η_{max}	Spatial multiplicity
θ	Angle of the grating
ν_B	Brillouin frequency shift
V_a	Acoustic velocity
R_D	Ring diameter
R_W	Ring width
w_g	Beam waist of gaussian beam
k	Wavevector
a	Axicon parameter
$\Delta\nu_B$	Brillouin gain linewidth
k_r	Radial wave vector
w_0	Beam waist of Gaussian beam at focus
R_r	Ring radius
k_z	Longitudinal wave vector

n	Refractive index of axicon material
α	Base angle of axicon

INTRODUCTION

Context of the research work

The single-mode fiber (SMF) has been the backbone of high-bandwidth optical telecommunication and the optical fiber sensing industry for several decades. Researchers have explored and exploited every attainable degree of freedom to its maximum, in their attempt to fully utilize the benefits of SMF. The introduction of SMFs with low-losses, the erbium doped fiber amplifier (EDFA), wavelength division multiplexing (WDM) and high-spectral efficiency coding using digital signal processing and coherent transmission, constitute some of the technological breakthroughs in the capacity to transmit data in the fiber-optic communication systems as shown in Fig. 0.1 (Essiambre et Tkach, 2012; Wang, Zhou et Zhang, 2014). Fueled by the ever-increasing demand for high-bandwidth multimedia applications, the ultimate data transmission capacity of a SMF is predicted to be reached within the next decade.

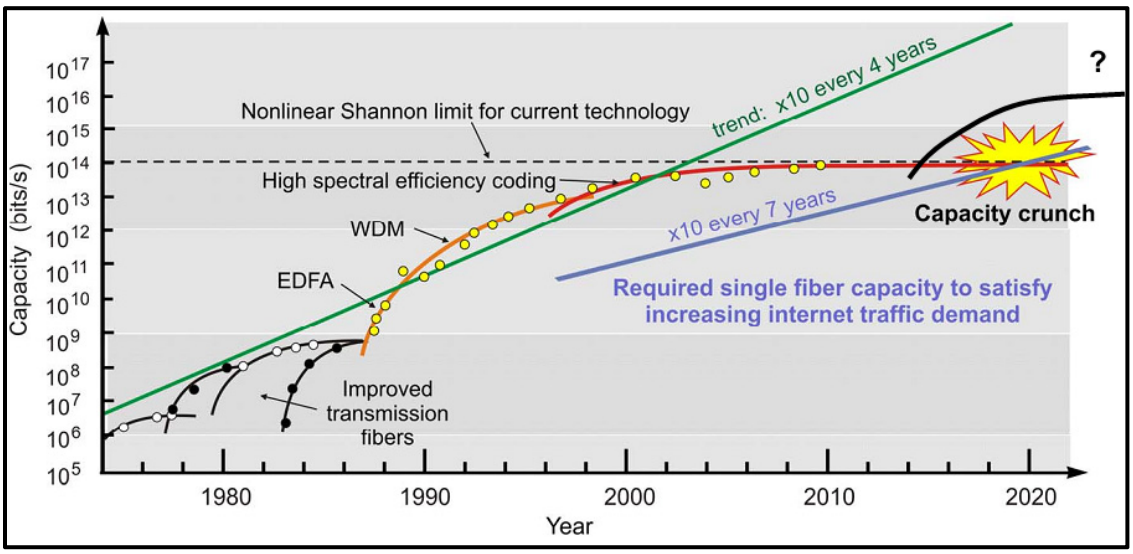

Figure 0.1 Data transmission capacity of fiber transmission systems as a function of year
Taken from Richardson et al. (2013, p.354)

The enhancement in the data transmitting capacity of single-mode fiber by 10,000 times in the past few decades has resulted in the steady improvement of optical communication

network traffic by a factor of 100 so far (Essiambre et Tkach, 2012; Richardson, Fini et Nelson, 2013). However, single-mode fiber transmission will no longer be able to satisfy the exponentially growing capacity demand as shown in Figure 0.1. The maximum limit of data transmission capacity in a standard single-mode fiber is predicted by theory to be around 100 Tb/s, based on the nonlinear Shannon limit (Richardson, Fini et Nelson, 2013). Several groups of researchers have been exploring and exploiting every attainable degree of freedom to its maximum (as shown in Figure 0.2), in their attempt to increase the data transmission rate utilizing SMF (Essiambre et Tkach, 2012).

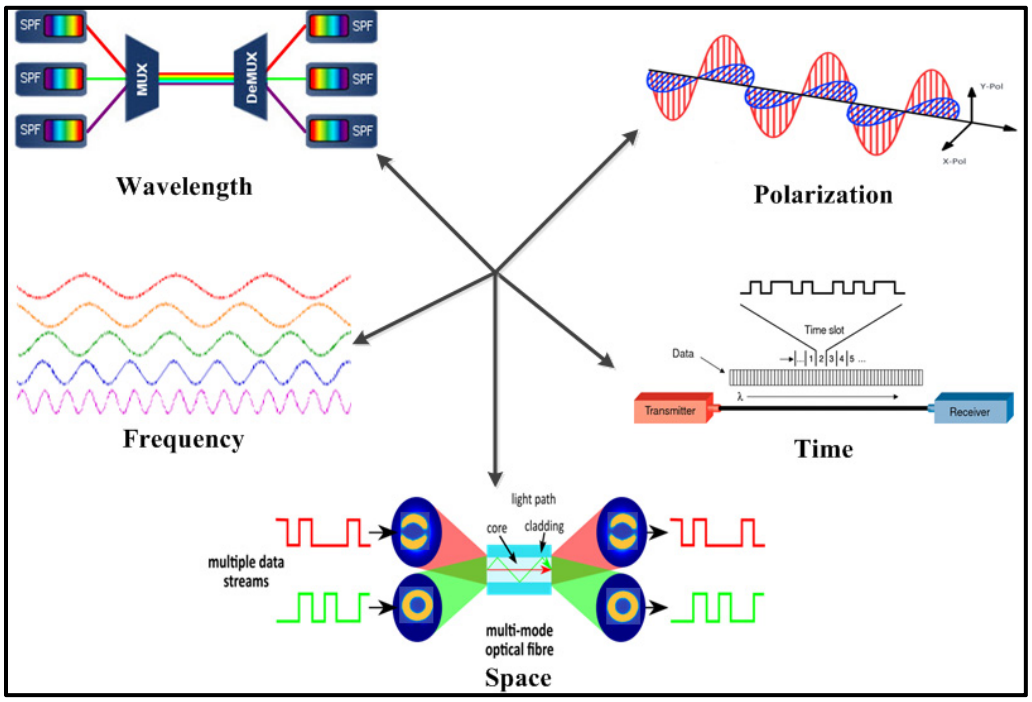

Figure 0.2 Spatial division multiplexing as a new, orthogonal, degree of freedom for data multiplexing in the future fiber-optic communication systems

Spatial division multiplexing aims to harness the rich spatial modes diversity available in multimode fibers (MMF) and few-mode fibers (FMF) towards increasing the aggregate transmission capacity within a single strand of fiber. Furthermore, it has been suggested that the same SDM techniques developed for the generation and control of modal transmission in MMF and FMF, could be exploited towards multi-parameter fiber-optic sensing (Chen et Koonen, 2017; Igarashi, Tsuritani et Morita, 2016; Kitayama et Diamantopoulos, 2017;

Rademacher et al., 2018b; Xu et al., 2016; Zhu et al., 2018). However, standard MMF supports over a hundred modes which makes receiving and processing the optical signals particularly difficult due to high modal crosstalk, whereas, FMF supports less than ten modes that it reduces the system complexity to an achievable level with current technologies. In particular, the few-mode fiber has attracted a lot of attention due to its potential applications in MDM systems in telecom and fiber-optic sensing (Igarashi, Tsuritani et Morita, 2016; Kitayama et Diamantopoulos, 2017; Li et al., 2012; Li et al., 2018; Liu et al., 2018; Niederriter, Siemens et Gopinath, 2015; Rademacher et al., 2018b; Weng et al., 2015a; Yaman et al., 2010).

The identified research problem and their potential solutions

Crosstalk management is one of the major challenges that have to be taken into consideration when dealing with fibers supporting several spatial modes. The energy efficiency of SDM links can be improved altogether using mode-division multiplexing that excites and propagates numerous optical modes in a parallel manner inside the FMF. The lack of an effective mode multiplexer/demultiplexer (mux/demux) for the insertion and separation of optical modes as well as the issue of intermodal crosstalk led to the design of MDM systems(Essiambre et al., 2013).

Few-mode fibers are particularly promising for MDM, where multiple information channels can be transmitted across spatial modes with minimum crosstalk thereby increasing the data capacity carried inside a single core fiber by many folds. However, the characterization and control of the higher-order modes in few-mode fibers can pose a great challenge. In order to maximally exploit the MDM system, the few-mode fiber needs to be fully characterized.

Recent researches have reported promising results in the development of high data transmission rate utilizing mode division multiplexing as well as multi-parameter and distributed sensors based on the LP modes of FMF (Li et al., 2015; Nejad et al., 2016; Wang et al., 2017b). Some of the works conducted on FMF (distributed fiber sensors, amplifiers,

switches, etc.) have already shown promising results of using FMF towards SDM technology (Bai et al., 2012; Carboni et Li, 2016; Genevaux et al., 2015; Salsi et al., 2012). Several of these breakthroughs towards the advancement of FMF in MDM and distributed sensors have exploited the LP modes of the fiber. Interestingly, OAM beams and linearly polarized beams can be achieved from the linear combinations on eigenmodes of fiber i.e. CVBs.

The demonstration towards the possibility of vector mode multiplexing can open window to utilize the eigenmodes of the fiber avoiding the utility of MIMO technology at the demultiplexing end (Liu et al., 2018). One of the reasons for scarce research works of CVBs towards MDM application corresponds to the scarce availability of specialty FMFs as well as the relatively high level of technical difficulty in the fabrication of photonic devices to excite and detect these vector beams. It becomes very essential to explore the properties of these vector beams for their potential applications in SDM fiber communication links and multi-parameter-based fiber-optic sensors. The generation and control of these CVBs in the FMF is regarded as primary importance. One key solution can be the development of photonic mode converters that can allow conversion of the fundamental mode of an FMF into a stable higher-order vector mode with high mode purity and conversion efficiency.

Objective of the research

The objective of the research is to investigate the specially-designed few-mode fiber as well as establish novel methods for the excitation and control of the guided higher-order modes including the cylindrical vector beam carrying orbital angular momentum states. Precise knowledge of these CVBs is critical in order to use them as tools for different applications in next-generation telecommunication systems and towards distributed sensing using FMF. Though different techniques have been proposed in this regard, still extensive research has to be carried out to design devices offering low loss and better isolation characteristics. The accurate characterization of this vector beam is critical in order to mitigate modal crosstalk.

The main objectives of the research work presented in this thesis are clearly displayed in figure 0.3 which are

1. To design and fabricate simple and robust free space as well as all-fiber based mode converters that can efficiently generate the CVBs and OAM supported by the FMF with high modal purity.

2. The second objective aims to characterize the vector beams supported by the FMF, which have not been fully explored until date. The accurate characterization of these vector beams is essential for obtaining the distributed measurements of the FMF, in order to exploit the vector beams to its maximum potential.

3. The final objective is to propose and demonstrate an alternate way to tailor the azimuthal intensity profile of the beam so as to maximize the free space coupling efficiency in specialty fibers.

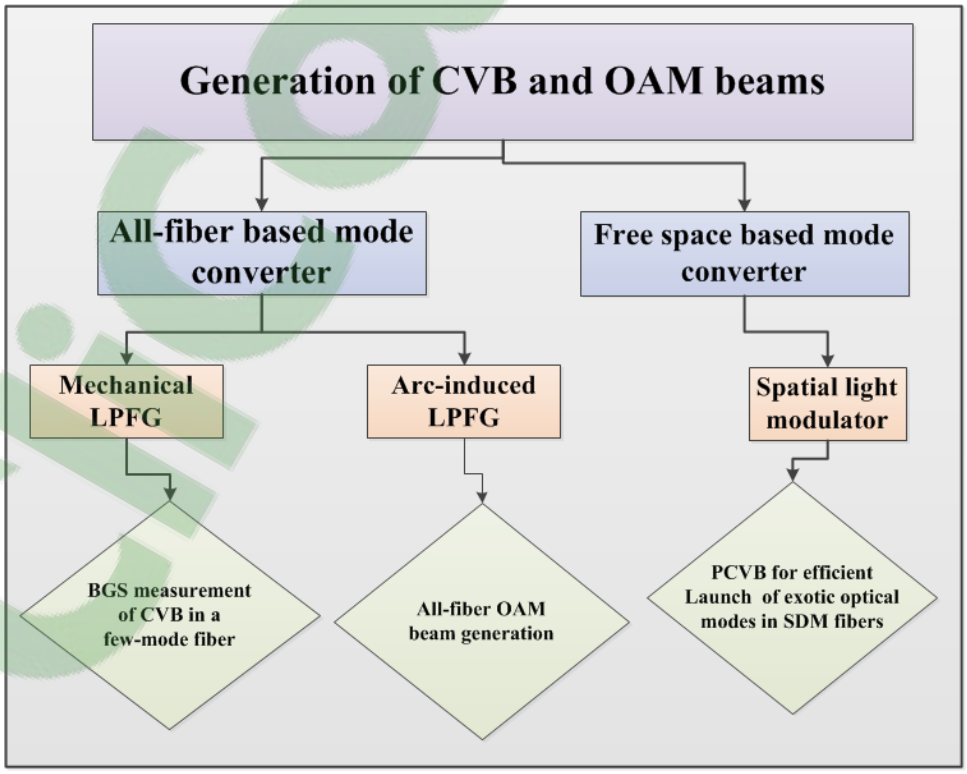

Figure 0.3 Schematic outline of the overall thesis research

The experimental part of the research work is selected as an original research paper based thesis, as recommended by the submission policies of ETS. During my PhD, I have contributed to the publication of 5 peer-reviewed journal articles (published/submitted), being first author of 3 articles and co-author for other 2 articles. The three articles as first author corresponds to the three chapters (2, 3 & 4) of this thesis. These three chapters from the journal article constitute an abstract, introduction, experimental techniques and results & discussion. The main content of the thesis comprises of abstract, introduction with objectives, literature review, conclusion and statement of original contribution with future recommendations.

Framework of the thesis:

The thesis has been organized as follows:

The first chapter of this thesis reviews the literature of techniques used for the production of passive components in order to generate CVBs and OAM beams. The chapter also reviews the highlights of some of the recent breakthroughs in the domain of SDM technology using FMF. The remaining three chapters present the methodology utilized for achieving the objective of the proposed research leading to journal publication.

The second chapter is an article published in Nature Scientific Reports in 2017:

In this article, the measurement of the Brillouin gain spectra of vector beams in a few-mode fiber using a simple heterodyne detection technique is demonstrated for the first time. A tunable long period fiber grating is used to selectively excite the vector beam supported by the few-mode fiber. Characterization of vector beams in a FMF gives a different and novel dimension to this research work when compared to the works that have been carried out till date using FMFs.

The third chapter of this thesis is an article published in IEEE Photonics Journal in 2018:

This article highlights the necessity of developing a technique to tailor the beam profile of CVBs for their potential applications in the efficient launch of exotic optical modes in specialty fibers, for super resolution microscopy and in the domain pertaining to optical tweezers. The method for producing high-purity PCVBs with tailorable transverse intensity profile (both ring width & ring diameter) controlled via a digital SLM and iris is reported in this chapter of the thesis. The technique proposed is highly adaptable for its robust nature to generate any arbitrary PCVBs as well as perfect vortex beams with any topological order, using the same experimental setup.

The fourth chapter of this thesis is an article submitted in Journal of lightwave technology:

In this article, all fiber-based mode converters designed to generate CVBs and OAM beams has been demonstrated. The long period fiber grating is written with the smallest grating pitch ever reported within a fiber that act as a mode converter fabricated using the common electric arc induced approach. Such passive fiber based mode converters can be used for the development of high energy CVB and OAM lasers.

The last chapter briefly concludes the thesis with future research recommendations.

CHAPTER 1

REVIEW OF THE STATE OF THE ART

This chapter reviews the studies on optical fiber communication systems including the different technologies employed and highlights the technological advancements that have happened across generations. The first generation of fiber-optic system came into existence with a bit rate of 45 Mb/s in 1978 (Maione, Sell et Wolaver, 1978). Over the years, the domains of fiber-optics communications have witnessed tremendous progress in the transmission rates. Each generation of optical fiber system came with increasing bit rates meeting the demands of the time. The invention of innovative smart technology reflects that there will never be a decline in the demand for higher bandwidths. The pursuit for higher bandwidths have paved way to 100 Gb/s data transmission rate up to several thousands kilometers to cope up with the ever increasing demand (Idachaba, Ike et Hope, 2014). The introduction and of the optical amplifier along with wavelength division multiplexing in the late 90s has unleashed the full potential and power of fiber-optic communication systems to enhance the data transmission rates even further. Despite the new technological advancements in the fiber-optic communication system, the so-called capacity crunch is one major issue of concern as the applied bandwidth is reaching its theoretical limit at a rapid rate.

At this juncture, the focus of the researchers is to meet the demands for higher bandwidth by maximally utilizing the available resources through novel approaches. Many techniques and approaches have been proposed by introducing specialty fibers to broaden the spectrum of telecommunication networks. Recently, space division multiplexing technology has made high impact in the scientific community (Richardson, Fini et Nelson, 2013). Several SDM fibers have been introduced to accomplish this goal. The knowledge of advancement of the special SDM based components is important to explore the possibility of improving the scalability of research. Therefore, the study of all-fiber based and free space based active and

passive devices are presented. Further, a review study of important fiber characterization tool that are useful towards fully exploiting modal properties of SDM fibers is discussed.

1.1 Space division multiplexing and its potential application

Spatial division multiplexing refers to a multiplexing technique that provides multiple data paths that are spatially distinguishable through the same fiber. SDM promises not only an increase in capacity per fiber but also reduction in cost per bit by increasing the energy efficiency (Winzer, 2014). But, the primary technical challenge would possibly be on crosstalk management. SDM can improve the bandwidth of new fiber optic systems by many folds through a method that can launch, transport and detect two or more optical channels operating at the same wavelength inside an optical fiber. This attribute makes SDM stand out among the other available multiplexing techniques while maintaining compatibility with time division multiplexing (TDM) and wavelength division multiplexing/dense wavelength division multiplexing (WDM/DWDM) techniques (Essiambre et Tkach, 2012; Richardson, Fini et Nelson, 2013), among others.

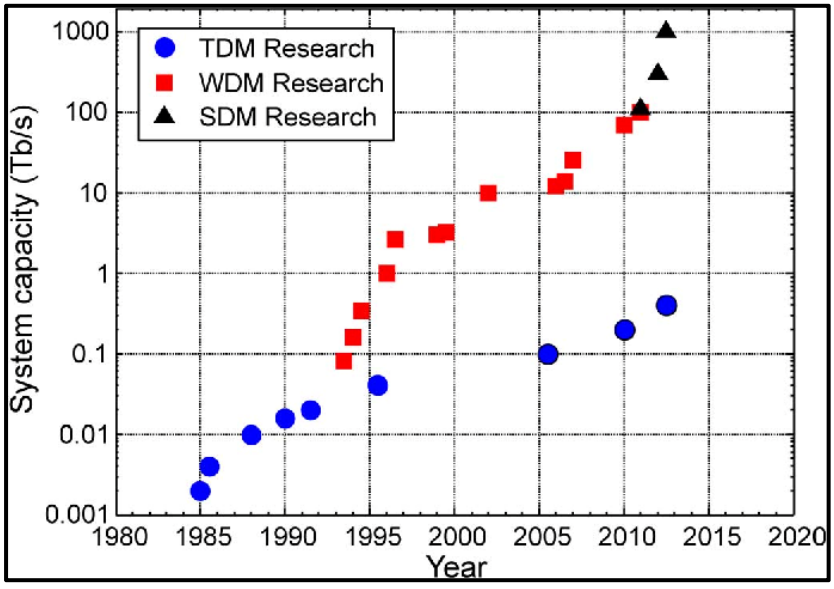

Figure 1.1 Demonstration of high capacity SDM systems
Taken from Essiambre et al. (2013, p.0701307)

1.2 SDM fibers and their outlook

As shown in Figure 1.1, the SDM technology in the upcoming years is expected to provide data capacity higher than 100 Tb/s which is much higher than the capacity that other multiplexing techniques can offer. In spatial multiplexing more than one spatial mode is guided by the fiber.

Several approaches have been reported to realize the potential benefits of SDM. The implementation of SDM depends on novel types of specialty fibers: FMFs, multicore fibers (MCFs) and hollow-core fibers (HCFs) as shown in Figure 1.2. MMFs and FMFs have found a variety of applications in telecommunication and optical sensing owing to the larger diversity in modes, lower optical non-linearities and higher power-handling; features that the conventional SMF does not offer.

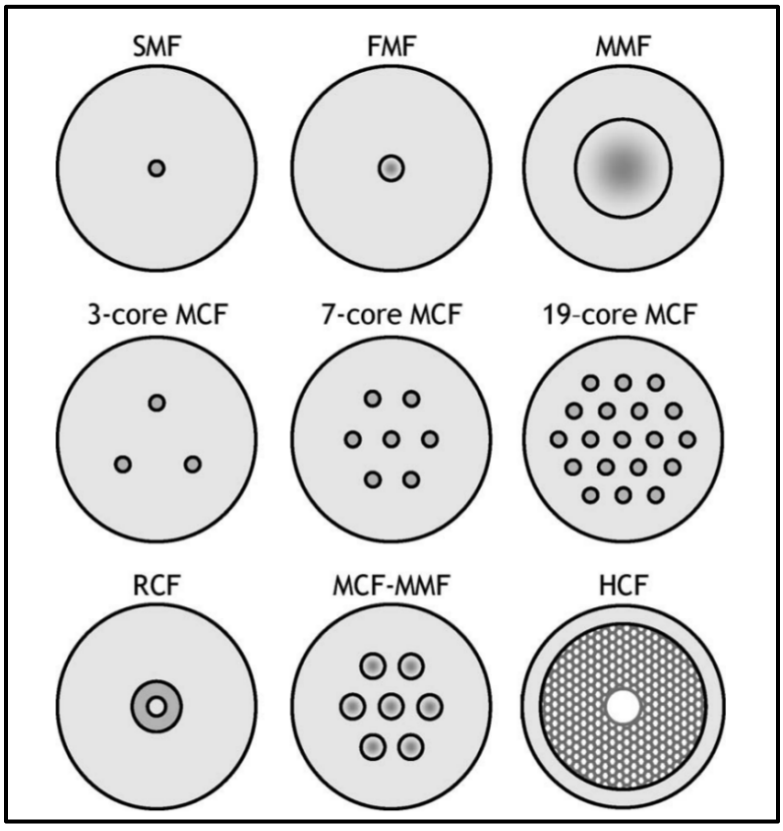

Figure 1.2 Cross-section of fibers supporting spatial division multiplexing
Taken from Essiambre et al. (2013, p.0701307)

However, standard MMF supports hundreds of modes, which makes the task of multiplexing/demultiplexing data along separate co-propagating modes virtually impossible at the moment. FMF supports less than ten modes that it reduces the system complexity to an achievable level (Kitayama et Diamantopoulos, 2017; Li et al., 2012). Though FMFs open exciting capacity-scaling scenarios with their ability to exploit more spatial channels, it is still very challenging to reliably excite, transmit and detect the different co-propagating modes independently. Some of the works have shown promising results on mode division multiplexing of LP_{01} and LP_{11} modes (Li et al., 2011a; Sillard et al., 2011; Wang et al., 2017b) and LP_{01} and two degenerate LP_{11} modes in FMF (Al Amin et al., 2011; Wang et al., 2017a).

The contemporary characterization methods of FMFs include the phase-shift method (Nicholson et al., 2003b), the S2 method (Nguyen et al., 2012) and the OLCI method (Gabet et al., 2015). However, the report on the FMFs characterization are based on the scalar LP mode groups measurements that have still left the windows of vector modes to be explored, that require greater spectral and spatial precision to be detected. These Eigen vector modes constitute the fundamental basis set of LP modes in the scalar approximation, where Figure 1.3 illustrates the LP_{11} mode degenerated into cylindrical vector beams: TE_{01}, HE_{21}even, HE_{21}odd and TM_{01}.

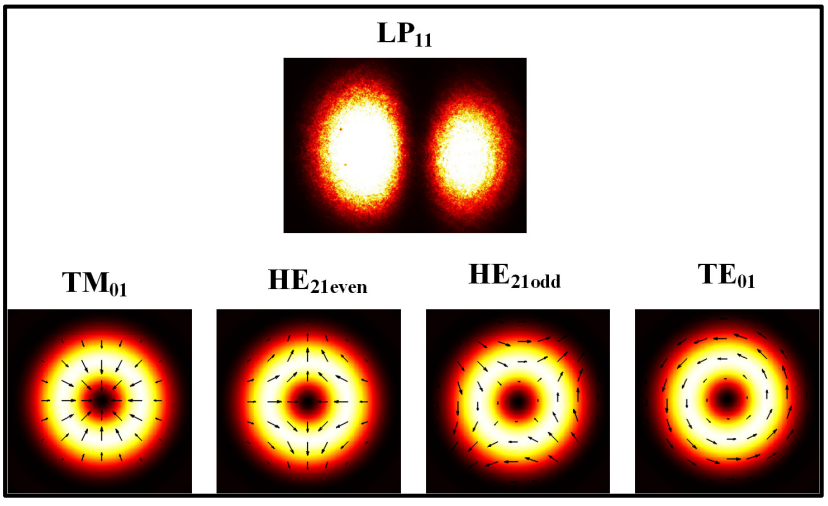

Figure 1.3 Scalar (top) and vector (bottom) representation of the first higher order anti-symmetric mode group

However, the deployment of these new fibers will be considered depending upon the efficiency, cost and performance compared to the equivalent number of SMF system. The motivation behind developing the SDM technology is not just to meet higher capacity demands but one of the most important factors is its cost per bit. The criteria that will determine the deployment of SDM technology in the commercial industry, if it:

i) Brings down the transmission cost per bit

ii) Increases energy efficiency

iii) Provides routing and switching flexibility needed in order to have efficient photonic mesh network

iv) Allows the smooth transition between the SDM systems and the already present SMF infrastructure.

1.3 Few-mode fibers for spatial division multiplexing

The pursuit for efficient and high-speed data transmission has drawn the attention of researchers towards the less exploited spatial dimensions in fibers. In this context, SDM that uses either FMF or MCF as the medium for data transmission forms the essential part of next-generation fiber telecommunication systems as summarized by Richardson et al. (Igarashi, Tsuritani et Morita, 2016; Kitayama et Diamantopoulos, 2017; Richardson, Fini et Nelson, 2013). The spatial spectral efficiency parameter termed “spatial multiplicity” has been brought forth keeping in view the space required for channel transmission. The spatial multiplicity (η_{max}) can be defined as the number of multiplexed spatial channels within the modes and cores excluding the polarization written as, (Mizuno et al., 2016)

$$\eta_{\max} = \frac{\text{spatial multiplicity}}{\text{cross sectional area}} \tag{1.1}$$

The aggregate spectral efficiency (ASE) can be measured if the spectral efficiency and spatial multiplicity are known. In the transmission experiments conducted earlier, the spatial multiplicity started from the value of 3 for the number of modes (Salsi et al., 2012) denoted by ‘M’ and a value of 7 for the number of cores (Zhu et al., 2011) which is denoted by ‘N’ in

multimode and multicore transmissions respectively. Later, the number of cores, 'N' was maximized to 19 thus increasing the multiplicity (Sakaguchi et al., 2012b). Spatial multiplicity above 30 could be attained by introducing the region of dense SDM, so as to improve the scalability (Mizuno et al., 2014). The results of various studies using MCF, MMF or FMF indicate great strides in the progress of data transmitting capacity of a single fiber link in the recent years (Igarashi, Tsuritani et Morita, 2016; Kitayama et Diamantopoulos, 2017; Minardo, Bernini et Zeni, 2014; Nikles, Thevenaz et Robert, 1997; Rademacher et al., 2018a; Rademacher et al., 2018b; Richardson, Fini et Nelson, 2013; Soma et al., 2018b; Song et Kim, 2013).

1.3.1 Few-mode multicore fiber for SDM transmission

Several techniques have been employed with a view to derive maximum benefit from SDM which can be accomplished in two different ways. Firstly, the SDM can be implemented by parallel propagation of several spatial channels in the same fiber. Another approach to introduce SDM systems is to insert multiple cores within a multicore fiber (MCF). Initial studies on transmission using a 7-core MCF reported a capacity increment of 100 Tb/s equal to the maximum SMF limit (Sakaguchi et al., 2012a). Certain studies have reported using around 19 independent optical cores inside a single clad fiber. Transmission experiments conducted with a 19-core fiber, reported a transmission rate of 305 Tb/s that is 3 times the SMF limit (Sakaguchi et al., 2012b). One of the studies has reported 1.01 Pb/s across 52 km distance in the transmission using a MCF having 12-cores (Takara et al., 2012). The highest data transmission rate of 1 Pb/s was reported with an ASE of 91.4 b/s/Hz by employing a 12 core fiber with a one-ring structure (Takara et al., 2012). A long haul transmission rate of 1 Eb/s could be accomplished using a 7 core, 12 core MCF over 7326 km 1700 km transmission distances (Igarashi et al., 2013). The second approach uses a guiding medium supporting multiple modes, like in a FMF that is capable of guiding only around 6 to 12 distinct modes inside a single core and is designed slightly larger than that of a SMF.

Table 1.1 Progress of SDM transmission system in optical fiber

Year	**Type of Fiber**	**No. of modes**	**Fiber length (km)**	**ASE (bit s^{-1} Hz^{-1})**	**Capacity−distance transmission (Pb s^{-1} km^{-1})**
2018	FMF-MCF (Soma et al., 2018)	6	11.3	1099.9	10.16
2018	FMF (Rademacher et al., 2018b)	3	3500	31.5	9.9
2018	FMF (Rademacher et al., 2018a)	3	1045	-	166
2018	FMF (Soma et al., 2018a)	10	48	30.5	0.25
2016	FM-MCF (Igarashi, Tsuritani et Morita, 2016)	6	9.8	456	2.05
2015	MMF (Ryf et al., 2015)	10	125	29	0.15
2014	OAM fiber (Wang et al., 2014a)	26	-	112.6	1.036
2013	FMF (Ryf et al., 2013)	6	177	30.72	4.35
2012	FMF (Wang et al., 2012)	32	1	95.7	0.002

FMF transmission has been exploited to demonstrate ASE of 32 bits/s/Hz making use of six spatial modes (Ryf et al., 2013). While ASE of 109 bits/s/Hz has been accomplished by

employing 12 cores in MCF transmission (Qian et al., 2012). The highest transmission rate reported for a 3 mode fiber transmission is 57.6 Tb/s over a distance of 119 km FMF (Sleiffer et al., 2012). Studies on hybrid multiplexing of multiple modes of MMF and multiple cores of MCF reported an ASE of 247.9 bits/s/Hz, which is 3 times greater than the 1 Pb/s reported in 12 core transmission (Takara et al., 2012). Uden et al., utilized WDM with 50 wavelength channels in a few-mode multicore fiber to demonstrate a data transmission of 255 Tb s^{-1} over a 1 km length of fiber (Van Uden et al., 2014). Further, spatial modes up to 15 have been reported for FMF transmission (Fontaine et al., 2015), and the length of fiber with 3 modes over 3500 km (Rademacher et al., 2018b) and 6 modes over 1600 km (Weerdenburg et al., 2017) have been reported. Most recently Soma et al., demonstrated 10.16-Peta-B/s ultradense SDM transmission over 6-mode 19-core fiber across the C+L band, which is one of the highest record fiber capacity reported in recent time (Soma et al., 2018b). The studies conducted by different groups reflect the tremendous growth over years in few-mode multicore as well as multimode transmission shown in Table 1.1.

1.3.2 Mux/demux: a crucial component for SDM system

The combinations of LP_{01} and modes including polarization and degeneracy are used to attain MDM in either two mode fiber (TMF) or FMF. The possibility of using MDM and multiple input multiple output (MIMO) to transmit data using FMF has been reported by different groups (Fontaine et al., 2015; Huang et al., 2015; Luís et al., 2018; Ryf et al., 2012; Shibahara et al., 2018; Sleiffer et al., 2012; Takara et al., 2012; Winzer et Foschini, 2011). Intense research is in progress on various aspects like fiber design (Grüner-Nielsen et al., 2015), amplification (Genevaux et al., 2015), transmission rate (Chen et al., 2015a) etc. for further advancements in FMF transmission technology. Some of the already existing FMF designs have used either with the step-index profile or graded-index profile. Fabrication of step-index profile is easy and does not require advanced processes such as stack and draw technique (needed for some micro structured and hollow core fibers) whereas, in graded index-profile, differential modal delay (DMD) within the modes can be reduced to a great extent. Desirable FMF designs will be engineered to lower the DMD to a much lower level,

decrease the non-linearity in fiber and also to minimize the propagation near levels currently possible with SMF(Ferreira, Fonseca et da Silva, 2014; Yaman et al., 2010).

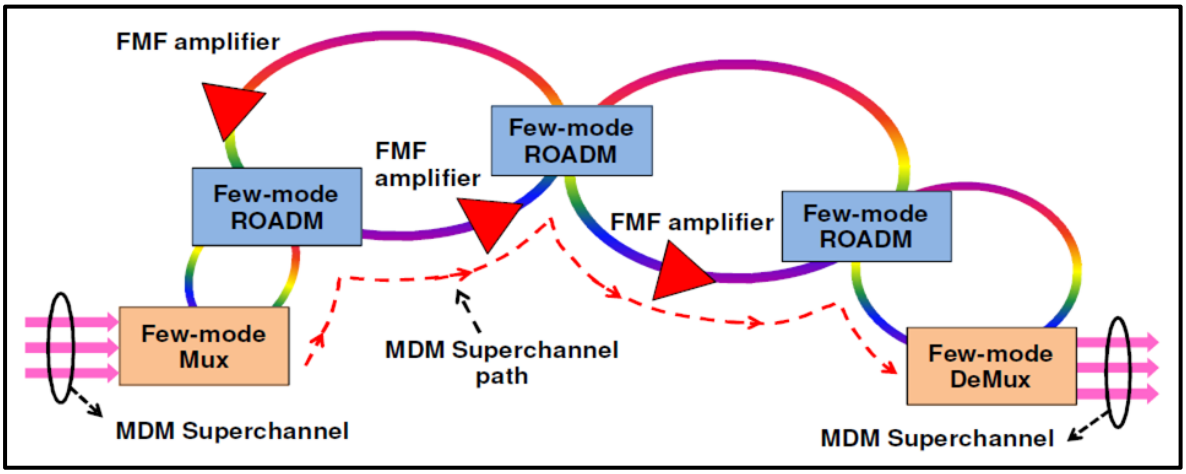

Figure 1.4 Illustration of mux/demux components in a SDM system
Taken from Chen et al. (2012, p.14303)

The MUX/DMUX of modes representcrucial components in the MDM transmission systems as shown in Figure 1.4. The optical add/drop multiplexer (OADM), mode converter (MC) and mode combiner are some of the components that have been reported for exploiting the MDM transmission systems (Chen et Zhou, 2014; Chen et al., 2012). There have been many experimental attempts to determine the utility of these components(Chen et al., 2013b; Ren et al., 2017; You, Jia et Wang, 2016). However, in-depth research is yet to be carried out in order to design a technically efficient and affordable SDM system overcoming the real time challenges. To MUX/DEMUX signals in multiple modes, Mizuno et al., described different kinds of MUX/DEMUX that can be devised such as LP mode converter as well as mode combiner, index matched mode couplers, phase plate or long period grating, mode coupler with cores in a arrayed fashion (Mizuno et al., 2015; 2016).

Moreover, some studies continue to progress the investigation to exploit the beams carrying OAM showing potential advantage to reduce the mode coupling and the requirements of DSP (Bozinovic et al., 2012; Brunet et al., 2014; Nejad et al., 2016; Ramachandran et Kristensen, 2013; Ung et al., 2014; Wang et al., 2016; Willner et al., 2015; Zhu et al., 2018; Zhu et al.,

2017). OAM modes, aka “vortex beams” have drew much attention in the research community with the recognition of light carrying orbital momentum first reported by Allen et al. (Allen et al., 1992). OAM encoding can enhance the multiplexing in multiple orthogonal spatial modes thereby providing a potential solution to the expected problem of capacity crunch and also efficiently improving the safety of quantum encryption networks. Bozinovic et al., demonstrated the transmission of light carrying OAM states over a distance of 0.9 km using FMF (Bozinovic et al., 2012). There are many such reports that have highlighted the importance of OAM modes for the efficient transmission of analog and digital signals in a FMF (Allen et al., 1992; Bozinovic et al., 2013; Ung et al., 2014; Wang et al., 2012). Some of the recent reports based on the OAM data multiplexing towards MIMO-free mode-division multiplexing systems (Nejad et al., 2016; Nejad et al., 2018; Wang et al., 2017b; Zhu et al., 2018; Zhu et al., 2017). OAM multiplexing will add a new dimension in increasing the data transmission capacity in the future communication system.

Most recent report from Liu et al. proposes and demonstrates the data multiplexing utilizing the vector eigenmodes in a 2-km large core FMF (Liu et al., 2018). The true vector modes present in this FMF can be used in efficient way to reduce the coupling between the modes. Researchers also have started utilizing these true vector modes of fiber that carry orbital angular momentum in order to reduce the complexity of MIMO processing at the receiver end. Such work on vector Eigen modes of fiber opens the future roadmap towards the possible vector mode multiplexing systems. The employment of efficient photonic integrated devices will help in the successful generation and MDM transmission of real eigenmodes of fiber i.e. CVBs. Since isolation of distinct modes to excite, transmit and separate is challenging, to accomplish desired performance in communication systems, the computer abd energy intensive MIMO technique has to be applied. The complexity of the electronic processing could be reduced using optical devices having better modal isolation. Though different techniques have been proposed in this regard, still extensive research is being carried out in designing devices offering low loss and high isolation characteristics (Eznaveh et al., 2017). Apart from SDM based amplifier and ROADM components, MUX/DEMUX) is needed to couple several spatial modes at one end and unscramble the crosstalk between the

modes at the other end. MUX/DEMUX is a key device to realize maximum potential of mode division multiplexed transmission.

1.4 Review on long period fiber grating as a mode converter

Mode converters can be either free space or inline fiber based. They are basically employed in order to convert light beams from the Gaussian-like fundamental LP_{01} mode into a higher-order LP_{11} mode or vice versa (Pradhan et al., 2015; Ramachandran et al., 2005; Savin et al., 2000; Vengsarkar et al., 1996a). The use of mode selective coupler (Blake, Kim et Shaw, 1986), intermodal couplers (Kim et Song, 2014), acousto-optic modulator (Kim et al., 1986), Kerr modulators (Andermahr et Fallnich, 2010), holographic mode mux/demux (Amphawan, 2011), and elliptical core fiber to lift modal degeneracy (Kim et al., 1987), are few techniques designed to achieve this target. In the past few years, several ways of writing LPFG techniques has been demonstrated. These methods include heating (Wonko, Marć et Jaroszewicz, 2017), electric arc-induced(Rego, 2016), microbending (Ramachandran et al., 2005), and etching process (Villar et al., 2017) which was demonstrated after the introduction of UV writing method (Bae et al., 2003).

1.4.1 Mechanical long period fiber grating

The characteristics of the transmission spectra in the LPFG rejection bands are affected by the writing method and the type of optical fiber employed. A specific transverse and longitudinal refractive index profile is generated in every inscription method. The coupling between fundamental LP_{01} mode and the higher-order LP_{11} modes can be determined from transverse index profile (Anemogiannis, Glytsis et Gaylord, 2003) while the position of the rejection bands is influenced by the longitudinal index profile (DeLisa et al., 2000). The optical characteristics of the rejections bands comprising the resonant wavelength position, depth of mode loss, birefringence, polarization dependent loss (PDL) and insertion loss and also the physical variables like stress, strain, bend, torsion and external refractive index are dependent on the total index profile and the type of fiber employed.

The fiber gratings enable coupling of guided modes to radiation modes when used as loss filters (Mizrahi et al., 1994). It can also be used to create cladding modes, as the cladding is surrounded by a lower refractive index medium like air (Vengsarkar et al., 1996a; Vengsarkar et al., 1996b). Switching and routing facility, dispersion management, polarization control and sensing, control of signal power, are some of the applications of long period fiber grating(Chen et al., 2018; Colaço et al., 2016; Huang et al., 2010; Masri et al., 2016; Ramachandran et Kristensen, 2013; Zhang et al., 2018). Transmission modes and reflection modes are the different operating modes on the basis of which fiber gratings are categorized, where, Bragg gratings and LPFGs periods are in the order of nanometer and micrometer respectively (Nemova et Kashyap, 2008). The proposed study focuses mainly on the inline conversion of transmission mode and therefore LPFG is proposed to achieve our objective.

The phase mask-based MC is a free space component that uses either spatial light modulator (SLM) or glass plate specially-fabricated for this purpose, whereas, LPFG based MC is a fiber-based component. The fiber-based components are compact and easy to integrate, and these characteristics give them an upper hand over the free-space components in telecom applications. It is straight forward to achieve mode conversion in a LPFG-based MC via periodic grating structure by applying pressure mechanically on FMF or TMF.

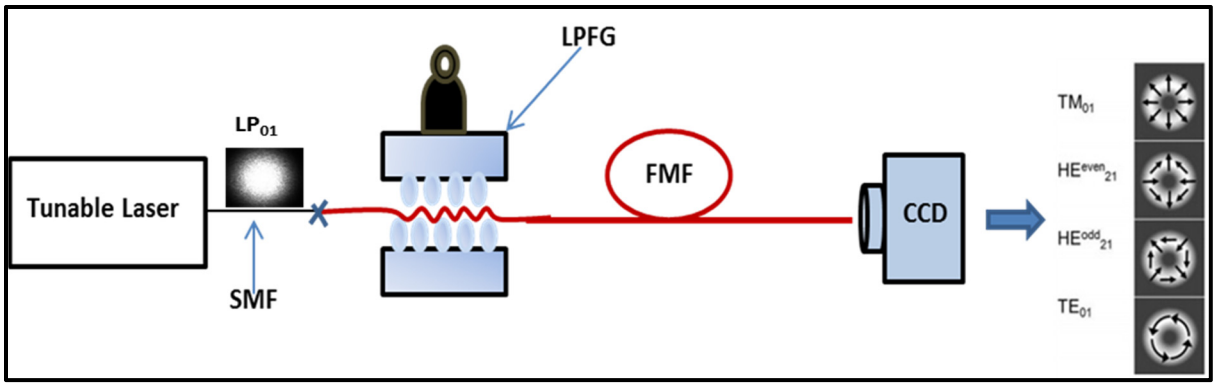

Figure 1.5 Mechanically induced LPFG as a mode converter

LPFG can be induced mechanically owing to its large index modulation period of some hundred micrometers as shown in Figure 1.5. The periodic index modulation is induced through the phenomenon of photo-elastic effect and was initially demonstrated in the polarization modes and the LP_{01} to the LP_{11} modes of the birefringent fibers and TMF respectively during the 1980s by (Kim et al., 1986; Kim et al., 1987). Lee et al., reported wire-winding LPFG technique by winding the wire periodically (pitch of 500 μm) around a cylindrical rod that demonstrated change in shift of 9 nm with transmission power difference of 2.5 dB in the higher-order LP modes by tuning the grating pitch (Lee et al., 2013).

Youngquist et al. used LPFG in birefringent fibers for coupling their polarization modes and also the conversion of LP_{01} to the LP_{11} mode in TMF (Youngquist, Brooks et Shaw, 1984). Using a simple 13-ridge device, Blake et al., demonstrated a potent LP_{01} to LP_{11} modal coupler for coupling the light between the modes (Blake, Kim et Shaw, 1986). Zhou et al., designed a tunable, reconfigurable and cost-effective mechanically-induced multi-π-shifted LPFG with filtering characteristics, which could induce up to nine π-shifts in a grating (Zhou et al., 2011). Ramachandran et al. have done extensive studies on LPFGs in FMF and have produced commendable results in this domain. One of their studies demonstrated the conversion of linearly polarized LP mode into a selected cylindrical vector beams (TM_{01}, HE_{21}even, HE_{21}odd and TM_{01}). Using LPFGs, 99% move conversion over 63 nm bandwidth was also demonstrated (Ramachandran et al., 2002; Ramachandran et al., 2005; Ramachandran et Kristensen, 2013; Ramachandran, Kristensen et Yan, 2009).

1.4.2 Long period grating written within a fiber

Another simple, flexible, low cost and efficient technique to fabricate LPFG is using electric arc induce method that allows the inscription of grating in all kind of fibers as shown in Figure 1.6. Several limitations exhibited by UV laser irradiation technique can be overcome by using electric arc induce method. Poole et al., introduced fabrication of LPFG in 1994, by utilizing two-step process of fiber cladding removal through laser ablation followed by arc discharge (Poole, Presby et Meester, 1994). LPFG fabrication solely based on electric arc

discharge was demonstrated by Dianove et al., in 1997 (Dianov et al., 1997). In 2006, the LPFG simulation showed the dependence of near field intensity distribution on the fiber that could lead to the coupling of core to cladding modes of different symmetries (André et al., 2006). In pure silica-core fibers, the micro-deformations were highlighted to be responsible for the grating formation (Rego et Ivanov, 2011).

For many years, several modifications to the LPFG setups were implemented to increase the reproducibility. Such improvements of advanced LPFG setups led to the flexible, compact, efficient and reproducible results allowing inscriptions in all kinds of fibers. The arc induced LPFG fabricated in different type of fiber includes photonics crystal fiber (Dobb, Kalli et Webb, 2006; Esposito et al., 2018), cladding etched fibers (Martinez-Rios, Monzon-Hernandez et Torres-Gomez, 2010), hollow core fibers (Iadicicco, Campopiano et Cusano, 2011; Iadicicco, Ranjan et Campopiano, 2015) and few-mode fibers (Ramachandran et al., 2002; Zhang et al., 2018; Zhao et al., 2017; Zhao et al., 2016). An automatic electric arc-based technique was reported by Yin et al., to improve the writing efficiency of LPFGs in SMF as well as PCF. For single-mode fiber, the grating pitch value could be varied within the range of 360-750 μm, and 480-580 μm for photonic crystal fiber employing a fully automated program in a fusion splicer (Yin et al., 2016). The modification in their fabrication involves absence of tension, application of compression, and even applying pressure to hollow core fiber on the time of arc discharge.

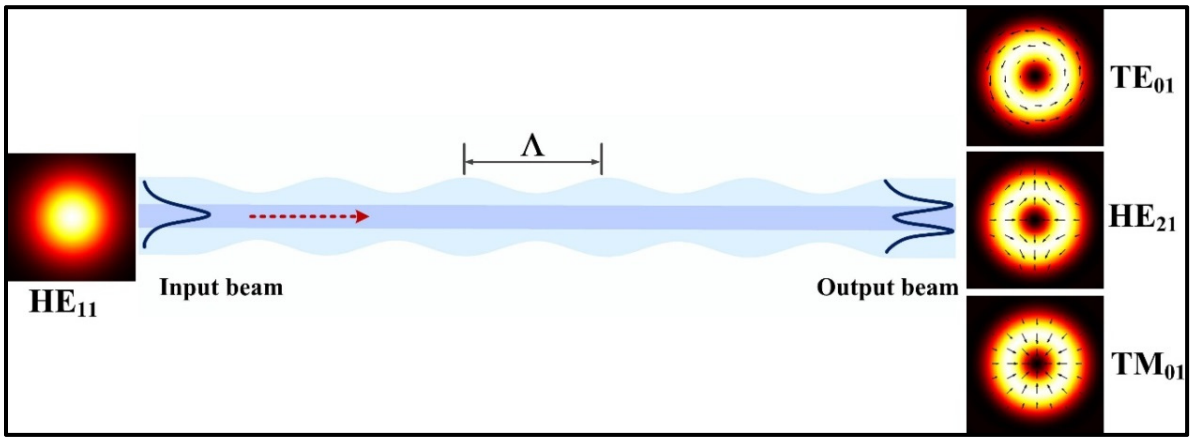

Figure 1.6 Arc induced LPFG as a mode converter

Recently, Du et al., fabricated a long period fiber grating with a period of 500 μm using an electric arc induce technique for simultaneous measurement of strain and temperature (Du, Wang et Zhao, 2018). Different characteristic features of arc induced LPFG as a function of different physical parameter such as temperature, strain, bending, pressure, torsion, effective refractive index have been reported (Rego, 2016). Along with their high-end applications in sensors, band-rejection filters, etc., LPFG have been demonstrated as a crucial component in MDM technology as a mode converter (as shown in Figure 1.6) to efficiently convert one guided mode to another in SDM fibers (Zhang et al., 2018).

Zhao et al., demonstrated an all fiber LPFG for the conversion of LP_{01} modes into other higher order modes (LP_{11}, LP_{21} and LP_{02}) (Zhao et al., 2017; Zhao et al., 2016). The period of the grating fabricated for the conversion of LP_{01}-LP_{11}, LP_{01}-LP_{21} and LP_{01}-LP_{02} using CO_2 laser were of the order 1750 μm, 630 μm and 420 μm. A temperature-insensitive LPFG mode converter was proposed by Dong et al., with a very high conversion effeciency >99% (Dong et Chiang, 2015). The generation of vortex beam is in high demand due to their novel applications in both telecommunications and sensing. The demonstration of mode conversion LP_{01}-LP_{11} (LP_{21}), for their potential application in high-order optical vortex pulsed lasers was reported by Wang et al (Wang et al., 2017c). Recent work performed on FMF have highlighted the potential for exploiting the LPFG towards the all-fiber generation of high-power CVB lasers as well as mode division multiplexing systems (Chen et al., 2018).

Although, fiber based techniques are highly preferred with the aim to reduce the overall loss incurred by the system, several reports towards generation and propagation of annular shaped beams can be still found based on free space. This is due to the ongoing design and fabrication of different types of optical fiber with an annular profile such as Inverse parabolic graded index profile fiber (Ung et al., 2014), graded index fiber(Huang et al., 2015), vortex fiber (Bozinovic et al., 2013), air core fiber (Brunet et al., 2015; Brunet et al., 2014; Kasahara et al., 2014) that requires test and validation, so as to make use of this SDM fibers to its full potential. However, the efficiency of free space coupling in such fibers can be optimized when the annular core dimension of the fiber and the beam intensity profile are perfectly

matched. These emerging applications of beams with doughnut shaped profile, both in free space optics as well as in fiber optics requires reliable excitation and propagation techniques.

1.5 Generation of perfect vector and vortex beams

A cylindrical vector beams associated with polarization singularity possesses cylindrical symmetry having its polarization varying spatially (Zhan, 2009). The unique properties of such cylindrical vector beams exhibiting complex polarization variations can give rise to peculiar focusing properties that allows one to achieve high resolution optical imaging and micro-particle optical manipulation (Kozawa et Sato, 2015). On the other hand, phase singularity is related to the field that is represented by azimuthal phase structure of the form $\exp(il\phi)$ in the transverse plane, where l is the topological charge and ϕ is the azimuthal angle. Typically, an optical vortex beam carrying orbital angular momentum is represented by a beam of light that possesses a helical phase front. Such beams with phase and polarization singularities have attracted tremendous research interests in many areas including laser material processing, optical trapping and quantum communication owing to their topological and spatial properties (Dennis, O'Holleran et Padgett, 2009; Kozawa et Sato, 2010; Milione et al., 2014; Porfirev, Ustinov et Khonina, 2016).

1.5.1 Review studies on perfect vortex beams

Although several methods have been introduced and demonstrated to generate vortex and vector beams with phase and polarization singularities, their launching efficiency in free space still remains an area of interest. The annular shaped beams in the optical fiber are excited in free space and the maximum coupling can be obtained when the overlap integral between the guided mode dimensions of the fiber and the input beam profiles is optimized.

One of the common shortcomings with these techniques originates from the strong dependence of inner and outer diameters of the annular intensity ring. In the case of conventional vortex beams, the ring diameter varies linearly with that of the order or a topological charge making coupling of several vortex beams problematic. Ostrovsky, et al.

first introduced the concept of perfect vortex beam in 2013 (Ostrovsky, Rickenstorff-Parrao et Arrizón, 2013). They used a special phase mask to demonstrate an annular intensity profile of the vortex beam independent of its topological charge. Further, Chen et al. experimentally demonstrated the particle dynamics in perfect optical vortex beams having fractional topological charge (Chen et al., 2013a). Some of these techniques used for the generation of perfect vortex beams have some extra rings. An improved technique was proposed by (Vaity et Rusch, 2015), to form a perfect vortex beam with controllable ring-width and ring diameter as shown in Figure 1.7. The complete mathematical description for the generation of PVB utilizing the Fourier transformation of Bessel beam was derived. They proposed that the ring diameter of the PVB could be controlled by controlling the radial wave vector of the Bessel-Gauss beam. For this purpose, they used a new phase mask with a combination of lens, axicon and spiral phase function.

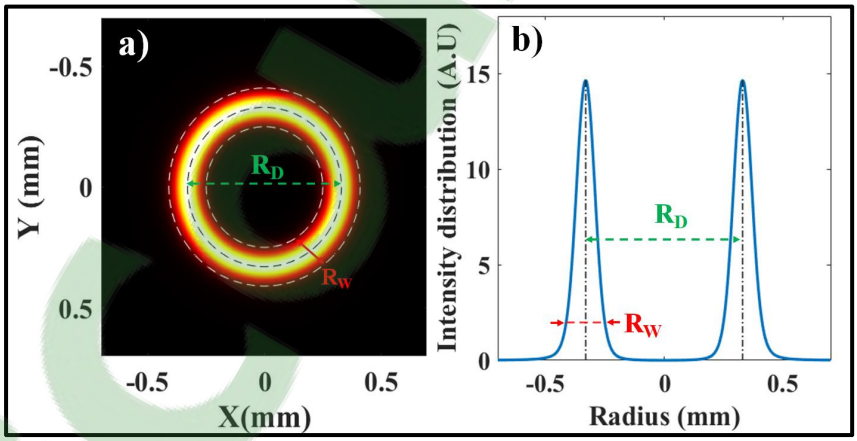

Figure 1.7 (a) Finite-element simulation of a perfect annular and its (b) azimuthal intensity profile shown with ring width R_W and ring diameter R_D parameters

Chen et al. reported an efficient technique to generate perfect vortex beam by use of a digital micro-mirror device with topological charge as large as $l = 90$ (Chen et al., 2015b). Later, Jabir et al., used the technique of Fourier transformation of the Bessel-Gauss beam to generate the perfect vortex beam by adjusting the distance between the lens and the axicon. The study of spontaneous parametric down conversion and their non-co-linear interactions using perfect vortices were reported (Jabir et al., 2016). In reference Ma et al., the method to

determine the position of the topological order of perfect vortices was proposed (Ma et al., 2017).

Furthermore, perfect vectorial vortex beams was proposed by (Li et al., 2016), where, a new class of perfect vector vortex beams whose ring diameter could be tailored irrespective of its polarization order was demonstrated. They utilized Sagnac interferometer technique to generate perfect vortex beams with elliptic and linear polarization order and experimentally demonstrated their propagation at a certain distance while maintaining their intensity profile. In 2017, Liu et al. designed Pancharatnam-Berry phase elements to demonstrate the generation of perfect vortex beam that possessed constant annular intensity profile and was equipped with polarizations that varied azimuthally (Liu et al., 2017a).

Though different techniques have been proposed towards successful generation and stable propagation of vector and vortex beams, still extensive research has to be carried out to design devices offering low loss and better isolation characteristics. There is a necessity in the characterization of these vector beams via Brillouin scattering process in the optical fiber, a nonlinear phenomenon that has invoked strong research interest recently owing to its promising applications in the domains of optical fiber communications and distributed fiber sensing.

1.6 Studies on stimulated Brillouin scattering in fiber

With the design and fabrication of specialty fibers for SDM technology, it becomes important to understand the modal properties of such fiber. Hence, characterization of these fiber utilizing phenomenon that are well understood can help in studying the properties of new SDM fibers(Minardo, Bernini et Zeni, 2014; Nikles, Thevenaz et Robert, 1997; Song et Kim, 2013). Stimulated Brillouin scattering (SBS) is a non-linear phenomenon that is implemented for various applications including the characterization of optical fiber (Li et al., 2014; Song et Kim, 2013), amplification (Gökhan, Göktaş et Sorger, 2018), and fiber sensing (Denisov, 2015; Li et al., 2015; Teng et al., 2015; Weng et al., 2015b; Xu et al., 2016). Research on

stimulated Brillouin scattering carried out over the years after their phenomenon was prefigured way back in 1922, however, it was experimentally observed only in 1964 by Chiao et al. (Chiao, Townes et Stoicheff, 1964). SBS in optical fiber results from the interaction of acoustic and optical waves that was demonstrated by Ippen and Stolen in 1972 as shown in Figure 1.8.

To obtain photonic functionalities like amplification (Olsson et Van der Ziel, 1986; Santagiustina et al., 2012), sensing (Hotate et Hasegawa, 2000; Li et al., 2014; Li, Hu et Shieh, 2013; Weng et al., 2015a; Zou, He et Hotate, 2009), optical delay lines (Li, Li et Vodhanel, 2012; Song et al., 2009), microwave photonics (Santagiustina et al., 2012) and polarization control (Thévenaz et al., 2008), SBS technology is highly is utilized. Brillouin gain spectra (BGS) are an important parameter that can offer relevant information along the length of the fiber, which includes the effective refractive index (ERI) of the modes guided by the fiber. The ERI of the guided modes of fiber are very sensitive to the temperature and strain parameters.

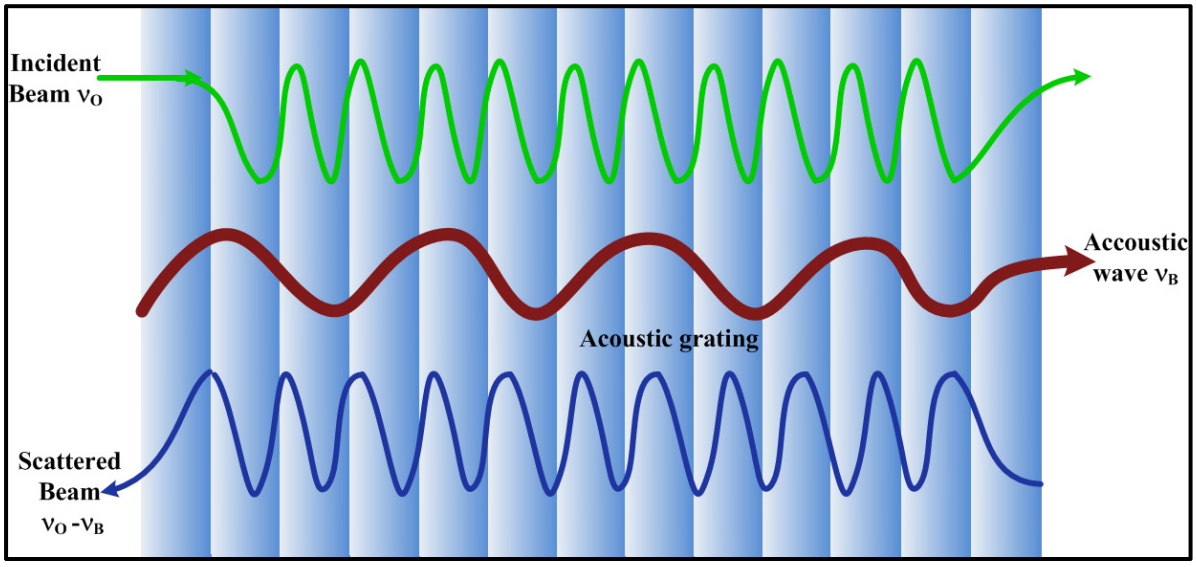

Figure 1.8 Brillouin scattering in an optical fiber resulting from an induced acoustic wave

The effect on the magnitude of BGS owing to the variation in ERI of fiber profile have also been the topic of studies (Florez et al., 2016; Li et al., 2014; Li, Hu et Shieh, 2013; Nikles,

Thevenaz et Robert, 1997; Song et Kim, 2013; Song, Kim et Kim, 2013). Brillouin gain arising from the interaction between acoustic and light waves in cylindrical waveguide geometry can be controlled on the basis of index profile design. Some of the early publications in this domain include studies by Cotter (Cotter, 1983) on SBS in single-mode fibers and Tkach et al. on spontaneous Brillouin scattering for fiber characterization in 1986 (Tkach, Chraplyvy et Derosier, 1986).

1.6.1 Stimulated Brillouin scattering techniques

Boyd proposed electrostriction and optical absorption as the two distinct mechanisms that influence the interactive index variation of the material resulting in Brillouin scattering (Boyd, 2003). SBS can allow distributed measurement as well as sensing using well-known techniques such as Brillouin optical time-domain reflectometer (BOTDR) (Nicholson et al., 2003b) or Brillouin optical time-domain analysis (BOTDA) (Nguyen et al., 2012). BOTDR technique (Xinlei, Qingxu et Wei, 2012; Zhou et al., 2013; Zhou et al., 2009; Zhou et al., 2007) is a valuable tool that is used to locate or identify the localized distributed strain in an optical fiber. The basic purpose of BOTDR technique is to diagnose the optical fiber cables enabling strain characterization and most importantly used for applications in strain and temperature measurements. This technique is a non-destructive test used for quality checking or troubleshooting of an installed fiber cable in an optical link and also for special strain and temperature environment tests. The BOTDR technique that uses Brillouin characteristics for measurement and detection principles has measured temperature error of 0.5 °C and spatial resolution of 10 m in a deployed optical fiber link of up to 80 km.

The Brillouin gain studies of standard SMF and PMF have reported in large numbers (Song et al., 2009; Song, 2011; Song et Yoon, 2010; Song et al., 2008; Teng et al., 2015; Zou, He et Hotate, 2009). However, there are only few studies reported on few-mode fiber. One of the recent studies on SBS characterization in an elliptic-core TMF reported significant Brillouin gain between the modes (Kim et Song, 2014; Li, Hu et Shieh, 2013). The Brillouin spectrum in single-mode fiber shows a Lorentzian profile. If any length is applied strain in fiber under

test, the maximum gain shifts to a different frequency. Beside the fiber birefringence, single-mode fiber possesses only single effective refractive index whereas on the basis of different effective acoustic velocities separate acoustic modes can produce different Brillouin frequency shift (BFS). Thus, Lorentzian spectral shapes peaking at different BFS are characterized on the basis of acoustic and optical mode field distributions that are spatially overlapped. In FMF, it becomes further complicated owing to the presence of numerous acousto-optic waves. The overall BGS is obtained from the optical and acoustic mode interaction travelling towards the path of the pump wave (Minardo, Bernini et Zeni, 2014). The recent studies on SBS reveal the dependency of BGS on the optical mode pairs present. A critical parameter involved in the characterization of TMF or FMF termed as intermodal beat length is measured by analyzing the effective refractive index difference between two spatial modes.

Song et al. categorized the interaction between the similar optical modes as intramodal SBS and that between dissimilar optical modes as intermodal SBS, and the BGS and gain co-efficient were determined using mode-division multiplexer (Song et Kim, 2013; Song, Kim et Kim, 2013). The magnitude of intramodal SBS gain was reported to be same or larger in comparison to the intramodal SBS gain. Determination of SBS threshold was focused in the studies of SBS in MMF which also revealed higher gain coefficient for lower-order modes than for the higher-order modes (Minardo, Bernini et Zeni, 2014). However, there are no reports on the SBS of cylindrical vector beams till date. We therefore intend to fill this void in the published literature.

Recently, SBS is being particularly utilized in the generation of localized and distributed dynamic Brillouin gratings (DBGs) (Denisov, 2015; Kim et Song, 2014; Li et al., 2014; Teng et al., 2015). Numerous DBG based applications such as high sensitive temperature and strain sensors, birefringence sensors, tunable delay lines, high resolution time-domain distributed sensors, and all-optical signal processing have been reported (Bao et Chen, 2012). To explore the process of DBG generation in optical fibers using SBS, various new techniques have been reported. One of the earliest techniques utilizing time domain analysis

of pulsed lightwave was introduced in 1989 (Horiguchi et Tateda, 1989). This technique has two scheme classifications: Brillouin optical time domain analysis (BOTDA) and Brillouin optical time domain reflectometry (BOTDR). In BOTDA, counter-propagating pump and probe configuration generates stimulated Brillouin scattering whereas, in BOTDR, a heterodyne interferometer detects the scattering. Demonstration of performance improvement and Brillouin spectrum characterization has also been carried out (Bao, Webb et Jackson, 1993). Brillouin optical correlation domain analysis (BOCDA), was another technique of interest and was studied in 1999 by a group of researchers (Hotate et Hasegawa, 2000). Through this technique, SBS was configured along a selected location of the optical fiber by adjusting the correlation between the pump and probe beams. Brillouin optical correlation domain reflectometry (BOCDR) on the basis of spontaneous Brillouin scattering is another technique proposed in 2009 (Mizuno, He et Hotate, 2009).

A novel dynamic grating technique was put forward by Song et al., using SBS in SMF, PMF and FMF revealing some promising experimental results (Song et Kim, 2013; Song et Yoon, 2010; Song et al., 2008). The distributed modal birefringence characterization in a FMF using distributed DBG was reported by Li et al., with higher spatial resolution and high accuracy (Li et al., 2014). Li et al., presented a distributed type FMF sensor with a pump-probe configuration where the temperature and strain coefficients could be measured independently for LP_{01} and LP_{11} modes (Li et al., 2015). Brillouin spectroscopic techniques have been adapted to obtain useful information about the scattering loss, the composition of fibers and the partition of optical power between the core and the cladding regions in optical fiber waveguides. The rigorous Brillouin spectrum analysis is important in order to precisely locate strain and temperature events. Different fiber types will have different Brillouin scattering properties which need to be considered in order to make accurate measurements of strain or temperature effects. Therefore, in applications like sensing utilizing special fibers like MCF, MMF or FMF (Pan, Weng et Wang, 2015), the BOTDR measurements play a very important role in order to characterize the Brillouin spectrum of the fiber.

1.7 Summary

This chapter of the thesis explained the initiation and motivation of the research work obtained from the background knowledge of earlier studies relevant to this research project. The description highlights the technological advancements that have already taken place and the research undertaken to facilitate high speed data transmission using SDM technology. The MDM seems to be a promising solution for the defined problem of capacity crunch in the upcoming telecommunication networks. Some of the early works done on mode converters are reviewed and the recent developments on FMF based devices that can act as independent information channels to use higher order guided modes, are discussed. Innovative and efficient technique employed for the characterization of fiber is reviewed in detail. Reviewing the literature has broadened the understanding on recent advancements in SDM that have benefitted domains like optical fiber sensors, apart from the domain of optical communications. To summarize, the photonic and SDM components that are proposed and demonstrated for characterizing optical fiber links, and their adoption in SDM technology have been reviewed.

The next three chapters of the thesis demonstrates the design, fabrication, characterization and experimental results of all-fiber and free space mux/demux devices utilized in the generation and characterization of CVBs in a few-mode fiber. To start with, the tunable mechanical fiber based converter is fabricated that has helped in the characterization of individual vector beams using the Brillouin scattering phenomenon. Further, the free space experimental set-up is designed and demonstrated to generate and tailor PCVBs that are demanded by some SDM fibers to increase the coupling efficiency. Finally, a simple and reliable mode converter that can support stable propagation of CVBs with high energy is demonstrated. The fabrication of such fiber-based devices has opened the possibility to create low-cost, compact and flexible mode converters in specialty few-mode fibers so as to generate CVBs and the so-called vortex beams.

CHAPTER 2

THE BRILLOUIN GAIN OF VECTOR MODES IN A FEW-MODE FIBER

P. Pradhan[a], B. Ung[b], C. Tremblay[c], D. Sengupta[d], S. LaRochelle[e] and L. Wang[f],

[a, b, c and d] Department of Electrical Engineering, École de technologie supérieure, 1100 Notre-Dame West, Montreal, Quebec, Canada H3C1K3
[e and f] Centre d'Optique, Photonique et Laser (COPL), Université Laval, Québec, QC, Canada G1V 0A6

Paper published in *Nature Scientific Reports*, April 2017

Résumé

Dans ce travail, nous démontrons pour la première fois la mesure des spectres de gain de Brillouin des modes vectoriels dans une fibre multimode en utilisant une simple technique de détection hétérodyne. Un réseau de fibres à longue période accordable est utilisé pour exciter sélectivement les modes vectoriels supportés par la fibre multimode. En outre, nous démontrons la mesure non-destructive des indices de réfraction effectifs absolus (n_{eff}) des faisceaux vectoriels avec une précision de ~10^{-4} basée sur les changements de fréquence de Brillouin enregistrés. La technique proposée représente un nouvel outil de mesure et de contrôle des faisceaux vectoriels ainsi que des modes portant un moment angulaire orbital dans les fibres optiques avec des applications potentielles dans les communications optiques de prochaine génération et les capteurs à fibres optiques multi-paramétriques.

2.1 Abstract

In this work, we demonstrate the measurement of the Brillouin gain spectra of vector modes in a few-mode fiber for the first time using a simple heterodyne detection technique. A tunable long period fiber grating is used to selectively excite the vector beam supported by the few-mode fiber. Further, we demonstrate the non-destructive measurement of the absolute effective refractive indices (n_{eff}) of vector modes with ~10^{-4} accuracy based on the acquired Brillouin frequency shifts of the modes. The proposed technique represents a new

tool for probing and controlling vector modes as well as modes carrying orbital angular momentum in optical fibers with potential applications in advanced optical communications and multi-parameter fiber-optic sensing.

2.2 Introduction

Recently, space division multiplexing (SDM) has been proposed to overcome the looming capacity crunch in conventional single-mode fibers (SMFs). In order to enable SDM in practice, many different types of specialty fibers have been devised (Richardson, Fini et Nelson, 2013). In particular, the few-mode fiber (FMF) has attracted a lot of attention due to its potential application in optical telecommunication and fiber sensing applications. Few-mode fibers are particularly promising for mode-division multiplexing (Ryf et al., 2012), where multiple information channels can be transmitted across independent spatial modes with minimum crosstalk, thereby enhancing the data carrying capacity inside a single core fiber by many folds. Moreover, recent research activities have reported promising results in the development of multi-parameter and distributed sensors based on the LP modes of FMFs (Li et al., 2015; Weng et al., 2015a; Xu et al., 2016). Both fields of application rely on harnessing the rich modal diversity in FMFs. In order to fully exploit this modal diversity, the nontrivial modal properties of the FMF must be characterized accurately. Specifically, the effective refractive indices (ERIs) of the modes and ERI differences (Δn_{eff}) between adjacent modes represent the key characteristics of FMFs that determine whether stable (i.e. low intermodal cross-talk) transmission of multiple discrete modes is possible in practice.

Several characterization methods and tools have been developed for single-mode fibers (Nikles, Thevenaz et Robert, 1997; Song, 2011) but, in the case of FMFs, new technical challenges arise due to the co-existence of multiple co-propagating modes. Some of the recent characterization techniques on FMF include the phase-shift method (Nicholson et al., 2003a), the S2 method (Nguyen et al., 2012), the time of flight method (Cheng et al., 2012), the microwave interferometric technique (Wang et al., 2014c) and the optical low-coherence interferometry method (Gabet et al., 2015). However, most of the work done on FMFs have

been limited to the measurements of the scalar LP mode groups and have so far neglected the underlying vector beam, which require delicate spectral and spatial control in order to be detected.

Vector modes in optical fibers constitute the fundamental basis set of LP modes (in the scalar approximation) as well as of modes carrying orbital angular momentum (OAM) which represent another potential avenue for SDM based communications (Willner et al., 2015). Therefore, fundamental information and control over the vector beam is critical for future SDM fiber communication links and OAM based fiber-optic sensors (Niederriter, Siemens et Gopinath, 2015). A recent characterization technique of vector beam based on permanently inscribed fiber Bragg gratings (FBGs) has been demonstrated (Wang et al., 2014b). While this technique is effective, the accuracy is limited by the perturbation induced by the refractive index modulation of the FBG, and its longitudinal spatial resolution and coverage are restricted by the length and number of FBGs present in the fiber under test.

Recent works performed on FMFs have highlighted the potential of exploiting the nonlinear stimulated Brillouin scattering in such fibers towards SDM (Song et Kim, 2013; Song, Kim et Kim, 2013) and fiber-optic sensing applications (Li, Hu et Shieh, 2013; Li et al., 2015). In this study, we report the non-destructive nonlinear characterization of vector beam in FMF – excited via a tunable long period fiber grating (LPFG) – by means of their Brillouin gain spectrum (BGS). We show how the BGS of the vector beam in FMF can be independently measured and analyzed, and how the corresponding ERIs of the vector beam can be subsequently retrieved from the data.

2.3 Experiment

The few-mode fiber used in the experiment is an inverse parabolic graded-index fiber designed to mitigate the modal crosstalk between different vector beam by ensuring large Δn_{eff} values between adjacent guided modes (Ung et al., 2014). This FMF with 3 μm core radius supports the fundamental HE_{11} (even and odd) mode, the TE_{01}, HE_{21} (even and odd),

TM_{01}, EH_{11} (even and odd), and HE_{31} (even and odd) vector beam in the C-band. We note that, in the scalar approximation, the LP_{11} mode group is created by a pairwise combination of the TE_{01}, HE_{21} (even and odd) or TM_{01} modes.

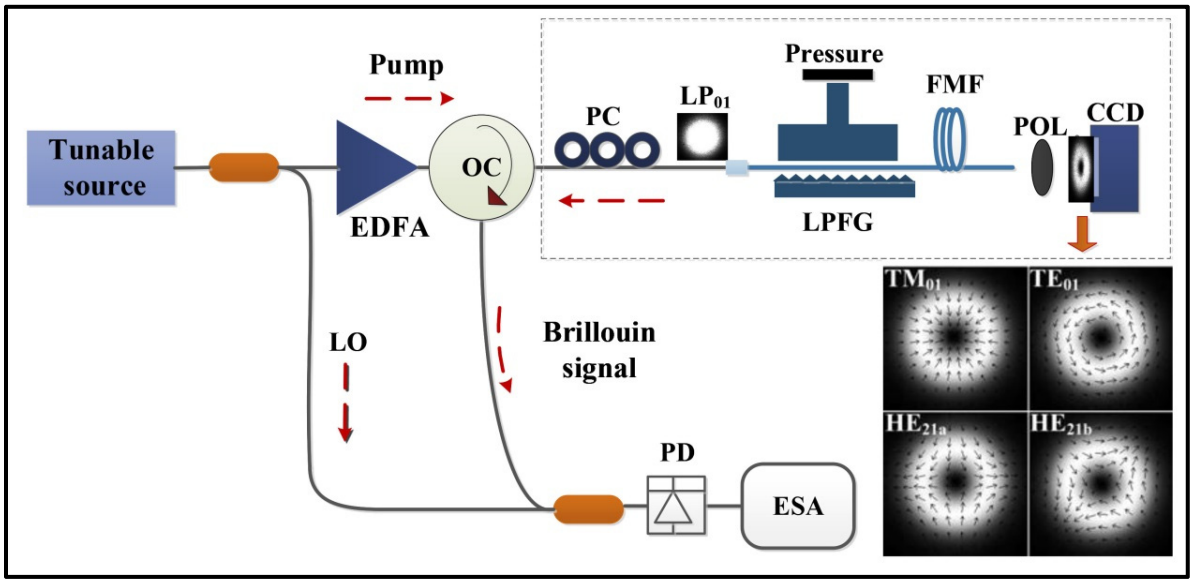

Figure 2.1 Experimental setup for the Brillouin gain spectra measurement of vector beam. (PC: polarization controller; LPFG: long period fiber grating; LO: local oscillator; FMF: few-mode fiber; POL: linear polariser; PD: photodetector; ESA: Electrical spectrum analyzer; EDFA: Erbium doped fiber amplifier; OC: optical circulator)
Inset: Electric field representation (arrows) of the TM_{01}, TE_{01}, HE_{21a} and HE_{21b} (LP_{11} mode group) calculated using FEM
Adapted from Ung et al. (2014, p.18047)

At 1550 nm, the FMF also supports up to 6 OAM modes through coherent combination of the degenerate high-order hybrid modes (HE_{21}, EH_{11}, HE_{31}). The ERIs of all the vector beam can be calculated by importing the measured refractive index profile (RIP) in a full-vector finite-element method (FEM) mode solver. The minimum Δn_{eff} value between the vector components (TE_{01}, HE_{21}, TM_{01}) of the LP_{11} group for this FMF is expected to be in the range of 2.9×10^{-4} and 3.7×10^{-4}. This large modal separation allows the stable propagation of these vector beams within the FMF.

On the other hand, the proximity of the EH_{11}, HE_{31} modes to modal cut-off induces very large modal losses (Ung et al., 2014) such that we can neglect the latter higher-order vector

beam. A tunable mechanical LPFG that efficiently excites the TE_{01}, HE_{21} and TM_{01} mode has been designed and fabricated (Pradhan et al., 2015). The LPFG is fabricated with a nominal grating period of Λ_O = 200 μm. This grating period can further be tuned by positioning the fiber at specific angles θ with respect to the grating lines. The angle of the grating can thus be varied from 0° (Λ_O = 200 μm) to 26°, corresponding to a maximum grating period of Λ = 222 μm. Strong coupling of the power from the fundamental HE_{11} towards a co-propagating higher-order mode occurs when the phase matching condition $\lambda = \Lambda \cdot \Delta n_{eff}$ is satisfied for a given vector mode, where λ is the resonant coupling wavelength, Δn_{eff} is the ERI difference between the fundamental and high-order vector beam, and $\lambda = \Lambda_O / \cos\theta$, is the designed grating period.

The experimental setup for measuring the BGS of different vector beam is illustrated in Figure 2.1. The upper branch of the setup (Figure 2.1 area inside dotted box) shows the arrangement utilized for the excitation and detection of different vector beam in the FMF. In the arrangement, the output of the SMF is spliced into the input of FMF after which the fundamental mode (HE_{11} or LP_{01}) is converted into the desired high-order vector mode by the LPFG. The latter scheme is reciprocal and thus also works in the opposite direction: any reflected power from vector beam in the FMF is converted back to the fundamental mode by the LPFG.

Polarization controllers and mode strippers are inserted to maximize the conversion efficiency of the LPFG. The average power conversion efficiency from the fundamental mode to each of the three different vector beam using LPFG is measured to be 98.4%. The end facet of the FMF is projected onto a CCD camera in order to dynamically monitor the excited modes. The images of different vector beam (in the LP_{11} mode group) exhibit a similar doughnut shaped intensity profile as shown in the inset of Figure 2.1. To discriminate and identify each vector mode, a polarizer (i.e. analyzer) is placed in front of the CCD camera and rotated at different angles as illustrated in Figure 2.2.

In the experimental configuration (Figure 2.1), a tunable laser with a 100-kHz linewidth is used as the light source. The 1550-nm CW light is split in two directions using a 50:50 single-mode fiber coupler. The upper path of the pump beam is first amplified to 25 dBm by an erbium doped fiber amplifier (EDFA) before being fed to the 50 m long FMF via an optical circulator (OC). The LPFG acts as the mode-converting device between the incident fundamental mode and the desired higher-order vector beam in the FMF (and vice-versa), as explained earlier.

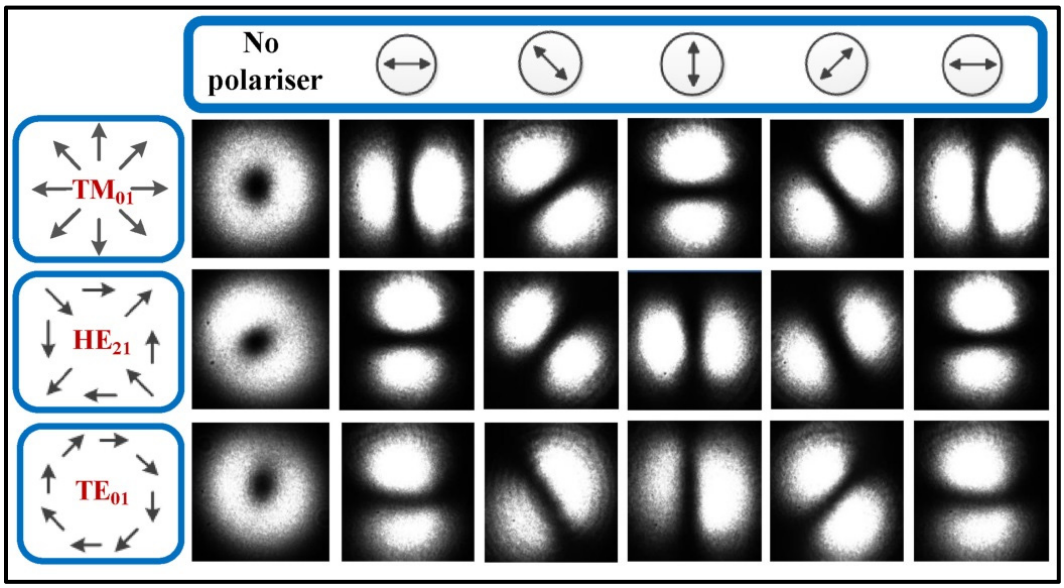

Figure 2.2 Identification of the TM_{01}, HE_{21} and TE_{01} vector beam via a linear polariser

2.3.1 Brillouin gain spectra

The reflected beam from the FMF contains a component at the same optical frequency as that of the incident beam (ν_0) and includes a slightly red-shifted spectral component owing to nonlinear Brillouin scattering. The Brillouin reflected signal (i.e. Stokes signal) – of frequency $\nu_0 - \nu_B$ where (ν_B) is the Brillouin frequency shift – is then optically mixed with the lower path beam (acting as a local oscillator) and the corresponding optical beat signal is measured by a fast photodiode and electrical spectrum analyzer (ESA). Figure 2.3 shows the Brillouin spectrum obtained by launching a fundamental mode into the FMF and analyzing the backscattered Stokes signal trace using the ESA.

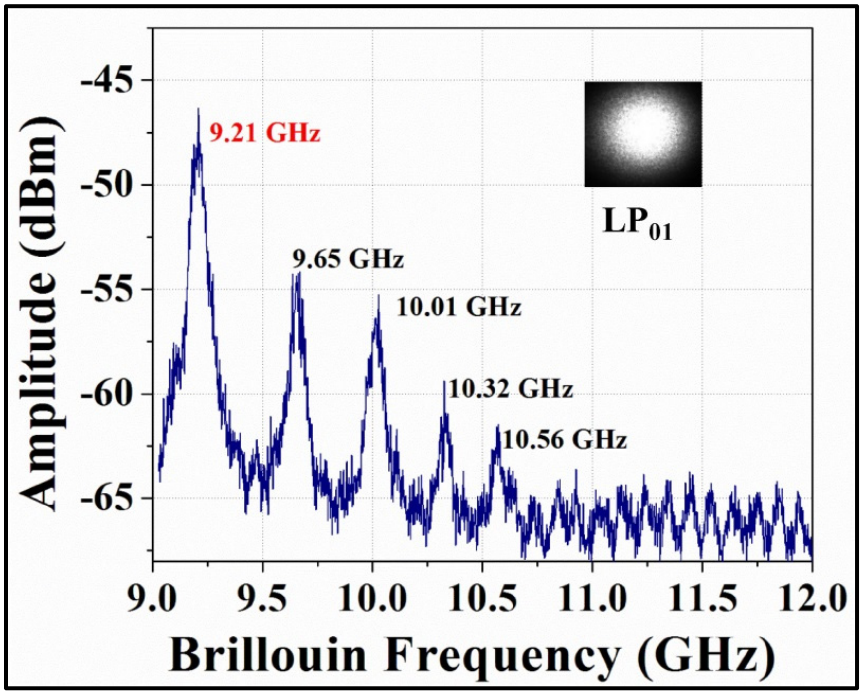

Figure 2.3 Full Brillouin gain spectra of the fundamental LP_{01} mode of FMF at 1550nm

The multiple peaks located at 9.21, 9.65, 10.01, 10.32 and 10.56 GHz correspond to the Brillouin scattering driven by various higher-order acoustic modes comprising both longitudinal and shear acoustic wave components (Xu et al., 2016). In this study, our analysis focuses on the fundamental acoustic mode (centered around 9.21 GHz) as it is the dominant peak with the strongest Brillouin scattering response. Nonetheless, the methodology presented hereafter could be extended to other acoustic modes of interest.

2.4 Results and Discussion

The measured Brillouin gain spectra for the fundamental LP_{01} optical mode and the vector components of the LP_{11} mode group are presented in Figure 2.4. To increase the signal to noise ratio of the BGS signal of each vector mode, ten sweeps were averaged before applying a Gaussian curve fit (Villafranca et al., 2005; Yeniay, Delavaux et Toulouse, 2002).

Although the excitation of all these guided modes is possible at 1550 nm if the LPFG is set at the proper angle, the measured BGS shown in Figure 2.4 were obtained at wavelengths slightly offset from the target 1550 nm wavelength (with the exception of the fundamental mode) due to imperfect fiber alignment on top of the LPFG's grating lines when the latter is set at a non-zero angle.

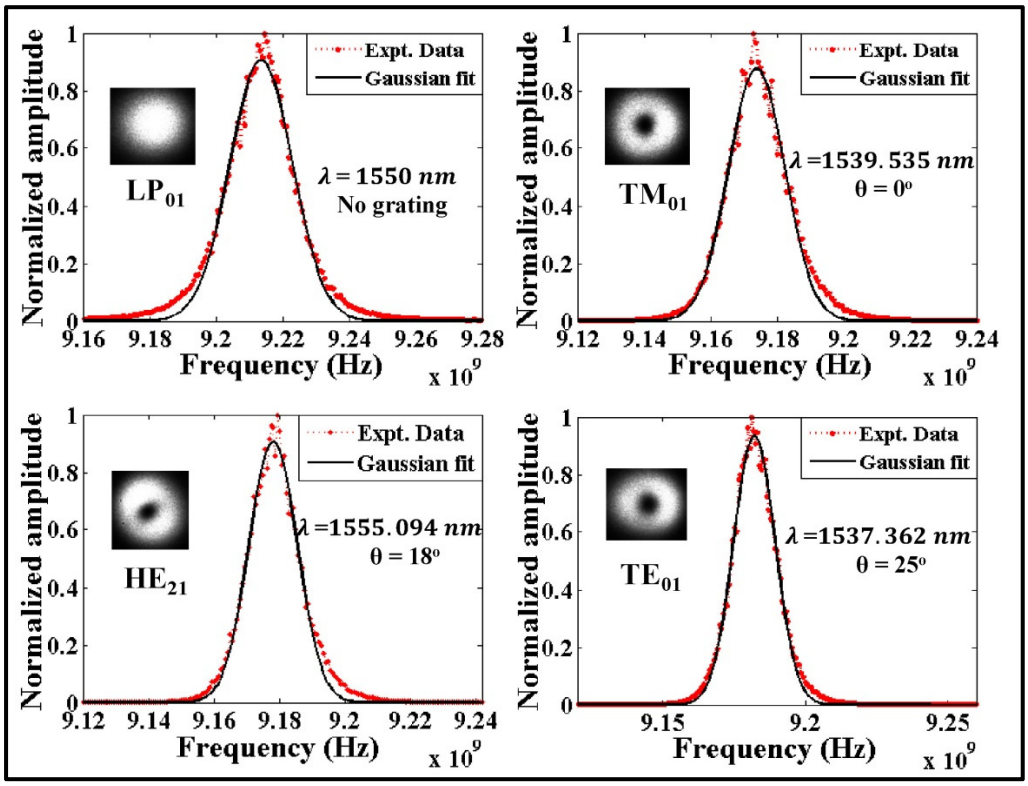

Figure 2.4 Measured Brillouin gain spectra for fundamental and high-order vector beam, and corresponding Gaussian fit curves

As a result, when pressure was applied on the fiber placed on top of the angled grating, it led to a non-uniformity of the grating period at some points along the ensuing LPFG. Therefore, in order to maximize the coupling efficiency of different vector beam, the phase-matching point was achieved by fine-tuning the resonance wavelength. Hence, in order to compare all BGS results at a common reference point, all the measurements (that were obtained at different wavelengths) were subsequently normalized to the same 1550 nm wavelength through a procedure detailed below.

2.4.1 Wavelength normalization of Brillouin gain spectra at 1550 nm

The variation of Brillouin frequency shift (BFS) ν_B for acoustic modes in terms of acoustic velocity V_a and optical modes with ERIs (n_{eff}) can be expressed as

$$\nu_B = \frac{2n_{eff}}{\lambda} V_a \tag{2.1}$$

where λ is the pump wavelength. The value of acoustic velocity (V_a) for germania-doped silica glass can be obtained through linear interpolation of the data based on the Makishima–Mackenzie model (Dragic, 2010). In this FMF, the maximum refractive index difference of - Δn ≈ 0.0442 at the core-cladding interface thus corresponds to a velocity of 4876 m/s for the fundamental longitudinal acoustic mode (Xu et al., 2016).

As seen from Eq. (2.1), using the latter value for V_a and the measured ν_B , we can deduce the n_{eff} values of the guided modes based on their specific BFS values at a given wavelength λ. Now, in order to retrieve the $n_{eff}{}'$ values of the TE_{01}, HE_{21} and TM_{01} modes at a common 1550 nm wavelength, the chromatic dispersion of their respective n_{eff} values [Figure 2.5] was taken into consideration via:

$$n_{eff}{}' = n_{eff} + \left(\frac{dn_{eff}}{d\lambda}\right)\Delta\lambda \tag{2.2}$$

Using Eq. (2.2) we are thus in a position to normalize the measurement of the BFS of different vector beam performed at different resonance wavelengths (λ) to the new wavelength (λ′ = 1550 nm) shifted by Δλ = (λ′ − λ).

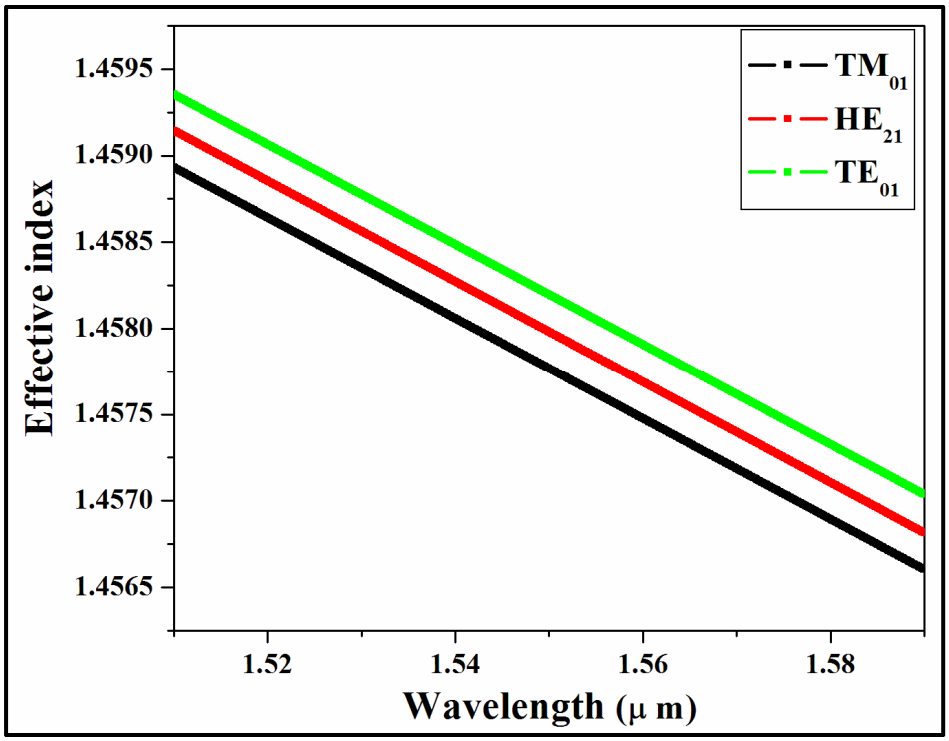

Figure 2.5 ERIs of the vector beam in the LP_{11} group calculated via FEM simulations based on the measured RIP of the FMF

The Brillouin frequency shift ν_B of the BGS measured for the fundamental and high-order vector beam in the 50 m FMF are summarized in Table 2.1. It is notable that the BFS of the vector components of the LP_{11} mode group are separated by small but non-negligible shifts that enable the independent characterization of these vector beams. Subsequently, the effective refractive indices of the vector beam, as well as their corresponding separations (Δn_{eff}), were extracted from the ν_B measurements using Eq. (2.1).

We note that the modal separations calculated via the BGS are almost two times larger than prior measurements (Ung et al., 2014; Wang et al., 2014b). We attribute these discrepancies to two main factors: a) the longitudinal variations in the fiber's refractive index profile (whose local effect on the fiber's n_{eff} values are accentuated by the very large core-cladding index contrast), and to its non-negligible birefringence which is capable of inducing significant deviations ($>10^{-4}$) in the ERI value of a vector mode (Wang et al., 2016),

Table 2.1 Characteristics of the Brillouin gain spectra of vector beam

Mode	**Brillouin frequency shift ν_B (GHz)**	**Effective refractive index n_{eff}**	**Modal separation Δn_{eff}**	**Brillouin gain linewidth $\Delta\nu_B$ (MHz)**	**Brillouin gain threshold (dBm)**
LP_{01}	9.2136 ± 0.0003	$1.46443\pm4\times10^{-5}$	$(5.0 \pm 0.1) \times 10^{-3}$	23.54±0.32	14.4
TE_{01}	9.1820 ± 0.0003	$1.45942\pm5\times10^{-5}$	$(5.9 \pm 0.9) \times 10^{-4}$	18.02±0.69	21.0
HE_{21}	9.1783 ± 0.0003	$1.45882\pm5\times10^{-5}$	$(6.5 \pm 0.7) \times 10^{-4}$	18.83±0.40	21.3
TM_{01}	9.1742 ± 0.0003	$1.45816\pm5\times10^{-5}$		21.01±0.36	18.3

b) the presence of a double-peak structure at the crest of the measured BGS (as shown in Figure 2.4) – ostensibly related to polarization mode dispersion (Wang et al., 2016) – introduces an unavoidable level of uncertainty in the curve fitting process. In fact, the double-peak is characterized by a spectral half-width of ~2 MHz which translates (via Eq. (2.1)) into a maximum error of ± 3.2×10^{-4} in the corresponding effective index value. The latter magnitude of the error allows to bring into agreement our results in Table 2.1 based on the BFS, with earlier reported results performed on the same fiber but via other methods (Li, Hu et Shieh, 2013; Wang et al., 2014b).

2.4.2 Brillouin threshold measurements

Finally, we measured the Brillouin threshold for each vector mode by varying the pump power from 9 dBm to 25 dBm. Plots of the Stokes signal power as a function of pump input power is presented in Figure 2.6. The Brillouin threshold of the vector beam are higher than that of the fundamental LP_{01} mode, and this difference is +4 dB for TM_{01} and +7 dB for HE_{21} and TE_{01}. We suspect that the lower Brillouin threshold observed for the TM_{01} mode (compared to the TE_{01} and HE_{21} modes) can be explained by a polarization-mode-dependent photon-phonon coupling efficiency arising from the interplay of the different in-homogeneously polarized vector beam with the specific refractive-index profile of the fiber supporting the photo-acoustic interactions (Florez et al., 2016; Van Deventer et Boot, 1994).

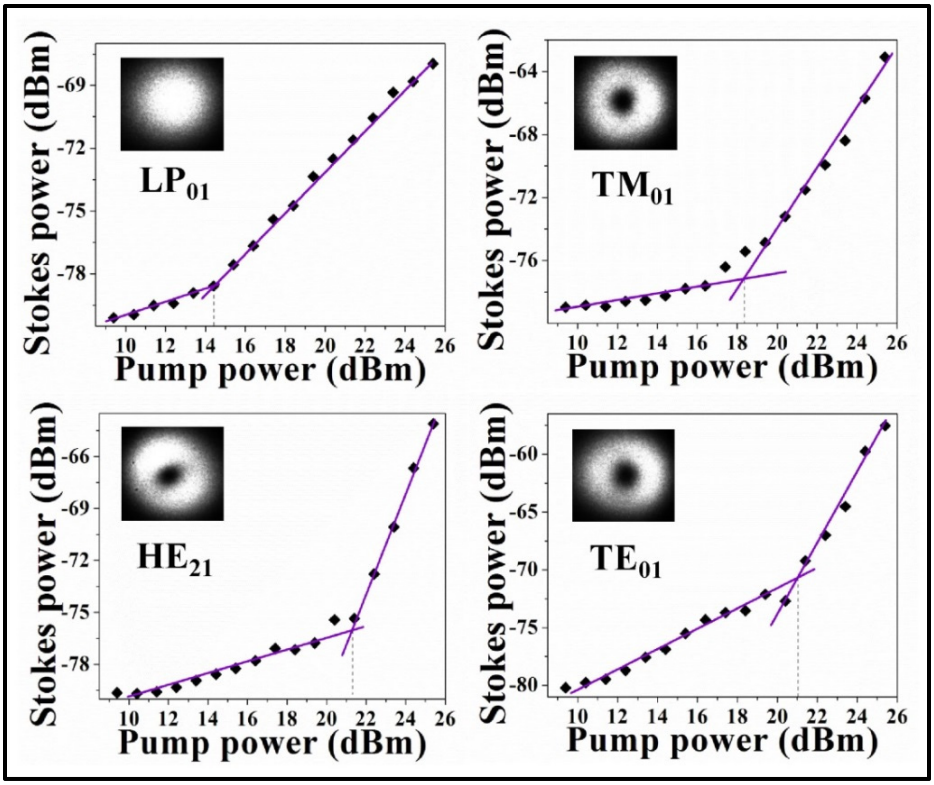

Figure 2.6 Brillouin threshold power of the LP_{01}, TM_{01}, HE_{21} and TE_{01} modes in the FMF

2.5 Conclusion

Measurement of the Brillouin gain spectra of the vector beam in a FMF has been demonstrated for the first time using a simple heterodyne detection technique. Based on the measured Brillouin frequency shifts, we were able to extract the effective refractive indices of the vector beam in the FMF in a completely non-destructive manner. We predict that this new characterization method of individual vector beam will have an impact in both light wave and fiber-optic sensing applications, which currently mostly rely on the scalar LP modes. Moreover, the ability of some specialty FMFs to lift the degeneracy of higher-order vector beam can be exploited in optical sensing (instead of their coupled LP modes counterpart), thereby bringing a larger number of independent states towards multi-parameter sensing. Because OAM mode-division multiplexing depends on the precise control of vector

modes, it is also expected that the proposed method will help in the remote and non-destructive modal diagnostic of OAM fibers and their design optimization towards stable OAM modes transmission or in narrow-linewidth Brillouin FMF lasers.

2.6 Acknowledgements

This work was supported by the Natural Sciences and Engineering Research Council of Canada (NSERC) and the FRQNT Strategic photonic cluster: Center for Optics, Photonics and Lasers (COPL).

2.7 Methods

Long period fiber grating as a mode converter: The LPFG was devised using 200 μm diameter steel wires placed on top of a rectangular aluminum block (6 cm long and 4 cm wide). The wire diameter determines both the height and nominal pitch Λ_O of the grating (Pradhan et al., 2015). As seen in Figure 2.7, the bare fiber was placed at varying angles θ with respect to the grating in order to excite individual vector beam. The angles calculated to excite TM_{01}, HE_{21} and TE_{01} were 0, 18 and 25 degrees respectively. The vector beam generated using LPFG were found to be stable over time and their modal purities (in dB) were calculated using the procedure outlined in ref. (Bozinovic, Kristensen et Ramachandran, 2011) : 22.5 dB, 19.7 dB and 18.8 dB for the TM_{01}, HE_{21} and TE_{01} modes respectively. The conversion efficiency of each vector mode was calculated by measuring the power transmitted at the output end of the fiber before and after the LPFG was used. Firstly, the power P_1 was measured at the output end of the fiber without the LPFG.

Then power P_2 was measured after the vector mode generation when the LPFG was applied. The calculation of corresponding mode conversion efficiency in dB was taken from (Wu et al., 2012)

$$\eta_{dB} = 10\log_{10}\left(\frac{P_1 - P_2}{P_1}\right) \tag{2.3}$$

Subsequently, the conversion efficiency in terms of percentage is given by

$$\eta_{\%} = \left(1 - 10^{\frac{\eta_{dB}}{10}}\right) \text{ X } 100\% \tag{2.4}$$

Proper identification of vector beam was ensured by using the polarizer in front of the CCD camera (see Figure 2.2) before recording measurements.

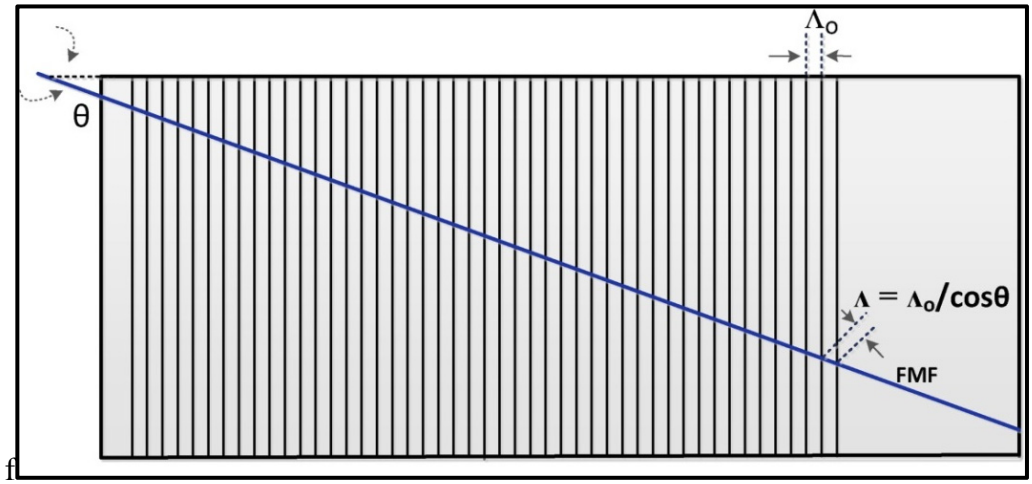

Figure 2.7 Positioning of the fiber at different angles w.r.t. LPFG (top view with angle θ) to vary the period

CHAPTER 3

GENERATION OF PERFECT CYLINDRICAL VECTOR BEAMS WITH COMPLETE CONTROL OVER THE RING WIDTH AND RING DIAMETER

P. Pradhan[a], B. Ung[b] and M. Sharma[c],

[a, b and c] Department of Electrical Engineering, École de technologie supérieure, 1100 Notre-Dame West, Montreal, Quebec, Canada, H3C1K3

Paper published in *IEEE Photonics Journal*, January 2018

Résumé

Nous proposons la génération de faisceaux vectoriels cylindriques parfaits de haute pureté (PCVB) en utilisant la transformation de Fourier des faisceaux vectoriels de Bessel-Gauss. La démonstration des PCVB est réalisée par une méthode interférométrique utilisant un modulateur spatial de lumière qui permet un contrôle totalement indépendant du diamètre de l'anneau (R_D) et de la largeur de l'anneau (R_W) du PCVB. Le schéma proposé permet de générer différents types de faisceaux vectoriels cylindriques avec des dimensions transversales précises définies par l'utilisateur. Le contrôle dynamique de la largeur et du diamètre de l'anneau ainsi que le type de PCVB souhaité est démontré de manière théorique et expérimentale. La configuration expérimentale proposée peut non seulement être employée dans la génération de PCVB arbitraire, mais également dans celle des faisceaux vortex parfaits. La capacité de générer des faisceaux vectoriels cylindriques et des faisceaux vortex parfaits a des implications pour l'excitation efficace de modes optiques exotiques dans les fibres spéciales, dans le domaine des pinces optiques ainsi que pour la microscopie à super résolution

3.1 Abstract

We propose the generation of high-purity perfect cylindrical vector beams (PCVB) using the Fourier transformation of Bessel–Gauss vector beams. The demonstration of PCVBs is

implemented via an interferometric method employing a spatial light modulator that allows a fully independent control of the ring diameter (R_D) and ring width (R_W) of the PCVB. The proposed scheme enables to generate different types of cylindrical vector beams with precise user-defined transverse dimensions. The dynamic control of the ring width, ring diameter, and the specific type of PCVBs desired is theoretically as well as experimentally demonstrated. The proposed experimental setup can not only be employed in the generation of arbitrary PCVB, but also in perfect vortex beams. The ability to generate fully tailorable cylindrical vector beams and vortex beams has implications for the efficient launch of exotic optical modes in specialty fibers, in the field of optical tweezers as well as for super resolution microscopy.

3.2 Introduction

There is a burgeoning transformation in the optics and photonics world, which so far had been driven by Gaussian light beams. Increasingly, scientists and engineers are finding new applications that benefit from a beam of light whose intensity profile takes the shape of a single doughnut ring(Chen et al., 2015b; Porfirev, Ustinov et Khonina, 2016; Zhan, 2009). In particular, the so-called cylindrical vector beams (CVBs) with radial and azimuthal distribution of polarization exhibit unique properties when focused, which provide distinctive light-matter interactions compared to conventional (Gaussian-like) beams with homogeneous polarization (Bomzon et al., 2002; Milione et al., 2015). For example, a radially polarized doughnut shaped beam enables a significantly improved imaging resolution by providing a symmetric and high numerical aperture focus (Dorn, Quabis et Leuchs, 2003; Youngworth et Brown, 2000). More recently, CVBs have shown to enhance the quality and control over the laser processing of materials (Duocastella et Arnold, 2012). Furthermore, CVBs have promising applications in optical micro-manipulation (Kozawa et Sato, 2010), super-resolution imaging (Kozawa et Sato, 2015; Török et Munro, 2004; Yu et al., 2016) and fiber optic transmission of exotic optical states (Brunet et al., 2014; Vaity et al., 2014). These emerging applications of CVBs, both in free space optics as well as in fiber optics, have

reached a threshold where further developments will require a greater control over the precise intensity profiles of the CVBs.

Precise control over the ring diameter and ring width of vortex beams (i.e. beams carrying orbital angular momentum) was recently achieved through the generation of perfect vortex beams, as demonstrated by a number of research groups (Chen et al., 2013a; Chen et al., 2015b; Jabir et al., 2016; Li et al., 2016; Ma et al., 2017; Ostrovsky, Rickenstorff-Parrao et Arrizón, 2013). These recent works report the ability to maintain the dimensions of the beam intensity pattern irrespective of their topological charge (l). Furthermore, the reported new class of perfect vector vortex beams has been demonstrated with tailorable ring diameter irrespective to the polarization order. Still to the best of our knowledge, the independent control of the ring diameter and ring width in perfect cylindrical vector beams (PCVB) has not yet been demonstrated in its entirety (Fu, Wang et Gao, 2016; Karahroudi et al., 2017; Liu et al., 2017b; Wang et al., 2017d).

So far, efforts towards the generation of PCVBs that would enable one to fully tailor the intensity profile of the CVBs of interest have yielded PCVBs with tunable ring diameter only that were of limited purity (Fu, Wang et Gao, 2016; Liu et al., 2017a; Wang et al., 2017d) (showing either residual light intensity in the beams center or significant intensity fringing) via a method of limited flexibility due to the use of static optical elements (Liu et al., 2017a). In this work, we demonstrate the generation of arbitrary PCVBs whose transverse intensity profile (i.e. ring width and ring diameter) can be independently and easily controlled via an iris and a diffractive phase mask implemented on a programmable spatial light modulator (SLM). The proposed method is highly adaptable as it can be used to generate any type of PCVB as well as any topological orders of perfect vortex beams, using the same experimental setup. Our experimental results are supported by a rigorous theoretical framework as well as full-vector finite-element simulations that are in agreement with theory and results.

3.3 Theory

Perfect cylindrical vector beams are here generated by the interference of two coherent sources: a left and a right circularly polarized beam stemming from the Fourier transformation of Bessel beams. The experimental formulation for the Fourier transform of an ideal Bessel function is not amenable in practice. Therefore, the Fourier transformation of the closely related Bessel-Gauss beams has been widely used instead in experiments. The Bessel-Gauss beam equation is mathematically written as (Vaity et Rusch, 2015)

$$E_{BG}(\rho,\varphi) = J_l(k_r\rho)\exp(il\varphi)\exp\left(\frac{-\rho^2}{w_g^2}\right) \tag{3.1}$$

Where (ρ,φ) are the polar co-ordinate system, J_l is the l^{th} order Bessel function of first kind, k_r is the radial wave vector, *l* is the topological charge of beam and w_g denotes the beam waist of the input Gaussian beam used to form the Bessel-Gauss beam.

In the case of the first circularly polarized Bessel-Gauss beam, the *x* and *y* *E*-field components transforms into a vector field given by (Maurer et al., 2007)

$$\vec{E}_{BG1}(\rho,\varphi,t) = J_l(k_r\rho)\exp\left(\frac{-\rho^2}{w_g^2}\right)\begin{pmatrix}\exp(il\varphi)\cos(\omega t)\\ \exp(il\varphi)\sin(\omega t)\end{pmatrix} \tag{3.2}$$

Likewise, the second circularly polarized Bessel-Gauss beam of opposite handedness and topological charge *l* can be written as

$$\vec{E}_{BG2}(\rho,\varphi,t) = J_l(k_r\rho)\exp\left(\frac{-\rho^2}{w_g^2}\right)\begin{pmatrix}\exp(-il\varphi)\cos(\omega t)\\ -\exp(-il\varphi)\sin(\omega t)\end{pmatrix} \tag{3.3}$$

The coherent superposition of these two opposite circularly polarized light beams thus yields a CVB with a Bessel-Gauss beam profile:

$$\vec{E}_{BG}(\rho,\varphi,t) \;= 2 * J_l(k_r\rho)\exp\left(\frac{-\rho^2}{w_g^2}\right)\begin{pmatrix}\cos(l\varphi)\cos(\omega t)\\ \sin(l\varphi)\sin(\omega t)\end{pmatrix} \tag{3.4}$$

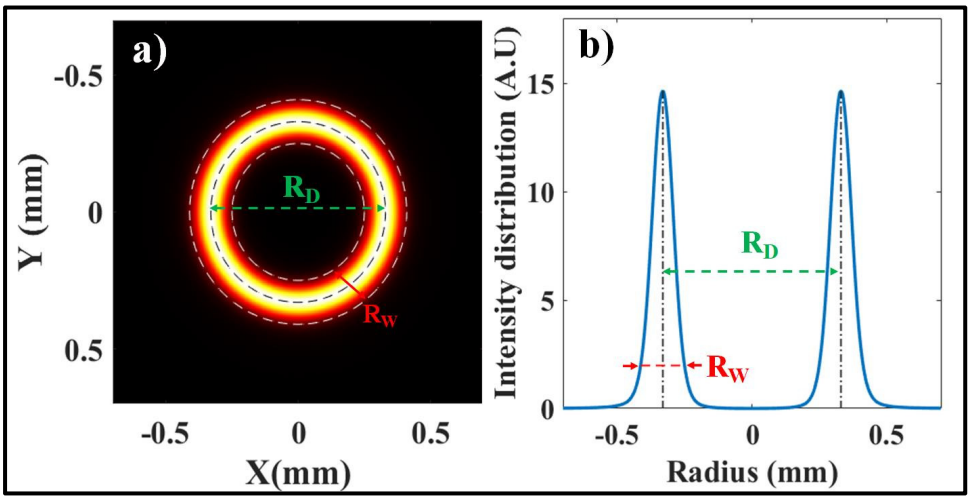

Figure 3.1 (a) Finite-element simulation of a perfect cylindrical vector beam and its (b) radial intensity profile shown with ring width R_W and ring diameter R_D parameters

The latter CVB is passed through a Fourier lens transformation that converts the CVB into the desired PCVB, which can be written as

$$\vec{E}_{BG}(R,\theta,t) \;= 2\cdot i^{l-1}\frac{w_g}{w_0}\exp\left(-\frac{R^2+R_r^2}{w_0^2}\right)I_l\left(\frac{2RR_r}{w_0^2}\right)\begin{pmatrix}\cos(l\theta+\emptyset)\cos(\omega t)\\ \sin(l\theta+\emptyset)\sin(\omega t)\end{pmatrix} \tag{3.5}$$

where $R = (\rho, \emptyset)$ is a shorthand notation for the polar coordinates, I_l is the l^{th} order modified Bessel function of first kind, $\emptyset$ is an offset phase added to tailor the relative phase between the two beams with opposite topological charges, $R_W = 2w_0$ denotes the "ring width" of PCVB (as shown in Figure 3.1) where $w_0 = \frac{2f}{kw_g}$ is the beam waist of the input Gaussian beam at focus, while the "ring radius" $R_r = \frac{R_D}{2}$ is governed by:

$$R_r = f\cdot\sin\big((n-1)\alpha\big) = k_r\, f\,/k \tag{3.6}$$

where n is the refractive index of the axicon material, α denotes the base angle of the axicon that is used to tune the ring radius of the PCVB, while $k = \sqrt{k_r^2 + k_z^2}$ and k_z respectively denote the total and longitudinal wave vectors. We note that a detailed description of the role and definition of the axicon parameter is given in Appendix A at the end of the paper. For large values of R_r at the Fourier plane, w_0 becomes small and the modified Bessel function can be approximated as

$$I_l\left(\frac{2RR_r}{w_0^2}\right) = \exp\left(\frac{2RR_r}{w_0^2}\right) \tag{3.7}$$

Hence the expression of the Fourier transformed CVB in Eq. (3.5) can be rewritten as

$$\vec{E}(R,\theta,t) = E_0 \exp\left(-\frac{(R-R_r)^2}{w_0^2}\right)\begin{pmatrix}\cos(l\theta+\emptyset)\cos(\omega t)\\ \sin(l\theta+\emptyset)\sin(\omega t)\end{pmatrix} \tag{3.8}$$

where we defined $E_0 = 2\cdot i^{l-1}\frac{w_g}{w_0}$. Further, the propagating PCVB is written as

$$\vec{E}(R,\theta,z,t) = E_0 \exp\left(-\frac{(R-R_r)^2}{w_0^2}\right)\exp\left(ikz - ik\left(\frac{R^2+{R_r}^2}{2z}\right)\right)\begin{pmatrix}\cos(l\theta+\emptyset)\cos(\omega t)\\ \sin(l\theta+\emptyset)\sin(\omega t)\end{pmatrix} \tag{3.9}$$

Finally, when the above equation is evaluated at the focal plane of the Fourier lens ($z = f$) it simplifies as

$$\vec{E}(R,\theta,f,t) = E_1 \exp\left(-\frac{(R-R_r)^2}{w_0^2}\right)\exp\left(-ik\frac{R^2+{R_r}^2}{2f}\right)\begin{pmatrix}\cos(l\theta+\emptyset)\cos(\omega t)\\ \sin(l\theta+\emptyset)\sin(\omega t)\end{pmatrix} \tag{3.10}$$

Where $E_1 = E_0 e^{(ikf)}$. Equation (3.10) describes the complex *E*-field amplitude of the PCVB at the focal plane of the Fourier transform lens. This equation is useful for guiding the experimental realization of PCVBs and to analyze the results. By controlling the input beam waist w_g one can tune the ring width (R_W) of the PCVB. Similarly, the ring diameter (R_D)

can be independently controlled by varying the radial wavevector K_r that is related to the axicon parameter in (3.6) and (3.12).

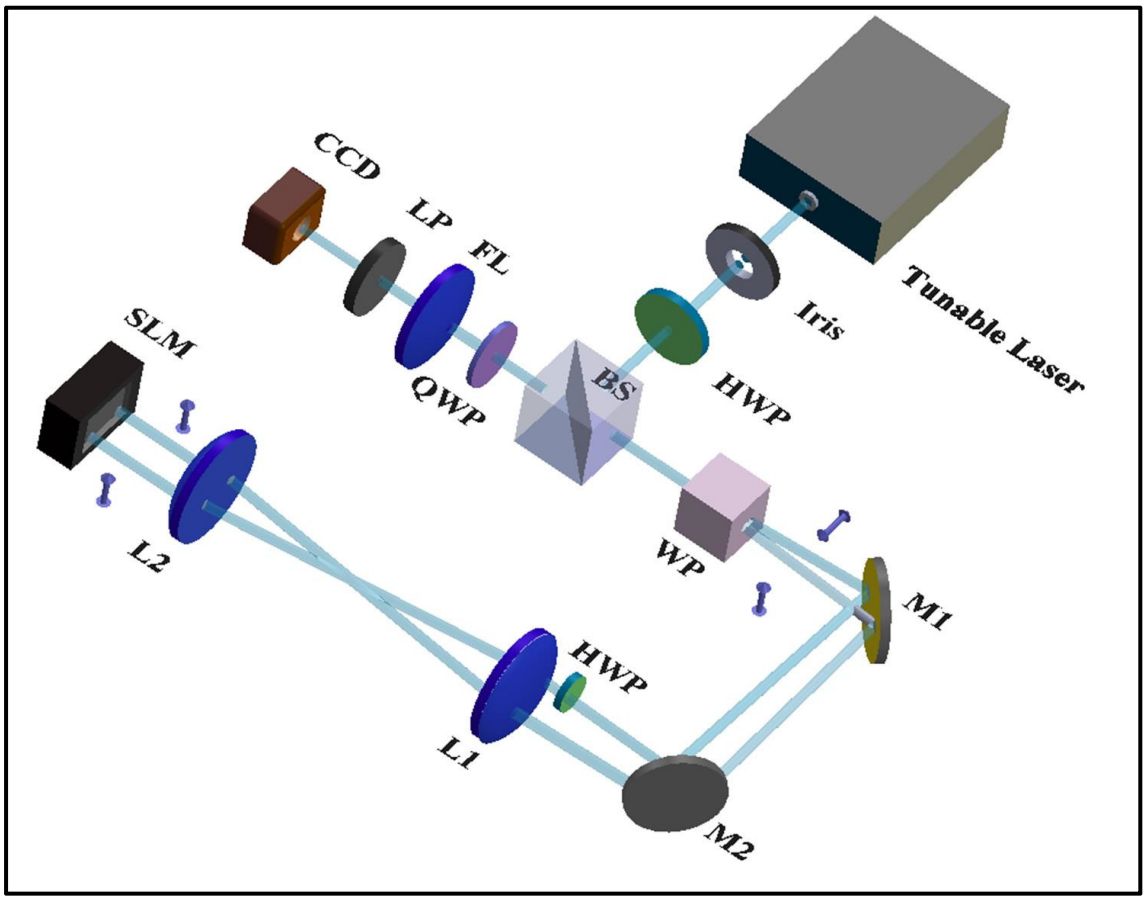

Figure 3.2 Experimental setup for the generation of PCVB incorporating HWP: half wave plate, BS: beam splitter, WP: Wollaston prism, mirror (M1, M2), lenses (L1, L2), SLM: spatial light modulator, LP: linear polarizer, QWP: quarter-wave plate, FL-Fourier lens and variable iris diaphragm

3.4 Experimental Setup

The experimental setup for the generation of PCVB is based on a common-path interferometric scheme and a spatial light modulator (SLM), as is schematically depicted in Figure 3.2. The linearly polarized input Gaussian beam from the tunable laser source at 1550 nm is collimated to a 3 mm diameter beam using an objective lens. This collimated beam is allowed to pass through an iris to adjust the incident beam diameter. A first half-wave plate

(HWP) is placed before a 50:50 non-polarizing beam splitter (BS) to ensure that the linearly polarized beam is at a 45◦ angle with respect to the plane of incidence. The Wollaston prism (WP) splits the input Gaussian beam into two beams of vertical and horizontal polarizations diverging at an angle of 1.3◦.

The horizontally polarized beam subsequently passes through a second HWP to make it vertically polarized in order to match the polarization dependence of the phase-only SLM. Further, a two-lens arrangement (L1 and L2) is employed to collimate the diverging beams before they interact with the phase masks digitally imprinted on the SLM. A blazed grating phase mask was designed using a homemade Matlab script and numerically transferred to the SLM in real-time. Henceforth, the two back-diffracted beams from the reflective SLM travels back through the same arrangement of lenses and prisms so that they recombine into a single coherent beam. The interference of the two orthogonally linearly polarized beams with opposite topological charges results in the formation of a vectorial beam exhibiting spatially inhomogeneous polarization. The role of the quarter-wave plate (QWP) is to convert the two orthogonally linearly polarized beams into left and right circularly polarized beams, respectively.

3.4.1 Role of spatial light modulator

The generation of different types of CVBs actually depends on the relative phase difference (φ) imparted by the phase mask of the SLM. The Fourier lens (FL) transforms the field distribution of the diffracted beams so as to generate a single PCVB at the focus. Finally, a CCD camera captures the intensity profile of the generated PCVB.

The screen of the reflective phase-only SLM (1920 × 1152 pixels) was divided into two equal halves, each addressing a different incoming beam, so as to produce two 1st-order diffracted beams with opposite topological charges whose intensity profiles are shown on the first two columns of Figure 3.3. The phase masks employed are blazed fork grating structures designed such that the total diffraction efficiency into the first order is maximal. We note that

the overall efficiency of the proposed scheme is currently limited to 25% due to the double passage through a beam splitter. Figure 3.3 also displays the experimental and simulated beam profiles of the generated PCVBs with the local E-field vectors denoted by arrows in the simulations.

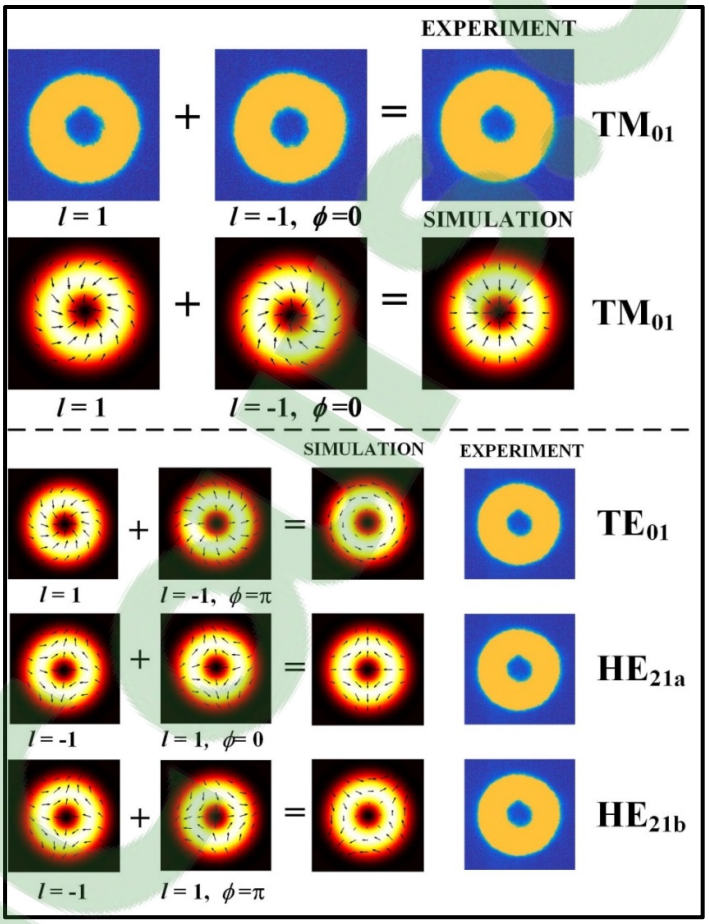

Figure 3.3 Experimental and simulated generation of PCVBs. The type of PCVB generated (here: TM_{01}, TE_{01}, even and odd HE_{21}) depends on the specific topological charge (l) and phase difference (ϕ) ascribed to each interfering beams

3.5 Result and discussion

For demonstration purposes, we applied the proposed method for the generation of three different types of CVBs: the radial and azimuthally polarized CVBs that are respectively analogous to the TM_{01} and TE_{01} modes of an optical fiber, as well as an in-homogeneously

polarized CVB with direct correspondence to the even and odd HE_{21} modes of a fiber. For the latter exemplar set of PCVBs, the relative phase difference between the two interfering beams (set by the phase masks on the SLM) was varied from $\phi = 0$ to $\phi = \pi$, as shown in Figure 3.3. Still, we again stress that the proposed method is in fact general since the SLM can be programmed with different phase and topological charges so as to generate any other types of PCVB or perfect vortex beams for that matter, all using the same experimental setup.

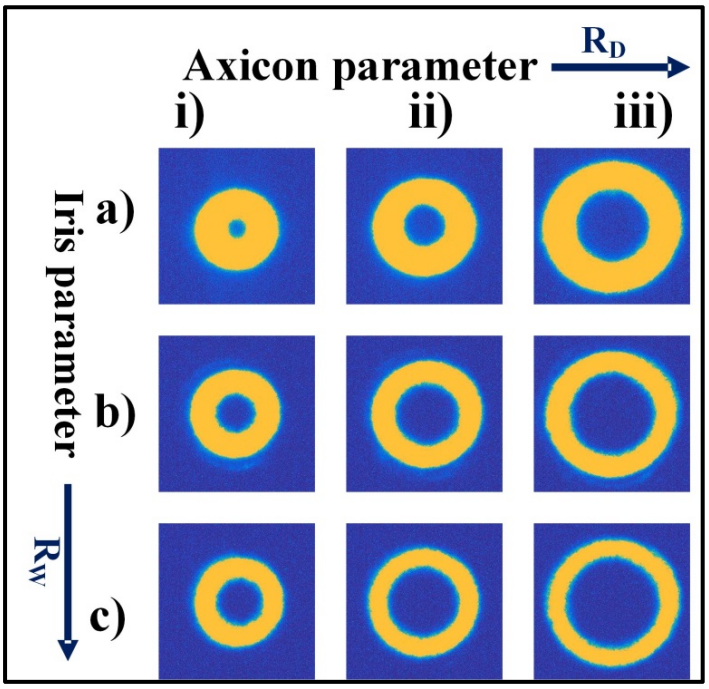

Figure 3.4 Experimental demonstration of PCVB (a radially polarized beam was here used). From left to right (i-iii) columns, the ring diameter R_D increases with the axicon parameter.From top to bottom (a-b-c) rows, the ring width R_W decreases with the iris parameter

As indicated earlier and suggested in Figure 3.1, the key feature of this work stems from the ability to tailor both the ring diameter and ring width of the PCVB independently from one another. The latter is here accomplished through two "knobs": the axicon parameter (a) and the iris parameter via the input Gaussian beam waist (w_g).

3.5.1 Process towards tailoring of cylindrical vector beam

The procedure to generate a PCVB is thus divided into two stages. In the first stage, the variable iris is used to control the diameter of the input Gaussian beam, which enables one to tune the ring width (R_W) of the PCVB. As the input beam width (w_g) increases, the ring width decreases in both directions, inward as well as outward. In the second stage, the axicon mask (along with the lens function) imprinted on the SLM allows the independent control of the ring diameter (R_D). The demonstration of PCVB with complete control over the transverse dimensions of the CVB is shown in Figure3.4 for increasing values of the axicon and iris parameters. The ring diameter (R_D) of PCVB was increased or decreased via the axicon parameter (a) for a given fixed input Gaussian beam width.

Table 3.1 Measured values of the R_D and R_W on the CCD Camera for Each PCVB shown in Figure 3.4

R_W (mm) \ R_D (mm)	i)	ii)	iii)
a)	0.61 / 0.25	0.73 / 0.22	0.87 / 0.21
b)	0.65 / 0.18	0.78 / 0.17	0.93 / 0.17
c)	0.65 / 0.16	0.79 / 0.14	0.93 / 0.14

Table 3.1 presents the measured values of the ring diameter (R_D) and ring width (R_W) that are shown in Figure 3.4. The results indicate an average fluctuation of around 3% for a given constant ring diameter (i.e. along a single column i, ii or iii) while the iris parameter (R_W) is varied. We ascribe this small error to the aperture diffraction incurred when the iris is gradually closed to modify the input beam width. This effect causes a slight reduction in the

brightness of the recorded beam, which in turn affects the intensity contrast (i.e. image sharpness) of the recorded beam profile.

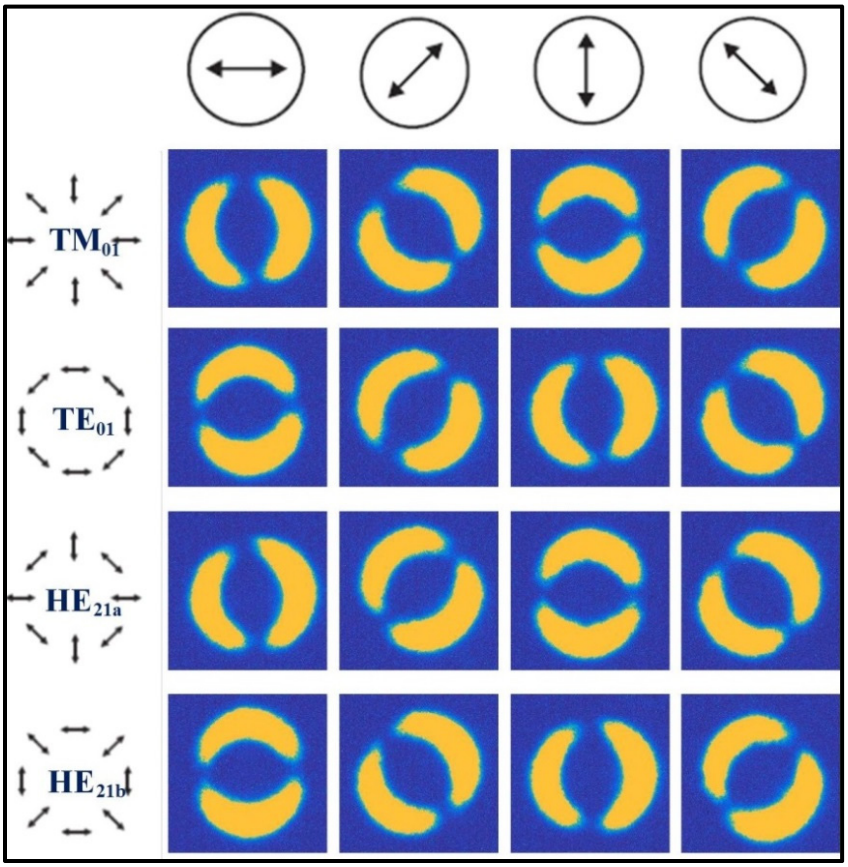

Figure 3.5 Experimental identification of the generated PCVBs (TM_{01}, TE_{01}, even and odd HE_{21} beams) via the rotation of a linear polarizer located in front of the CCD camera

We note that the ultimate size of ring width possible with this method is only limited in practice by the aperture of the iris utilized (see Figure 3.2). However, this iris could be replaced by a lens arrangement (i.e. tunable beam expander) that would extend the input beam diameters possible with this approach. The maximum achievable size of ring diameter is mainly restricted by the aperture stop of the lenses and half wave plate located before the SLM. On the other hand, the minimum size of the ring diameter is limited by the minimum input size of the Gaussian beam. Measurements in Table 3.1 further indicate that for a given constant ring width (along a single row a, b or c) there is an average error of 5% in the stability of the ring width (R_W) while the ring diameter (R_D) is varied. This small fluctuation

stems from the Fourier transformation of the Bessel-Gauss beams as pointed out in (Vaity et Rusch, 2015).

The experimental validation of the kind of PCVB generated was performed with the well-known method of the rotating analyzer (Figure 3.), as described in (Pradhan et al., 2017a; Zhan, 2009). The first column in Figure 3. presents a schematic representation of the *E*-field vector distribution of the PCVBs of interest. By rotating the linear polarizer in front of the CCD camera (first row) and by simultaneously monitoring the resulting intensity profiles on the camera (subsequent rows), one can deduce the type of PCVB (TM_{01}, TE_{01} and even or odd HE_{21}) at hand. We note that the intensity distributions of the TM_{01} and TE_{01} modes rotate in the same direction while rotating the linear polarizer in front of the CCD camera, whereas the intensity distributions of the even or odd HE_{21} modes rotate in the opposite direction.

Table 3.2 Mode Purity Measurement of PCVBs

PCVBs	**Simulation (dB)**	**Experimental (dB)**
TE_{01}	33.65	19.10
TM_{01}	33.65	18.13
$HE_{21,even}$	33.65	18.23
$HE_{21,odd}$	33.65	18.53

To determine the mode purity of the PCVBs generated with this method, the azimuthal intensity distribution of the doughnut shaped intensity profiles was recorded. A calculation based on the visibility of the intensity ring pattern reveals that the PCVBs produced in this work were of high purity (>18 dB) as indicated in Table 3.2. The approach used to determine the mode purity is detailed in Appendix B.

3.6 Conclusion

We have proposed and demonstrated the generation of high-purity perfect cylindrical vector beams (PCVB) whose transverse profile dimensions (i.e. ring width and ring diameter) can be independently controlled using an iris and a diffractive phase mask implemented on a digital spatial light modulator (SLM). Although the work was restricted to the generation of well-known PCVBs (the HE_{21} mode, radially and azimuthally polarized TM_{01} and TE_{01} modes), we emphasize that the proposed method can be directly generalized to any arbitrary PCVB as well as for the generation of perfect vortex beams, using the same experimental setup. The ability to generate PCVBs and tune their dimensions through a digitally addressable SLM obviates the need for the repeated tedious manipulation and re-alignment of bulk optics in the setup. The ensuing perfect cylindrical vector beams and perfect vortex beams are of high topical interest in the areas of laser material processing, super-resolution microscopy, fiber launching of exotic optical states and spin-orbit optical interactions, among others.

3.7 Appendix A

The interference of the two perfect vortex beams (of opposite topological charges) leading to the generation of a PCVB with the desired spatial polarization and transverse dimensions, depends on the user-defined phase masks imprinted on the SLM. A given phase mask is here designed by combining an axicon phase, a lens function and a spiral phase function that also implements the appropriate relative phase shift (between the two interfering beams). The resulting complex phase mask is given by (Vaity et al., 2014):

$$\exp\left(\frac{-\mathrm{ikR}^2}{2\mathrm{f}} - \mathrm{i}a\mathrm{R} + \mathrm{i}l\theta\right) \tag{3.11}$$

where k denotes the total wavevector, f is the focal length and a the axicon parameter. The first term of (3.11) represents a lens function while the next term is the axicon function that is used to control the ring diameter ($\mathrm{R_D}$) of the PCVB. The axicon parameter used in this phase mask has a relationship between the radial and total wavevector defined by

$$a = \mathrm{k}\sin^{-1}\left(\frac{\mathrm{k_r}}{\mathrm{k}}\right) \tag{3.12}$$

with $\mathrm{k_r} = 2.405/\mathrm{B_0}$ and $\mathrm{B_0}$ being the first zero of the zero-order Bessel beam. Finally, the third term of (3.11) represents a spiral phase function that is used to produce two beams with opposite topological charges ($l = \pm 1$). The practical implementation of this complex phase mask is schematically described Figure 3.5.

Figure 3.5 shows the physical procedure for transforming an input Gaussian beam into a PCVB. The input Gaussian beam sequentially passes through the three different stages of the complex phase mask described in (3.11) that is imprinted on one half-side of the SLM. In the example of Figure 3.5, here a right(-left) circularly polarized input Gaussian beam after passing through the spiral phase function yields a Laguerre-Gauss beam of prescribed

topological charge ($l = \pm 1$). Next, the beam is transmitted through the axicon function thus generating a Bessel-Gauss beam.

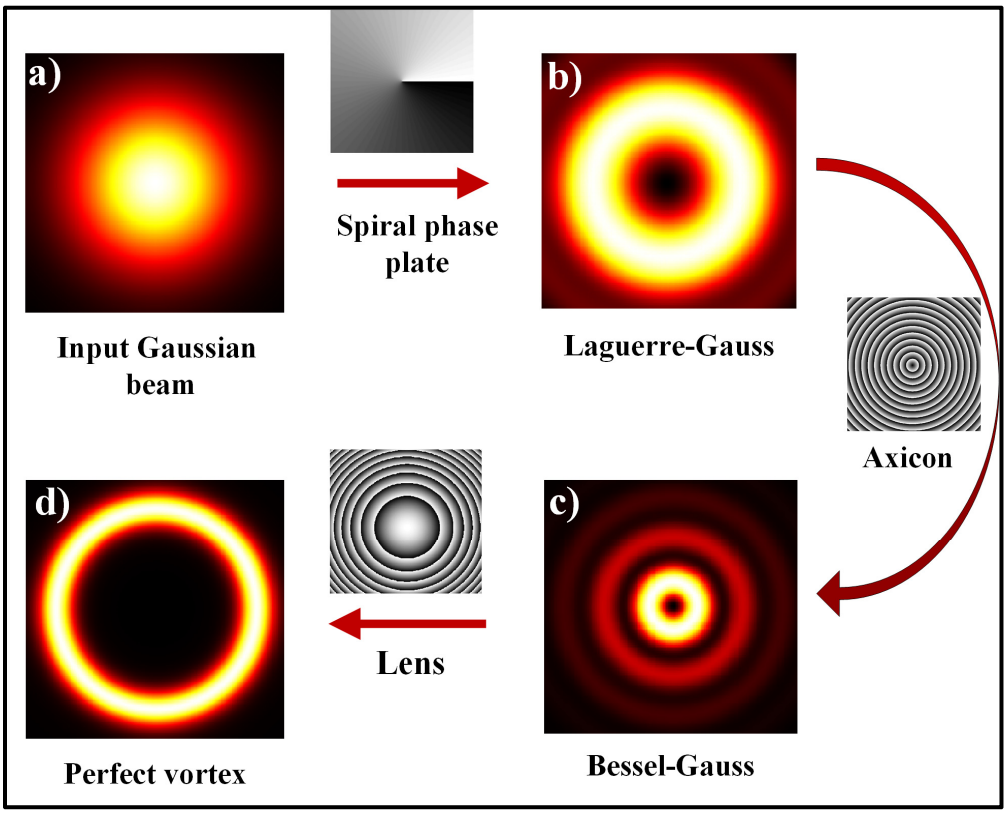

Figure 3.5 Simulation of the (a) input Gaussian beam, (b) Laguerre-Gauss beam after passing through the spiral phase function, (c) Bessel-Gauss beam after undergoing the axicon function, and (d) the perfect vortex beam is obtained after the lens function

Subsequently, the Bessel-Gauss beam is Fourier transformed into a perfect vortex beam after passing through the lens function. The latter procedure is performed on both arms of the common-path interferometric arrangement (but using different phase masks on each half-side of the SLM). Finally, when the two perfect vortex beams of opposite topological charges are made to interfere, the ensuing optical beam forms the desired type of PCVB (TM_{01}, TE_{01} or even and odd HE_{21} modes) as shown in Figure 3.3.

3.8 Appendix B

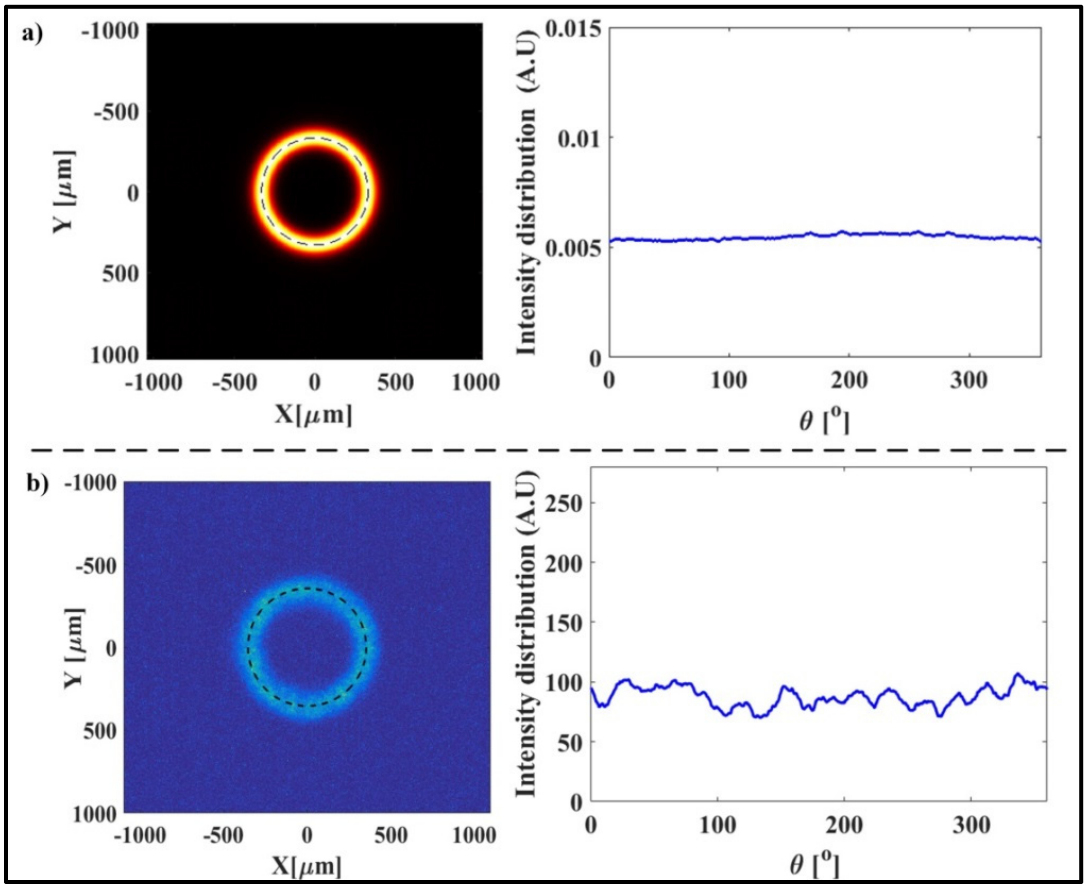

Figure 3.6 (a) Simulated and (b) experimental TE_{01} PCVB with the centered azimuthal intensity profile recorded along the dashed line. This azimuthal profile is ultimately used to calculate the beam purity

To test the quality of the PCVB generated using our experimental setup, we measured the purity of the TM_{01}, TE_{01} or even and odd HE_{21} beams based on the visibility of their intensity pattern given by (Bozinovic, Kristensen et Ramachandran, 2011)

$$V = \frac{I_{max} - I_{min}}{I_{max} + I_{min}} \tag{3.13}$$

Where I_{max} and I_{min} are the intensity maxima and minima of the beam along the azimuthal intensity distribution. Hence, the mode purity is calculated using

$$\text{Mode purity (dB)} = 10\log_{10}\left(\frac{1+\sqrt{1-V}}{V}\right)^2 \quad (3.14)$$

Figure 3.6 (a) shows the azimuthal intensity distribution along the ring for an ideal TE_{01} mode obtained from simulation. Keeping the simulated result as reference, we then present the azimuthal intensity distribution of the experimentally obtained TE_{01} PCVB as displayed in Figure 3.6 (b). The beam purity measurements of the TM_{01} and HE_{21} PCVBs were similarly calculated and their values reported in Table 3.2.

CHAPTER 4

CYLINDRICAL VECTOR BEAM GENERATION BASED ON ARC-INDUCED LONG PERIOD GRATINGS IN FEW-MODE FIBER

P. Pradhan[a], B. Ung[b], C. Tremblay[c], D. Sengupta[d],

[a, b, c and d] Department of Electrical Engineering, École de technologie supérieure, 1100 Notre-Dame West, Montreal, Quebec, Canada, H3C 1K3

Paper submitted for publication, April 2018

Résumé

Nous rapportons un réseau longue période à fibre (LPFG) avec le plus petit pas fabriqué en utilisant l'approche commune via arc électrique. Avec ce LPFG écrit dans une fibre faiblement multimode, nous avons démontré l'excitation efficace des faisceaux vectoriels cylindriques (CVBs) d'ordre supérieur, à savoir les modes TE_{01}, HE_{21} et TM_{01}. L'efficacité de conversion moyenne pour la production de CVB est mesurée à environ ~81%. En outre, la génération de faisceaux avec moment angulaire orbital (OAM) a été accomplie avec succès et détectée à la sortie de la fibre faiblement multimode. Ce travail démontre que la méthode couramment accessible d'écriture à l'arc électrique pour la fabrication de LPFG peut être étendue à des fibres spéciales faiblement multimodes qui nécessitent souvent de très petites valeurs de pas du réseau. Les résultats présentés sont pertinents pour le domaine de l'illumination structurée, en particulier pour la génération de faisceaux CVB et OAM de puissance élevée.

4.1 Abstract

We propose and demonstrate the use of the cost-effective electric arc writing method for the all-fiber CVB and OAM mode generation in few-mode fibers for the first time to the best of our knowledge. We show that this technique enables the writing of long-period fiber gratings (LPFGs) with pitch values as small as 238 μm, such is required in some high-index contrast specialty fibers tailored for the stable guiding of CVB and OAM modes. Conversion

efficiencies around 81 % are measured for three different symmetric CVBs. The polarization-dependent properties of the fabricated LPFG are elucidated and we report a polarization-dependent loss of about 2.5 dB accross the different CVBs. By means of a fabricated LPFG, we further demonstrated the all-fiber generation of the OAM states with topological charge (±1) at the output of the few-mode fiber. The results are relevant to the fields of laser material processing, space-division multiplexing and novel optical sensors that would benefit from a compact source of quality CVB and OAM beams of high average optical power.

4.2 Introduction

Over the past few decades, studies on few-mode fibers (FMFs) and multimode fibers (MMFs) have been explored intensively in view of their potential to overcome the capacity crunch of optical fiber communications based on the single-mode fiber (SMF) (Kitayama et Diamantopoulos, 2017; Rademacher et al., 2018b; Richardson, Fini et Nelson, 2013). Few-mode fibers are particularly promising for mode-division multiplexing, where multiple information channels can be devised across independent spatial modes with minimum crosstalk, thereby enhancing the data carrying capacity inside a single core fiber by many folds (Ryf et al., 2012). Moreover, recent research activities have reported promising results in the development of multi-parameter and distributed sensors based on the linearly polarized (LP) modes of FMFs (Li et al., 2015; Weng et al., 2015b). Conventionally, the linearly polarized (LP) modes have been widely utilized because the modes forming this basis are more readily observed than the real eigenmodes of an optical fiber.

Recently, cylindrical vector beams (CVB) (Maurer et al., 2007; Pradhan et al., 2017b; Youngworth et Brown, 2000; Zhan, 2009), orbital angular momentum (OAM) (Brunet et al., 2014; Jabir et al., 2016; Karahroudi et al., 2017; Török et Munro, 2004; Ung et al., 2014) and vectorial vortex beams (Fu, Wang et Gao, 2016; Jabir et al., 2016; Li et al., 2016; Liu et al., 2017b; Wang et al., 2017d) have received increased scrutiny as new spatial mode basis sets. The unique properties of higher-order cylindrical vector beams exhibiting inhomogeneous polarization give rise to peculiar focusing properties that can achieve high resolution optical imaging and micro-particle optical manipulation (Dorn, Quabis et Leuchs, 2003; Kozawa et Sato, 2010; Yu et al., 2016), among other. These emerging applications of CVBs, both in free

space optics as well as in fiber optics, have reached a threshold where further developments will require a generation of these CVBs with strong coupling efficiency and high power handling. For this purpose, it is essential to develop efficient methods to generate these CVBs (and OAM beams).

Some of the current methods of generating CVBs employ spatial light modulator (Ostrovsky, Rickenstorff-Parrao et Arrizón, 2013; Pradhan, Sharma et Ung, 2018), spiral phase plate (Liu et al., 2017b), mechanical LPFG (Pradhan et al., 2015; Ramachandran, Kristensen et Yan, 2009) and offset fiber coupling (Fang et al., 2013). However, all-fiber based mode converters with an advantage of cost, fabrication, integration, stability and low loss are often favored towards applications in mode division multiplexing systems. Although several inscribing mechanisms based on CO_2 laser (Dong et Chiang, 2015; Wang et al., 2015), femtosecond laser (Li et al., 2011b) as well as UV laser writing (Smietana, Bock et Mikulic, 2010) are reported, the electric arc-induced method remains a well-established and low-cost technique to write stable and efficient long-period fiber gratings (LPFG) (Ivanov et Rego, 2007; Rego et al., 2001; Rego et al., 2005; Smietana et al., 2010).

Recent work performed on FMF has highlighted the potential for exploiting the LPFG towards the all-fiber generation of high-power CVB lasers as well as in mode division multiplexing applications (Chen et al., 2018). In this work we develop an all-fiber mode converter that can efficiently generate CVBs of potentially high power and support their stable fiber propagation with high mode purity by means of the arc-induced writing technique to realize LPFGs with grating pitches as small as 238 μm, as required to excite CVBs in some specialty FMFs.

4.3 Theory and experimental configuration

The LP modes of the optical fiber are extensively used because of their convenience in many applications and simple mathematical description. In particular, the first higher-order LP_{11} mode may randomly degenerate into its even and odd states (plus two orthogonal polarizations) while propagating in the fiber. On the other hand, the true eigenmodes of the fiber, if properly excited, may retain their original shape and polarization state as they

propagate along the fiber. This is due to the invention of a new class of specialty fibers designed to lift the polarization degeneracy of the antisymmetric LP_{11} mode so that the propagation constants of its constituting eigenmode components are separated by sufficiently large phase gaps. Meanwhile, it is instructive to describe the relationship between these LP modes and the eigenmodes supported by the fiber (Ramachandran, Kristensen et Yan, 2009; Ung et al., 2014). In the weakly guiding approximation, the fiber modes are represented as linearly polarized LP_{lm} modes, where 'l' is the azimuthal number and 'm' is the radial mode order. For m=1, the LP mode group in any fiber can have four unstable transverse electric field distributions represented as (Han et al., 2016; Huang et al., 2015)

$$\begin{pmatrix} LP_{l,1}^{ox} \\ LP_{l,1}^{ey} \\ LP_{l,1}^{ex} \\ LP_{l,1}^{oy} \end{pmatrix} = K_{l.m}(r) \begin{pmatrix} \sin l\emptyset & 0 \\ 0 & \cos l\emptyset \\ \cos l\emptyset & 0 \\ 0 & \sin l\emptyset \end{pmatrix} \begin{pmatrix} \hat{x} \\ \hat{y} \end{pmatrix} \quad l \geq 1 \tag{4.1}$$

Where l denotes the topological charge, $\emptyset$ is the azimuthal coordinate and $K_{l,m}(r)$ represents the radial field distribution. The linear combinations of these modes through the symmetric and antisymmetric combinations represent the first four eigenmodes modes of the fiber.

$$\begin{pmatrix} LP_{1,1}^{ox} \\ LP_{1,1}^{ey} \\ LP_{1,1}^{ex} \\ LP_{1,1}^{oy} \end{pmatrix} = \begin{pmatrix} 1 & -1 & 0 & 0 \\ 1 & 1 & 0 & 0 \\ 0 & 0 & 1 & 1 \\ 0 & 0 & -1 & 1 \end{pmatrix} \begin{pmatrix} HE_{21}^{o} \\ TE_{01} \\ HE_{1,1}^{e} \\ TM_{01} \end{pmatrix} \quad l = 1 \tag{4.2}$$

The expressions of the eigenmodes and their corresponding electric field vectors in a weakly guided fiber (for l=1) are represented as (Snyder et Love, 2012)

$$e_{HE^{o}_{21}} = K_{l.m}(r)\{\sin\emptyset\hat{x} + \cos\emptyset\hat{y}\} \quad (4.3)$$

$$e_{TE_{01}} = K_{l.m}(r)\{\sin\emptyset\hat{x} - \cos\emptyset\hat{y}\} \quad (4.4)$$

$$e_{HE^{e}_{21}} = K_{l.m}(r)\{\cos\emptyset\hat{x} - \sin\emptyset\hat{y}\} \quad (4.5)$$

$$e_{TM_{01}} = K_{l.m}(r)\{\cos\emptyset\hat{x} + \sin\emptyset\hat{y}\} \quad (4.6)$$

In our experiment, we have used an inverse parabolic graded-index profile FMF that supports three mode groups (including 8 CVBs) in the C-band: LP_{01} (HE_{11x}, HE_{11y}), LP_{11} (TE_{01}, HE_{21odd}, HE_{21even} and TM_{01}) and LP_{21} (EH_{11odd}, EH_{11even}, HE_{31odd}, HE_{31even}) (Ung et al., 2014). The effective refractive index difference Δn_{eff} between the eigenmodes (TE_{01}, HE_{21}, TM_{01}) of the LP_{11} group in this FMF is expected to be in the range of 2.1×10^{-4} and 3.7×10^{-4}. This large modal separation helps to mitigate the modal crosstalk between different vector modes by ensuring proper discrimination of n_{eff} values between adjacent guided modes thus enabling their stable transmission in the FMF.

In addition, these eigenmodes can also serve as the basis to form OAM guided modes. In the vicinity of 1550 nm, the FMF thus supports up to 6 OAM modes through the coherent combination of degenerate CVBs, i.e. the high-order hybrid modes (HE_{21}, EH_{11}, HE_{31}) (Wang et al., 2014b).

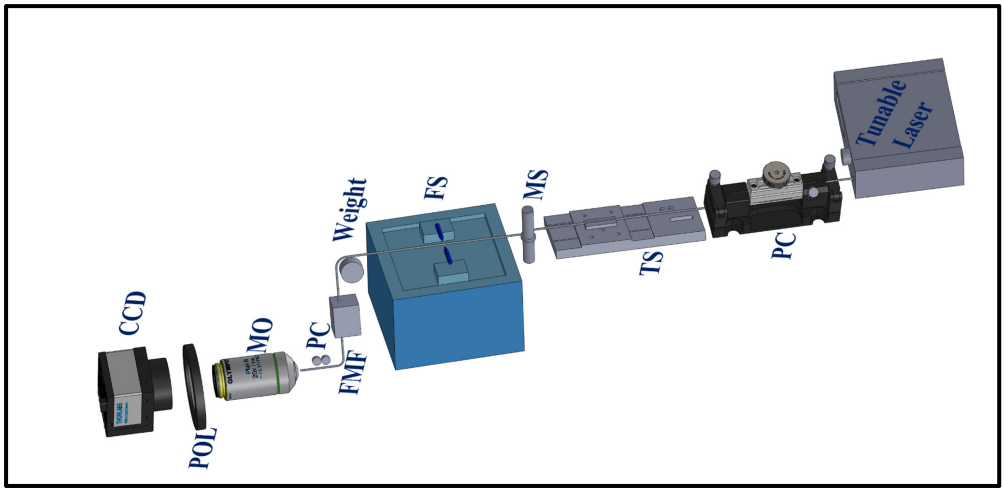

Figure 4.1 Experimental setup for the generation of CVBs using LPFG in few-mode fiber
PC: polarization controller; TS: translation stage, FMF: few-mode fiber; MS: mode stripper; FS: fusion splicer; MO: microscope objective; POL: linear polarizer

To excite the CVBs, the LPFG was engineered to realize core-guided mode coupling from the fundamental LP_{01} mode to each of the high-order eigenmodes (TE_{01}, HE_{21}, TM_{01}). The schematic of the fabrication process for arc-induced long-period fiber grating is shown in Fig. 4.1, in which an electric-arc with exposure time of 200 ms, provided by a Fujikura FSM-30 fusion splicer is maintained between two electrodes where the FMF sits. A linear translation stage with 1 μm resolution displaces the fiber after each electric discharge by a distance equal to the desired grating period. The proximal part of the FMF remains fixed on a motorized translation stage while the distal end was attached to a weight (10g). A single mode fiber was spliced to the input port of the FMF with an in-line fiber polarization controller (PC) inserted between the tunable laser and the LPFG in order to optimize the conversion efficiency of the LPFG. To ensure that only the fundamental LP_{01} mode is launched into the FMF, a mode stripper (MS) is placed at the input side of FMF.

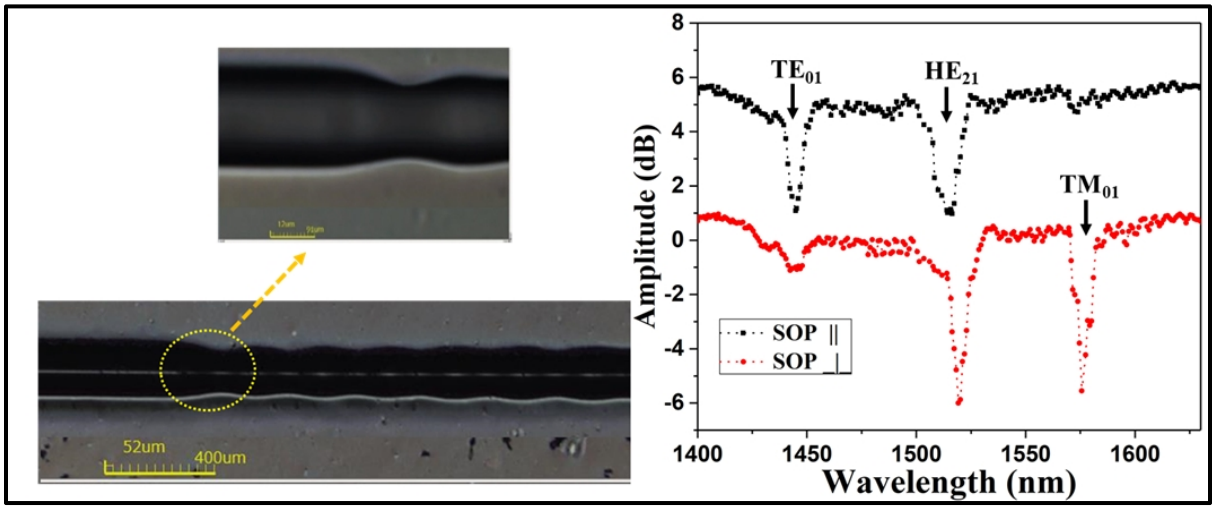

Figure 4.2 a) Side view on the microscope and partially enlarged tapered region of the LPFG induced in FMF by the electric-arc discharges, b) Polarization dependent transmission spectrum of the LPFG.

Figure 4.2a shows the periodic geometrical modulations in the fabricated LPFG that gives rise to the mode coupling from the LP_{01} core-guided mode to a higher-order core-guided CVB. The LPFG fabrication process involves the application of a constant force upon the FMF to create axial tension. As a result, small tapers are formed at each fiber point exposed to an electric arc discharge. The linear stage then moves the fiber to the next point so as to create a periodic refractive index modulation.

The shape of the tapered structure depends on the applied tension and arc discharge parameters. The main effect of the arc discharge are twofold, based on previous reports (Esposito et al., 2017; Rego et al., 2001; Rego, Ivanov et Marques, 2006): i) a localized geometrical modification of the optical fiber, i.e. tapering, within the transverse cross-section of the core and cladding regions; ii) a change in the silica refractive index due to the stress relaxation induced by the softened hot spots. Further, the local perturbation created by the electric arc in the fiber is asymmetric, owing to the side-writing configuration, thus making the LPFG polarization dependent (Masri et al., 2016; Rego, Ivanov et Marques, 2006).

Figure 4.2b shows the polarization dependent transmission spectra of the fabricated LPFG recorded by launching input light from a broadband source through an inline polarizer to control the input state of polarization (SOP). Here, the transmission spectra clearly demonstrate the strict dependence of input SOP corresponding to the TE_{01} and TM_{01} mode. When the input SOP is transverse to the LPFG, only the TE_{01} and HE_{21} modes are excited, whereas for the input SOP perpendicular to the LPFG, only the TM_{01} and HE_{21} resonances occur. Since the HE_{21} mode is polarization insensitive, it can be excited regardless of the input SOP as expected (Masri et al., 2016; Ramachandran et al., 2005).

4.4 Result and discussion

In order to observe the excitation of the various CVBs, the tunable laser was set at the resonant excitation wavelength of the desired eigenmode. Figure 4.3 shows the fiber output intensity profiles after the one-meter long FMF captured on a CCD camera. Through the intensity profiles and the help of a linear polarizer we were able to confirm that all CVBs of interest (i.e. TE_{01}, HE_{21}, TM_{01}) were successfully excited. In this regard, the linear polarizer (i.e. analyzer) was placed in front of the CCD camera and rotated (first row) and by simultaneously monitoring the resulting intensity profiles on the camera (subsequent rows), one can deduce the type of CVB (TM_{01}, TE_{01} and HE_{21}) at hand (Maurer et al., 2007; Pradhan et al., 2017b; Ramachandran, Kristensen et Yan, 2009; Volpe et Petrov, 2004).

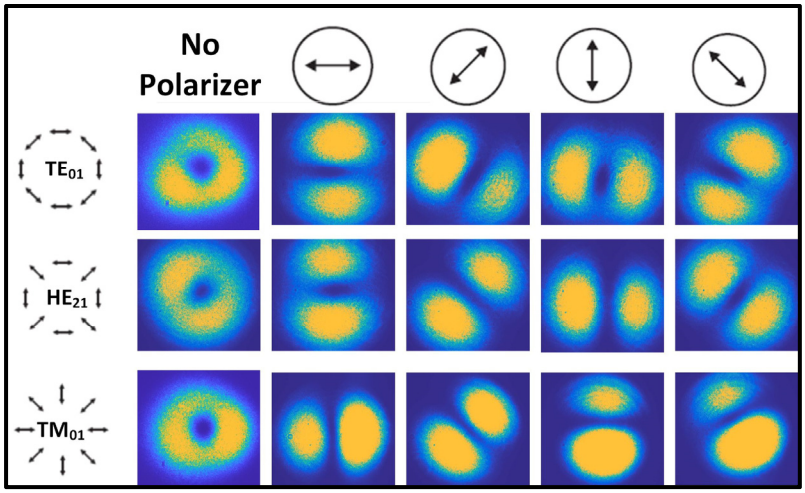

Figure 4.3 Measured intensity profiles of the CVBs in FMF excited by the LPFG

The grating pitches written in the FMF for mode conversion between LP_{01} and the CVBs (TM_{01}, TE_{01}, HE_{21}) are 238 µm, 250 µm, 265 µm and the corresponding length of the grating of each LPFG is around 3.5 cm respectively. The grating pitch of the LPFG was calculated prior to fabrication in order to ensure that the resonance wavelength falls within the tuning range of our C-band laser, as based on the phase matching condition given by (Pradhan et al., 2015):

$$\Lambda = \frac{\lambda}{n_{effLP_{01}} - n_{effLP_{11}}} \tag{4.7}$$

where Λ is the pitch of the grating, λ is the resonance wavelength, and $n_{effLP_{01}}$ and $n_{effLP_{11}}$ are the effective indices of the two coupled modes.

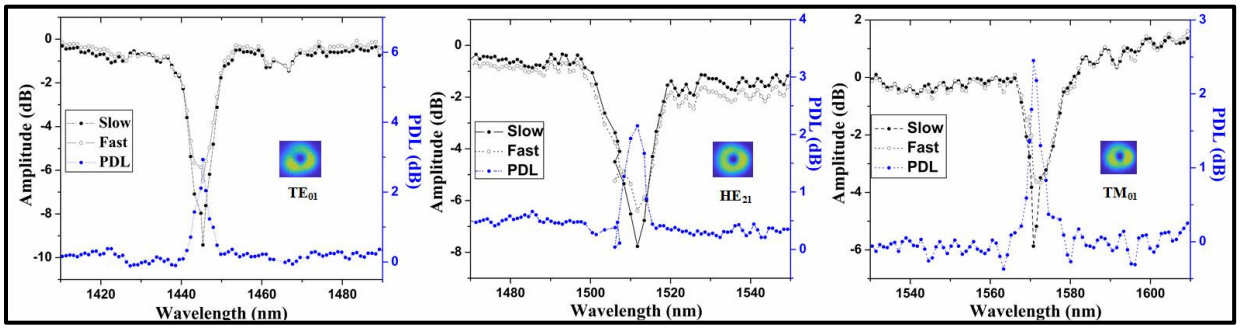

Figure 4.4 Transmission spectra of LPFG and their corresponding PDL spectra

The PDL characteristics of the LPFG are measured by placing the in-line polarization controller at both the ends of the fabricated LPFG as shown in the experimental setup in Fig. 4.1. The transmission spectra for different CVBs excited by LPFG at two different orthogonal input polarizations are recorded by the optical spectrum analyzer and their corresponding PDL are displayed in Fig. 4.4. The solid black line represents the transmission spectra when both the polarization axis is well aligned, whereas the dotted lines represent PDL evolution when the two-polarization axis is orthogonal to each other. The maximum PDLs between fundamental mode and TE_{01}, HE_{21} and TM_{01} mode are measured to be 2.9, 2.2 and 2.6 dB, respectively. The explanation towards polarization dependence of LPFG is related to the ellipticity introduced into the core shape by the side-writing electric arc process. This fact has been demonstrated elsewhere using a similar side-writing configuration (Wu et al., 2017). This large local perturbation in the core geometry results in a significant perturbation of the core-guided modal fields that in turn breaks the orthogonality between eigenmodes of a perfectly circular fiber.

Prior work on arc-induced LPFG reported the coupling of antisymmetric LP modes in a standard optical fiber using such asymmetric grating (Rego, Ivanov et Marques, 2006). The same asymmetry in the transverse grating structure here allows the linearly polarized fundamental mode to couple with the symmetric core guided eigenmodes through the non-zero overlap integral of their transverse E-field distributions, as predicted by coupled mode theory. Furthermore, the specialty FMF used in this work is designed (by means of its high-index annular profile) to lift the modal degeneracy of antisymmetric LP_{11} modes, thereby enabling the LPFG to efficiently couple light to the symmetric CVB modes depending on the input SOP. (Pradhan et al., 2017b). The extinction ratio of the LP_{01}-TE_{01}, LP_{01}-HE_{21} and LP_{01}-TM_{01} mode are found to be 89%, 82% and 73%, respectively. The fact that weak grating spectrum is measured compared to the earlier reported literature, we believe this due to the smaller grating period required to excite these vector modes. The width of the arc limits the smallest grating period that can be fabricated which leads to the overlapping of the tapered region when the grating period is smaller than 250 um (Colaço et al., 2016; Smietana et al., 2010).

4.4.1 OAM state measurements

An OAM beam (also known as a vortex beam) is represented by a beam of light that possesses a helical phase front proportional to exp($il\phi$) in the transverse plane, where l is the topological charge and ϕ is the azimuthal angle. The FMF theoretically supports 6 $OAM_{\pm l,m}^{\pm s}$ states through the superposition of even and odd hybrid modes: $OAM_{\pm 1,1}^{\pm} = HE_{21even} \mp iHE_{21odd}$, $OAM_{\mp 2,1}^{\pm} = EH_{11even} \mp iEH_{11odd}$, and $OAM_{\pm 2,1}^{\pm} = HE_{31even} \mp iHE_{31odd}$, where, the $\pm s$ superscript represents the OAM polarization state, the $\pm l$ subscript its topological charge and m denotes the radial order (Wang et al., 2014b). In this work, we restricted our demonstration to the generation of $OAM_{\pm 1,1}$ mode that originate from the π-shifted superposition of odd and even HE_{21} modes.

The experimental setup towards all-fiber OAM beams generation is shown in Fig. 4.5. To confirm that the excited vector beam does indeed carry OAM, the LPFG was prepared firstly to realize core modes coupling from the LP_{01} to the HE_{21} mode. Then by adjusting the polarization controller (PC) placed after the LPFG to create a π/2 phase-shifted linear combination of the even and odd HE_{21} modes, the $OAM_{\pm 1,1}$ beam were obtained. Subsequently, the OAM beam was combined and interfered with the reference Gaussian beam (retrieved from another arm of the SMF-coupled laser source) through a non-polarization beam splitter.

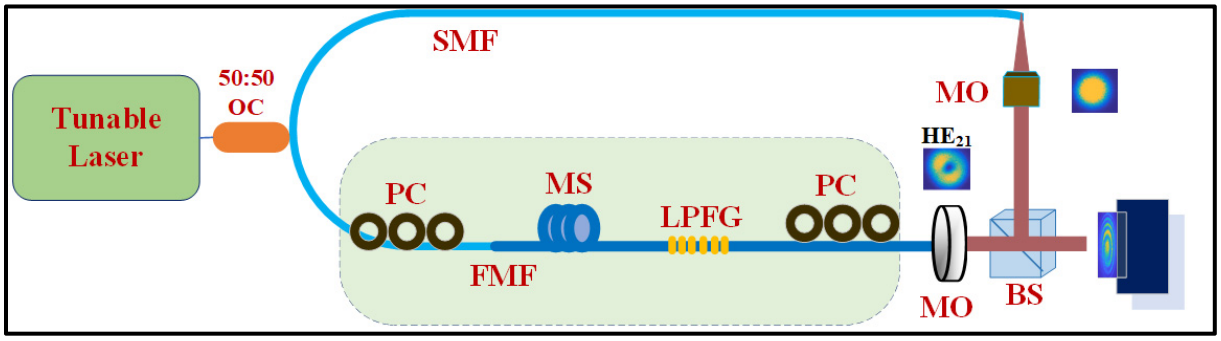

Figure 4.5 Experimental setup for the generation and detection of OAM beams

Figure 4.5 shows the interference pattern of the $OAM_{1,1\pm}$ beams (generated via the LPFG in FMF) with the reference Gaussian beam. We note that the topological charge (l) of the OAM

state generated in the FMF can be simply tuned through the inline PC so as to control the relative phase shift between the HE_{21even} and HE_{21odd} modes. The experimental results shown in Fig. 4.6 confirm that the LPFG mode converter can generate the CBVs as well as the $OAM_{1,1\pm}$ modes successfully.

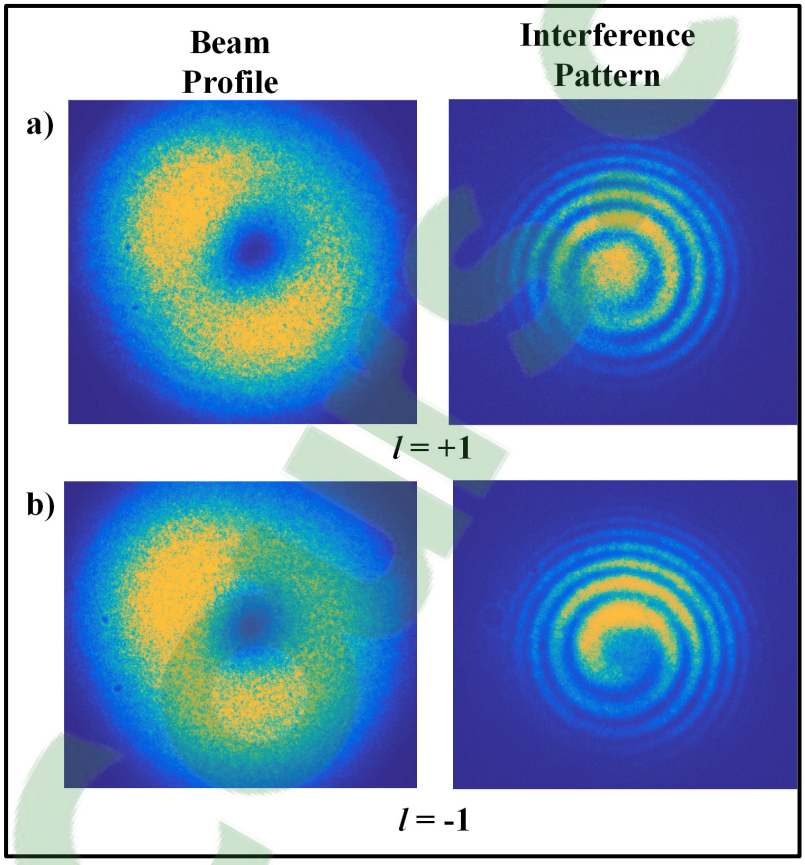

Figure 4.6 Intensity profiles and spiral interference patterns of the generated beams a) $OAM_{1,1+}$ b) $OAM_{1,1-}$

4.4.2 Purity measurements of CVBs and OAMs

Finally, we measured the mode purity of the CVBs (or OAM beam) generated with the LPFG as calculated by recording the azimuthal intensity distribution of the doughnut shaped intensity profiles (Pradhan, Sharma et Ung, 2018). This calculation based on the visibility of the intensity ring pattern reveals that the mode purity of CVBs and $OAM_{1,1\pm}$ beams produced using the LPFG fabricated with the electric arc technique was found to be 19.5 dB on

average. Figure 4.7 shows the azimuthal intensity distribution along the ring of an exemplar CVB (the HE_{21} mode in this instance) obtained with our experimental setup.

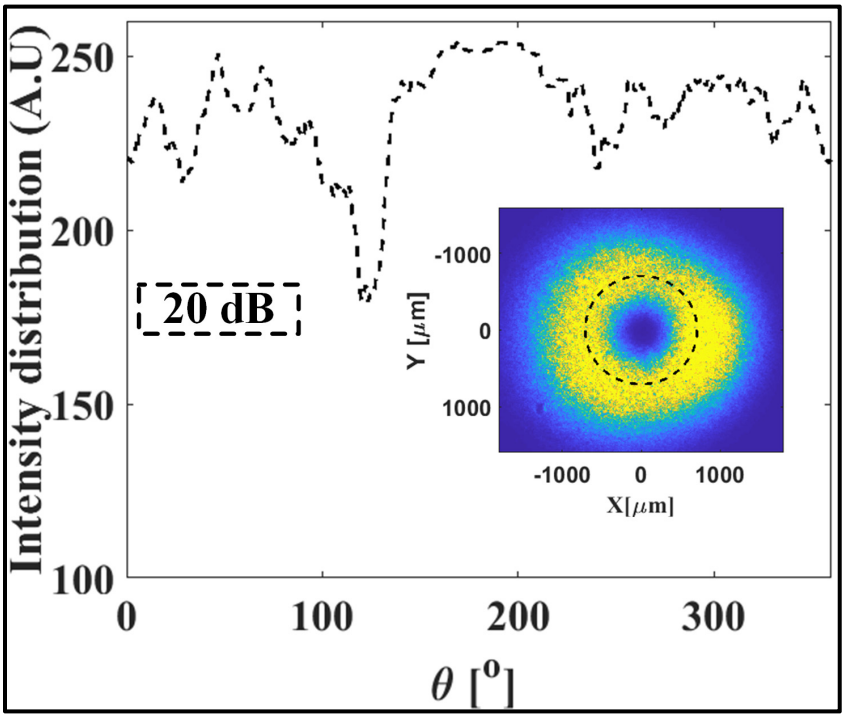

Figure 4.7 Beam purity (20.9 dB) of the generated HE_{21} beam calculated from the azimuthal intensity profile

4.5 Conclusion

In conclusion, we have fabricated LPFG by means of the cost-effective electric arc writing method and demonstrated for the first time, to the best of our knowledge, the all-fiber generation of cylindrical vector beams (CVB) and modes carrying orbital angular momentum (OAM) in a specialty few-mode fiber. The ensuing LPFGs obtained with a side-writing configuration exhibited polarization dependence with a mode-specific polarization-dependent loss on the order of 2.5 dB. The extinction ratios (i.e. conversion efficiencies) measured from the grating transmission spectra for three different CVBs of interest TM_{01}, TE_{01}, HE_{21} are found to be 81 % on average. The demonstration of $OAM_{1,1\pm}$ states was validated by the spiral fringe pattern yielded by the interference of the OAM beam with that of a reference gaussian beam. Our results indicate that the common electric arc fusion splicer can be used to create

low-cost, compact and flexible mode converters in specialty few-mode fibers so as to generate CVBs and the so-called vortex beams (i.e. OAM beams). A caveat is related to the achievable minimum grating period, here found to be around 220 μm, which limits the applicability of this method for some few-mode fibers. The high-power all-fiber generation of CVB and OAM beams has potential applications in laser material processing, super-resolution imaging and mode-division multiplexing.

4.6 Acknowledgement

The authors would like to thank Mr. A. Zalzal and Mr. S. Gagne for the technical support provided in this work.

CONCLUSION

The research goal - generation of cylindrical vector beams and their subsequent characterization- is a demonstration of methods developed for the excitation of CVBs in few-mode fibers. Even though, CVB are the true eigen vector modes of an optical fiber whose linear combination can be utilized for the synthesis of LP and OAM beams, many reports can be found still based on the generation and measurements of the scalar LP modes of FMF. The techniques towards the delicate spectral and spatial controls of CVBs in order to be detected are yet to be fully explored. To fill this void, this thesis reports a simple, flexible and cost-effective technique that allows an efficient generation of the CVB and OAM beams while reducing the overall losses incurred by the system to 0.2 dB. It is intended towards the development of a mode converter that can dynamically generate cylindrical vector beams of potentially high optical output power and enable the stable fiber propagation with high mode purity in specialty fibers.

To start with, three different techniques for the generation of CVB and OAM beams with high output mode purity are utilized. The two mode converters designed and fabricated for the CVB generation are all-fiber based. The first one is a mechanical mode converter with a novelty in its tunability generates cylindrical vector beams of the LP_{11} mode group supported by the FMF. The non-destructive characterization of CVB in a few-mode fiber is demonstrated by utilizing the phenomenon of stimulated Brillouin scattering for the first time. The aim of the experiment was to demonstrate the independent measurement, identification and the complete analysis of the Brillouin gain spectra of vector beams in specialty few-mode fibers. The photonic device was also utilized to retrieve the corresponding effective refractive indices of the individual vector beams supported by the FMF. As described in the reported article in chapter 2, the proposed technique represents a new tool for probing and controlling vector beams as well as modes carrying orbital angular momentum in optical fibers with potential applications in advanced optical communications and multi-parameter fiber-optic sensing.

The second device is an all-fiber based mode converter designed to generate CVBs and OAM beams while increasing the stability of beam propagation for long length fiber transmission. The grating is written within a fiber that act as a mode converter design fabricated using the common electric arc induced approach. In addition, such all-fiber mode converter provides the possibility of utilizing high-energy laser beam demanded by many non-linear experiments. Such low-cost, reliable and compact device opens road toward exploiting the all-fiber generation of high-power CVB and vortex laser as well as mode multiplexing applications.

If the above-described two all-fiber based LPFGs are compared, writing LPFG using electric arc within the fiber can generate stable CVB output than the mechanical LPFG which are stable for short period of time. An electric arc-based mode-converter can be monitored real-time whereas mechanical grating can be utilized after they are fabricated. The tunability to produce all the desired CVBs provide a destructive advantage of mechanical grating. Overall, both the all-fiber based LPFG can generate CVBs with high coupling efficiency (>90%) and high mode purity (<20 dB). However, the overall insertion loss of the electric arc-based LPFG is measured to be 0.2 dB, while 0.1 dB of insertion loss is obtained in the case of mechanical LPFG. On the other hand, the power handling capacity of both the device can resist more than few watts.

The final mode converter is a programmable spatial light modulator that was utilized to generate CVB in free space. The efficiency of free space coupling can be optimized when the annular core dimension of the fiber and the beam intensity profile are perfectly matched. Although several methods have been introduced and demonstrated to generate vortex and vector beams, their launching efficiency in free space still remains an area of interest. The annular shaped beams in the optical fiber are excited in free space and the maximum coupling can be obtained when the beam dimension of the fiber and the beam profile are optimized. One of the common shortcomings with these techniques originates from the strong inter-dependence of inner and outer diameter of the annular intensity ring. In the case of conventional vortex beams, the ring diameter varies linearly with the topological charge

thus making the co-generation (and fiber co-propagation) of several different vortex beams problematic.

It is thus crucial to control the ring diameter and width of CVB as well as OAM beams. There are already some reports on the generation of perfect vortex beams for tailoring the annular beam of the vortex beam with any order of topological charge to the same size. Still many of the reports are limited to monitoring of ring diameter only and have produced beam with limited purity. Therefore, we have proposed the generation of high-purity perfect cylindrical vector beams using the Fourier transformation of Bessel–Gauss vector beams. The different types of cylindrical vector beams are generated with precise transverse dimensions demanded by the specialty fibers. The dynamic control of the ring width, ring diameter, and the specific type of PCVBs desired is theoretically as well as experimentally demonstrated. The proposed experimental setup can be employed to tailor any breed of annular shaped beams. The ability to generate fully tailorable CVB and OAM beams has implications for the efficient launch of exotic optical modes in specialty fibers, for super resolution microscopy and in the field of optical tweezers. With this technique, the overall efficiency of the proposed scheme is currently limited to 25% due to the double passage through a beam splitter. Further, the power handling capacity of the setup can only be few hundreds of miliwatts, limited by the threshold of splatial light modulator.

The proposed research will impact the development of novel metrological techniques for next-generation SDM networks, a recent topic of research that is of high relevance for both applied research and industrial end-users. Moreover, the investigation of novel types of FMFs tailored for the stable transmission of vector modes carrying OAM states, as well as the dynamic characterization of their properties along the fiber, constitute fundamental topics of research that will help scientists and engineers alike to control the propagation of light on the most fundamental level. Finally, the development of a fully-distributed multimodal fiber sensing system is expected to be a significant technological contribution to the fields of fiber-optic sensors and civil structural monitoring.

STATEMENT OF ORIGINAL CONTRIBUTION & FUTURE RECOMMENDATIONS

Statement of original contribution

The original contributions to the research described in this thesis are summarized below:

1. Novelty in the design and in-lab fabrication of cost-effective tunable mechanical grating using stainless steel needles for generation of CVBs;
2. Brillouin gain measurement of the cylindrical vector beams in a few-mode fiber is reported for the first time;
3. The dynamic control of the ring width, ring diameter, and the specific type of desired PCVBs is theoretically as well as experimentally demonstrated for the first time;
4. LPFG with small pitch (<250 um) fabricated in specialty FMF using the low-cost electric arc-induced method has been demonstrated to allow the generation of CVB and OAM modes for the first time.

Recommendations for future work

The area of structured light (i.e. CVB and OAM beams), as well as its emerging applications, remains rich in photonic discoveries. We propose below some research topics that would merit further exploration so as to extend the work and science encovered in this thesis:

1. Fiber based mode converters and their utility in applications

In comparison to the fabrication methods (mechanical and electric arc) of LPFG reported in this thesis, laser irradiation-based inscription is an effective means to fabricate LPFGs for its potential to precisely and uniformly write gratings of very small pitch values often demanded by SDM fibers. The conversion efficiency, stability and flexibility of the three different techniques (mechanical, arc-induced and laser irradiation) ought to be compared for their

application in fiber-optic communication and sensing. Such fiber based mode converters will act as key components to provide a stable, low loss, mux/demux capability in SDM transmission.

2. Few mode fiber and advanced characterization techniques

The Brillouin experiment has allowed to extract the absolute effective refractive indices (n_{eff}) of vector modes with ~10^{-4} accuracy based on the acquired Brillouin frequency shifts of the modes. Further, the accurate characterization of these individual vector beams can be accomplished via the generation of a dynamic Brillouin grating in the few-mode fiber, an advanced metrological technique with promising applications in fiber-optic communications and distributed fiber sensing. Dynamic Brillouin grating (DBG) is a novel technique based on SBS, which has drawn significant attention over the recent years owing to its promising applications in the longitudinal characterization of optical fiber, optical amplification, for optical storage and delay lines, and for distributed optical sensing. DBG based on CVBs can be achieved by simultaneously launching two independent higher-order vector beams as CW probe waves inside the FMF and a counter-propagating pulse-modulated pump wave in the fundamental mode. The resulting two DBGs will allow us to unambiguously detect any local changes in temperature and/or strain along the FMF. This technique has potential benefits of harnessing the vector beams in the development of novel SDM characterization techniques and multi-parameter distributed fiber-optic sensors.

3. All-fiber based CVB and OAM lasers using a long period fiber grating

Active approaches towards the generation of CVB and OAM beams directly from a laser cavity have attracted lot of interests and hence being proposed by many research groups. Compared to the acoustically induced and mode selective coupler, arc induced and laser inscribed LPFG based mode converter demonstrates several advantages including broadband response, ease of fabrication and robustness. Therefore, a simple and efficient all–fiber LPFG based mode converter towards the all-fiber CVB and OAM laser generation is highly

desirable at the telecom band offering high conversion efficiency. So, the LPFG based mode converter fabricated and reported (chapter 3 of the thesis) towards CVB and OAM generation can be further utilized in the production of all-fiber based CVB and vortex lasers.

LIST OF PUBLICATIONS

Pradhan, Prabin, Dipankar Sengupta, Lixian Wang, Christine Tremblay, Sophie LaRochelle et Bora Ung. 2017. « The Brillouin gain of vector modes in a few-mode fiber ». *Scientific Reports,* vol. 7.

Pradhan, Prabin, Manish Sharma et Bora Ung. 2018. « Generation of perfect cylindrical vector beams with complete control over the ring width and ring diameter *». IEEE Photonics Journal*, vol. 10, no 1, p. 1-10.

Pradhan, Prabin, Dipankar Sengupta, Christine Tremblay et Bora Ung. 2017. « Cylindrical vector beam generation based on arc-induced long period gratings in few-mode fiber ». #JLT-23254-2018 Submitted to *Journal of lightwave technology* (2018).

Facchinello, Yann, Éric Wagnac, Bora Ung, Yvan Petit, Prabin Pradhan, Louis-Marie Peyrache et Jean-Marc Mac-Thiong. 2017. « Development of an instrumented spinal cord surrogate using optical fibers: A feasibility study ». *Medical Engineering and Physics*, vol. 48, p. 212-216.

Facchinello, Yann, Éric Wagnac, Bora Ung, Yvan Petit, Prabin Pradhan, Louis-Marie Peyrache et Jean-Marc Mac-Thiong. « The use of embedded optical fibers to assess the compression distribution within soft materials: case of an instrumented physical spinal cord surrogate ». Submitted to *IEEE Transactions on Biomedical Engineering (TBME)* in December (2017).

PROCEEDINGS IN PEER-REVIEWED CONFERENCES

Pradhan, Prabin, Dipankar Sengupta, Christine Tremblay et Bora Ung. « Small Period Gratings Written in Few-Mode Fiber Using Electric Arc Discharges ». ». *In Photonics North*, 2018. p. 1-3. IEEE.

Pradhan, Prabin, Dipankar Sengupta, Lixian Wang, Véronique Francois, Christine Tremblay, Sophie LaRochelle et Bora Ung. 2016. « Brillouin gain spectra measurement of vector modes in a few-mode fiber ». *In Lasers and Electro-Optics (CLEO), 2016 Conference on*. p. 1-2. IEEE.

Pradhan, Prabin, Dipankar Sengupta, Haythem Rehouma, Véronique Francois, Christine Tremblay et Bora Ung. 2015. « Excitation of vector modes in few-mode fiber using

wire-based mechanical long period fiber grating ». *In Photonics North*, 2015. p. 1-1. IEEE.

Facchinello, Yann, Éric Wagnac, Bora Ung, Yvan Petit, Prabin Pradhan, Louis-Marie Peyrache et Jean-Marc Mac-Thiong. 2017b. « Instrumented spinal cord surrogate using optical fiber: role of the fiber's location ». *In Biomedical Engineering (BioMed), 2017 13th IASTED International Conference on*. p. 229-232. IEEE.

Facchinello, Yann, Eric Wagnac, Bora Ung, Yvan Petit, Prabin Pradhan, Louis-Marie Peyrache et Jean-Marc Mac-Thiong. 2017a. « The development of a physical spinal cord surrogate with localized transverse compression sensing capabilities ». *In Proceedings of the 3rd World Congress on Electrical Engineering and Computer Systems and Science (EECSS'17)*: ICBES 129

Conference presentation

Pradhan, Prabin, Dipankar Sengupta, Lixian Wang, Christine Tremblay, Sophie LaRochelle et Bora Ung. 2017. « The Brillouin gain of vector modes in a few-mode fiber ». In STARACOM 2017, Montreal (poster).

Pradhan, Prabin, Dipankar Sengupta, Lixian Wang, Véronique Francois, Christine Tremblay, Sophie LaRochelle et Bora Ung. « Investigation on suppression of laser speckle noise in multimode fiber ». In IONS Quebec, 2016.

Dipankar Sengupta, Julien Duchamp, Prabin Pradhan et Bora Ung. « Investigation on suppression of laser speckle noise in multimode fiber ». In IONS Quebec, 2016 (poster).

Facchinello, Y., Wagnac E., Ung B., Petit Y., Pradhan P., Peyrache L.-M. and Mac-Thiong J.-M. (2017). Development Of An Instrumented Spinal Cord Surrogate Using Embedded Optical Fiber: A Feasibility Study. American Spinal Injury Association Annual Scientific Meeting. 29 Apr. Albuquerque, NM, USA

BIBLIOGRAPHY

Al Amin, Abdullah, An Li, Simin Chen, Xi Chen, Guanjun Gao et William Shieh. 2011. « Dual-LP 11 mode 4x4 MIMO-OFDM transmission over a two-mode fiber ». *Optics express,* vol. 19, nº 17, p. 16672-16679.

Allen, Les, Marco W Beijersbergen, RJC Spreeuw et JP Woerdman. 1992. « Orbital angular momentum of light and the transformation of Laguerre-Gaussian laser modes ». *Physical Review A,* vol. 45, nº 11, p. 8185.

Amphawan, Angela. 2011. « Holographic mode-selective launch for bandwidth enhancement in multimode fiber ». *Optics express,* vol. 19, nº 10, p. 9056-9065.

Andermahr, Niklas, et Carsten Fallnich. 2010. « Long-period fiber gratings for transverse mode conversion induced by the optical Kerr effect ». In *Conference on Lasers and Electro-Optics*. p. CWL6. Optical Society of America.

André, PS, RA Sá Ferreira, CML Correia, H Kalinowshy, Xin Xiang-Jun et JL Pinto. 2006. « Demodulating the response of optical fibre long-period gratings: genetic algorithm approach ». *Chinese Physics Letters,* vol. 23, nº 9, p. 2480.

Anemogiannis, E, Elias N Glytsis et Thomas K Gaylord. 2003. « Transmission characteristics of long-period fiber gratings having arbitrary azimuthal/radial refractive index variations ». *Journal of Lightwave Technology,* vol. 21, nº 1, p. 218.

Bae, Jun Kye, Sang Hyuck Kim, Jun Hee Kim, Jinho Bae, Sang Bae Lee et Je-Myung Jeong. 2003. « Spectral shape tunable band-rejection filter using a long-period fiber grating with divided coil heaters ». *IEEE Photonics Technology Letters,* vol. 15, nº 3, p. 407-409.

Bai, Neng, Ezra Ip, Yue-Kai Huang, Eduardo Mateo, Fatih Yaman, Ming-Jun Li, Scott Bickham, Sergey Ten, Jesús Liñares et Carlos Montero. 2012. « Mode-division multiplexed transmission with inline few-mode fiber amplifier ». *Optics express,* vol. 20, nº 3, p. 2668-2680.

Bao, Xiaoyi, et Liang Chen. 2012. « Recent progress in distributed fiber optic sensors ». *Sensors,* vol. 12, nº 7, p. 8601-8639.

Bao, Xiaoyi, David J Webb et David A Jackson. 1993. « 22-km distributed temperature sensor using Brillouin gain in an optical fiber ». *Optics letters,* vol. 18, nº 7, p. 552-554.

Blake, JN, BY Kim et HJ Shaw. 1986. « Fiber-optic modal coupler using periodic microbending ». *Optics letters,* vol. 11, nº 3, p. 177-179.

Bomzon, Ze'ev, Gabriel Biener, Vladimir Kleiner et Erez Hasman. 2002. « Radially and azimuthally polarized beams generated by space-variant dielectric subwavelength gratings ». *Optics letters,* vol. 27, nº 5, p. 285-287.

Boyd, Robert W. 2003. *Nonlinear optics*. Academic press.

Bozinovic, Nenad, Poul Kristensen et Siddharth Ramachandran. 2011. « Long-range fiber-transmission of photons with orbital angular momentum ». In *Lasers and Electro-Optics (CLEO), 2011 Conference on*. p. 1-2. IEEE.

Bozinovic, Nenad, Yang Yue, Yongxiong Ren, Moshe Tur, Poul Kristensen, Hao Huang, Alan E Willner et Siddharth Ramachandran. 2013. « Terabit-scale orbital angular momentum mode division multiplexing in fibers ». *science,* vol. 340, nº 6140, p. 1545-1548.

Bozinovic, Nenad, Yang Yue, Yongxiong Ren, Moshe Tur, Poul Kristensen, Alan Willner et Siddharth Ramachandran. 2012. « Orbital angular momentum (OAM) based mode division multiplexing (MDM) over a Km-length fiber ». In *European Conference and Exhibition on Optical Communication*. p. Th. 3. C. 6. Optical Society of America.

Brunet, Charles, Bora Ung, Lixian Wang, Younès Messaddeq, Sophie LaRochelle et Leslie A Rusch. 2015. « Design of a family of ring-core fibers for OAM transmission studies ». *Optics express,* vol. 23, nº 8, p. 10553-10563.

Brunet, Charles, Pravin Vaity, Younès Messaddeq, Sophie LaRochelle et Leslie A Rusch. 2014. « Design, fabrication and validation of an OAM fiber supporting 36 states ». *Optics express,* vol. 22, nº 21, p. 26117-26127.

Carboni, Christian, et Guifang Li. 2016. « Novel applications of space-division multiplexing ». *Frontiers of Optoelectronics,* vol. 9, nº 2, p. 270-276.

Chen, Haoshuo, et AMJ Ton Koonen. 2017. « Spatial division multiplexing ». In *Fibre Optic Communication*. p. 1-48. Springer.

Chen, Ming-Yang, et Jun Zhou. 2014. « Design of add-drop multiplexer based on multi-core optical fibers for mode-division multiplexing ». *Optics express,* vol. 22, nº 2, p. 1440-1451.

Chen, Mingzhou, Michael Mazilu, Yoshihiko Arita, Ewan M Wright et Kishan Dholakia. 2013a. « Dynamics of microparticles trapped in a perfect vortex beam ». *Optics letters,* vol. 38, nº 22, p. 4919-4922.

Chen, Ruishan, Jinghao Wang, Xiaoqiang Zhang, Anting Wang, Hai Ming, Feng Li, Dick Chung et Qiwen Zhan. 2018. « High efficiency all-fiber cylindrical vector beam laser using a long-period fiber grating ». *Optics letters,* vol. 43, nº 4, p. 755-758.

Chen, Xi, An Li, Jia Ye, Abdullah Al Amin et William Shieh. 2012. « Reception of mode-division multiplexed superchannel via few-mode compatible optical add/drop multiplexer ». *Optics express,* vol. 20, nº 13, p. 14302-14307.

Chen, Xi, An Li, Jia Ye, Abdullah Al Amin et William Shieh. 2013b. « Demonstration of few-mode compatible optical add/drop multiplexer for mode-division multiplexed superchannel ». *Journal of Lightwave Technology,* vol. 31, nº 4, p. 641-647.

Chen, Yingkan, Adriana Lobato, Yongming Jung, Haoshuo Chen, Vincent AJM Sleiffer, Maxim Kuschnerov, Nicolas K Fontaine, Roland Ryf, David J Richardson et Berthold Lankl. 2015a. « 41.6 Tbit/s C-Band SDM OFDM transmission through 12 spatial and polarization modes over 74.17 km few mode fiber ». *Journal of Lightwave Technology,* vol. 33, nº 7, p. 1440-1444.

Chen, Yue, Zhao-Xiang Fang, Yu-Xuan Ren, Lei Gong et Rong-De Lu. 2015b. « Generation and characterization of a perfect vortex beam with a large topological charge through a digital micromirror device ». *Applied Optics,* vol. 54, nº 27, p. 8030-8035.

Cheng, Ji, Martin EV Pedersen, Ke Wang, Chris Xu, Lars Grüner-Nielsen et Dan Jakobsen. 2012. « Time-domain multimode dispersion measurement in a higher-order-mode fiber ». *Optics letters,* vol. 37, nº 3, p. 347-349.

Chiao, RY, CH Townes et BP Stoicheff. 1964. « Stimulated Brillouin scattering and coherent generation of intense hypersonic waves ». *Physical Review Letters,* vol. 12, nº 21, p. 592.

Colaço, Celso, Paulo Caldas, Ignacio Del Villar, Rui Chibante et Gaspar Rego. 2016. « Arc-induced long-period fiber gratings in the dispersion turning points ». *Journal of Lightwave Technology,* vol. 34, nº 19, p. 4584-4590.

Cotter, D. 1983. « Stimulated Brillouin scattering in monomode optical fiber ». *Journal of Optical Communications,* vol. 4, nº 1, p. 10-19.

DeLisa, Matthew P, Zheng Zhang, Mira Shiloach, Saeed Pilevar, Christopher C Davis, James S Sirkis et William E Bentley. 2000. « Evanescent wave long-period fiber Bragg grating as an immobilized antibody biosensor ». *Analytical chemistry,* vol. 72, nº 13, p. 2895-2900.

Denisov, Andrey. 2015. « Brillouin dynamic gratings in optical fibres for distributed sensing and advanced optical signal processing ».

Dennis, Mark R, Kevin O'Holleran et Miles J Padgett. 2009. « Singular optics: optical vortices and polarization singularities ». In *Progress in Optics*. Vol. 53, p. 293-363. Elsevier.

Dianov, EM, VI Karpov, MV Grekov, KM Golant, SA Vasiliev, OI Medvedkov et RR Khrapko. 1997. « Thermo-induced long-period fibre gratings ». In *Integrated Optics and Optical Fibre Communications, 11th International Conference on, and 23rd European Conference on Optical Communications (Conf. Publ. No.: 448)*. Vol. 2, p. 53-56. IET.

Dobb, H, Kyriacos Kalli et David J Webb. 2006. « Measured sensitivity of arc-induced long-period grating sensors in photonic crystal fibre ». *Optics Communications,* vol. 260, nº 1, p. 184-191.

Dong, Jiangli, et Kin Seng Chiang. 2015. « Temperature-insensitive mode converters with CO 2-laser written long-period fiber gratings ». *IEEE Photonics Technology Letters,* vol. 27, nº 9, p. 1006-1009.

Dorn, Ralf, S Quabis et G Leuchs. 2003. « Sharper focus for a radially polarized light beam ». *Physical review letters,* vol. 91, nº 23, p. 233901.

Dragic, Peter D. 2010. « The Acoustic Velocity of Ge-Doped Silica Fibers: A Comparison of Two Models ». *International Journal of Applied Glass Science,* vol. 1, nº 3, p. 330-337.

Du, Chao, Qi Wang et Yong Zhao. 2018. « Long-period fiber grating sensor induced by electric-arc discharge for dual-parameter measurement ». *Instrumentation Science & Technology,* vol. 46, nº 1, p. 1-11.

Duocastella, Marti, et Craig B Arnold. 2012. « Bessel and annular beams for materials processing ». *Laser & Photonics Reviews,* vol. 6, nº 5, p. 607-621.

Esposito, Flavio, Rajeev Ranjan, Stefania Campopiano et Agostino Iadicicco. 2017. « Experimental study of the refractive index sensitivity in arc-induced long period gratings ». *IEEE Photonics Journal,* vol. 9, nº 1, p. 1-10.

Esposito, Flavio, Rajeev Ranjan, Stefania Campopiano et Agostino Iadicicco. 2018. « Arc-Induced Long Period Gratings from Standard to Polarization-Maintaining and Photonic Crystal Fibers ». *Sensors,* vol. 18, nº 3, p. 918.

Essiambre, R-J, R Ryf, NK Fontaine et S Randel. 2013. « Breakthroughs in photonics 2012: Space-division multiplexing in multimode and multicore fibers for high-capacity optical communication ». *IEEE Photonics Journal,* vol. 5, nº 2, p. 0701307-0701307.

Essiambre, René-Jean, et Robert W Tkach. 2012. « Capacity trends and limits of optical communication networks ». *Proceedings of the IEEE,* vol. 100, nº 5, p. 1035-1055.

Eznaveh, Z Sanjabi, JE Antonio-Lopez, JC Alvarado Zacarias, A Schülzgen, CM Okonkwo et R Amezcua Correa. 2017. « All-fiber few-mode multicore photonic lantern mode multiplexer ». *Optics Express,* vol. 25, nº 14, p. 16701-16707.

Fang, Zhiqiang, Yao Yao, Kegui Xia, Minqiang Kang, Ken-ichi Ueda et Jianlang Li. 2013. « Vector mode excitation in few-mode fiber by controlling incident polarization ». *Optics Communications,* vol. 294, p. 177-181.

Ferreira, Filipe M, Daniel Fonseca et Henrique JA da Silva. 2014. « Design of few-mode fibers with M-modes and low differential mode delay ». *Journal of Lightwave Technology,* vol. 32, nº 3, p. 353-360.

Florez, Omar, Paulo F Jarschel, Yovanny AV Espinel, CMB Cordeiro, TP Mayer Alegre, Gustavo S Wiederhecker et Paulo Dainese. 2016. « Brillouin scattering self-cancellation ». *Nature communications,* vol. 7, p. 11759.

Fontaine, Nicolas K, Roland Ryf, Haoshuo Chen, Amado Velazquez Benitez, JE Antonio Lopez, R Amezcua Correa, Binbin Guan, Burcu Ercan, Ryan P Scott et SJ Ben Yoo. 2015. « 30× 30 MIMO transmission over 15 spatial modes ». In *Optical Fiber Communications Conference and Exhibition (OFC), 2015*. p. 1-3. IEEE.

Fu, Shiyao, Tonglu Wang et Chunqing Gao. 2016. « Generating perfect polarization vortices through encoding liquid-crystal display devices ». *Applied optics,* vol. 55, nº 23, p. 6501-6505.

Gabet, Renaud, Elodie Le Cren, C Jin, M Gadonna, Bora Ung, P Sillard, HG Nguyen, Y Jaouën, Monique Thual et S LaRochelle. 2015. « Complete dispersion characterization of few mode fibers by OLCI technique ». *Journal of Lightwave Technology,* vol. 33, nº 6, p. 1155-1160.

Genevaux, Philippe, Christian Simonneau, Guillaume Le Cocq, Yves Quiquempois, Laurent Bigot, Jean-François Morizur et Gabriel Charlet. 2015. « Amplification of 5 modes carrying each 100Gb/s with a few mode EDFA ». In *Optical Fiber Communications Conference and Exhibition (OFC), 2015*. p. 1-3. IEEE.

Gökhan, Fİkrİ Serdar, Hasan Göktaş et Volker J Sorger. 2018. « Analytical approach of Brillouin amplification over threshold ». *Applied optics,* vol. 57, nº 4, p. 607-611.

Grüner-Nielsen, Lars, Yi Sun, Rasmus V Jensen, Jeffrey W Nicholson et Robert Lingle. 2015. « Recent advances in low DGD few-mode fiber design, fabrication, characterization and experiments ». In *Optical Fiber Communications Conference and Exhibition (OFC), 2015*. p. 1-3. IEEE.

Han, Ya, Yan-Ge Liu, Wei Huang, Zhi Wang, Jun-Qi Guo et Ming-Ming Luo. 2016. « Generation of linearly polarized orbital angular momentum modes in a side-hole ring fiber with tunable topology numbers ». *Optics express,* vol. 24, nº 15, p. 17272-17284.

Horiguchi, Tsuneo, et Mitsuhiro Tateda. 1989. « BOTDA-nondestructive measurement of single-mode optical fiber attenuation characteristics using Brillouin interaction: Theory ». *Journal of lightwave technology,* vol. 7, nº 8, p. 1170-1176.

Hotate, Kazuo, et Takemi Hasegawa. 2000. « Measurement of Brillouin Gain Spectrum Distribution along an Optical Fiber Using a Correlation-Based Technique--Proposal, Experiment and Simulation ». *IEICE transactions on electronics,* vol. 83, nº 3, p. 405-412.

Huang, Hao, Giovanni Milione, Martin PJ Lavery, Guodong Xie, Yongxiong Ren, Yinwen Cao, Nisar Ahmed, Thien An Nguyen, Daniel A Nolan et Ming-Jun Li. 2015. « Mode division multiplexing using an orbital angular momentum mode sorter and MIMO-DSP over a graded-index few-mode optical fibre ». *Scientific reports,* vol. 5, p. 14931.

Huang, Wei-Bo, Li-Wei Liu, Yu-Li Wang, Wen-Fung Liu et Cheng-Ling Lee. 2010. « Dispersion control in liquid core arc-induced long-period fiber gratings ». In *OptoElectronics and Communications Conference (OECC), 2010 15th*. p. 656-657. IEEE.

Iadicicco, Agostino, Stefania Campopiano et Andrea Cusano. 2011. « Long-period gratings in hollow core fibers by pressure-assisted arc discharge technique ». *IEEE Photonics Technology Letters,* vol. 23, nº 21, p. 1567-1569.

Iadicicco, Agostino, Rajeev Ranjan et Stefania Campopiano. 2015. « Fabrication and characterization of long-period gratings in hollow core fibers by electric arc discharge ». *IEEE Sensors Journal,* vol. 15, nº 5, p. 3014-3020.

Idachaba, Francis, Dike U Ike et Orovwode Hope. 2014. « Future trends in fiber optics communication ». In *Proceedings of the World Congress on Engineering*. Vol. 1, p. 2-4.

Igarashi, Koji, Takehiro Tsuritani et Itsuro Morita. 2016. « Ultra-high-capacity transmission over few-mode multi-core fibers ». In *OptoElectronics and Communications Conference (OECC) held jointly with 2016 International Conference on Photonics in Switching (PS), 2016 21st*. p. 1-3. IEEE.

Igarashi, Koji, Takehiro Tsuritani, Itsuro Morita, Yukihiro Tsuchida, Koichi Maeda, Masateru Tadakuma, Tsunetoshi Saito, Kengo Watanabe, Katsunori Imamura et

Ryuichi Sugizaki. 2013. « 1.03-Exabit/skm Super-Nyquist-WDM transmission over 7,326-km seven-core fiber ». In *Optical Communication (ECOC 2013), 39th European Conference and Exhibition on*. p. 1-3. IET.

Ivanov, OV, et G Rego. 2007. « Origin of coupling to antisymmetric modes in arc-induced long-period fiber gratings ». *Optics Express,* vol. 15, nº 21, p. 13936-13941.

Jabir, MV, N Apurv Chaitanya, A Aadhi et GK Samanta. 2016. « Generation of "perfect" vortex of variable size and its effect in angular spectrum of the down-converted photons ». *Scientific reports,* vol. 6.

Karahroudi, Mahdi Khodadadi, Bahman Parmoon, Mohammadreza Qasemi, Abolhasan Mobashery et Hossein Saghafifar. 2017. « Generation of perfect optical vortices using a Bessel–Gaussian beam diffracted by curved fork grating ». *Applied optics,* vol. 56, nº 21, p. 5817-5823.

Kasahara, Motoki, Kunimasa Saitoh, Taiji Sakamoto, Nobutomo Hanzawa, Takashi Matsui, Kyozo Tsujikawa et Fumihiko Yamamoto. 2014. « Design of three-spatial-mode ring-core fiber ». *Journal of lightwave technology,* vol. 32, nº 7, p. 1337-1343.

Kim, BY, JN Blake, HE Engan et HJ Shaw. 1986. « All-fiber acousto-optic frequency shifter ». *Optics Letters,* vol. 11, nº 6, p. 389-391.

Kim, Byoung Yoon, James N Blake, Shang-Yuan Huang et Herbert J Shaw. 1987. « Use of highly elliptical core fibers for two-mode fiber devices ». *Optics Letters,* vol. 12, nº 9, p. 729-731.

Kim, Yong Hyun, et Kwang Yong Song. 2014. « Mapping of intermodal beat length distribution in an elliptical-core two-mode fiber based on Brillouin dynamic grating ». *Optics express,* vol. 22, nº 14, p. 17292-17302.

Kitayama, Ken-ichi, et Nikolaos-Panteleimon Diamantopoulos. 2017. « Few-mode optical fibers: Original motivation and recent progress ». *IEEE Communications Magazine,* vol. 55, nº 8, p. 163-169.

Kozawa, Yuichi, et Shunichi Sato. 2010. « Optical trapping of micrometer-sized dielectric particles by cylindrical vector beams ». *Optics Express,* vol. 18, nº 10, p. 10828-10833.

Kozawa, Yuichi, et Shunichi Sato. 2015. « Numerical analysis of resolution enhancement in laser scanning microscopy using a radially polarized beam ». *Optics Express,* vol. 23, nº 3, p. 2076-2084.

Lee, Jonghun, Cherl-Hee Lee, Kwang Taek Kim et Jaehee Park. 2013. « Fabrication and Mode Coupling of Long-Period Fiber Grating by Winding a Wire Around an Optical Fiber Fixe
d to a Cylindrical Metal Rod ». In *Current Trends in Short-and Long-period Fiber Gratings*. InTech.

Li, An, Abdullah Al Amin, Xi Chen et William Shieh. 2011a. « Transmission of 107-Gb/s mode and polarization multiplexed CO-OFDM signal over a two-mode fiber ». *Optics Express,* vol. 19, nº 9, p. 8808-8814.

Li, An, Xi Chen, Abdullah Al Amin, Jia Ye et William Shieh. 2012. « Space-division multiplexed high-speed superchannel transmission over few-mode fiber ». *Journal of Lightwave Technology,* vol. 30, nº 24, p. 3953-3964.

Li, An, Qian Hu, Xi Chen, Byoung Yoon Kim et William Shieh. 2014. « Characterization of distributed modal birefringence in a few-mode fiber based on Brillouin dynamic grating ». *Optics letters,* vol. 39, nº 11, p. 3153-3156.

Li, An, Qian Hu et William Shieh. 2013. « Characterization of stimulated Brillouin scattering in a circular-core two-mode fiber using optical time-domain analysis ». *Optics Express,* vol. 21, nº 26, p. 31894-31906.

Li, An, Yifei Wang, Jian Fang, Ming-Jun Li, Byoung Yoon Kim et William Shieh. 2015. « Few-mode fiber multi-parameter sensor with distributed temperature and strain discrimination ». *Optics letters,* vol. 40, nº 7, p. 1488-1491.

Li, Benye, Lan Jiang, Sumei Wang, Hai-Lung Tsai et Hai Xiao. 2011b. « Femtosecond laser fabrication of long period fiber gratings and applications in refractive index sensing ». *Optics & Laser Technology,* vol. 43, nº 8, p. 1420-1423.

Li, Jianping, Jianbo Zhang, Fan Li, Xincheng Huang, Shecheng Gao et Zhaohui Li. 2018. « DD-OFDM transmission over few-mode fiber based on direct vector mode multiplexing ». *Optics express,* vol. 26, nº 14, p. 18749-18757.

Li, Peng, Yi Zhang, Sheng Liu, Chaojie Ma, Lei Han, Huachao Cheng et Jianlin Zhao. 2016. « Generation of perfect vectorial vortex beams ». *Optics Letters,* vol. 41, nº 10, p. 2205-2208.

Li, Shenping, Ming-Jun Li et Richard S Vodhanel. 2012. « All-optical Brillouin dynamic grating generation in few-mode optical fiber ». *Optics letters,* vol. 37, nº 22, p. 4660-4662.

Liu, Jun, Shi-Mao Li, Long Zhu, An-Dong Wang, Shi Chen, Charalambos Klitis, Cheng Du, Qi Mo, Marc Sorel et Si-Yuan Yu. 2018. « Direct fiber vector eigenmode

multiplexing transmission seeded by integrated optical vortex emitters ». *Light: Science & Applications,* vol. 7, nº 3, p. 17148.

Liu, Yachao, Yougang Ke, Junxiao Zhou, Yuanyuan Liu, Hailu Luo, Shuangchun Wen et Dianyuan Fan. 2017a. « Generation of perfect vortex and vector beams based on Pancharatnam-Berry phase elements ». *Scientific Reports,* vol. 7, p. 44096.

Liu, Yachao, Yougang Ke, Junxiao Zhou, Yuanyuan Liu, Hailu Luo, Shuangchun Wen et Dianyuan Fan. 2017b. « Generation of perfect vortex and vector beams based on Pancharatnam-Berry phase elements ». *Scientific Reports,* vol. 7.

Luís, Ruben S, Georg Rademacher, Benjamin J Puttnam, Yoshinari Awaji et Naoya Wada. 2018. « Long distance crosstalk-supported transmission using homogeneous multicore fibers and SDM-MIMO demultiplexing ». *Optics express,* vol. 26, nº 18, p. 24044-24053.

Ma, Haixiang, Xinzhong Li, Yuping Tai, Hehe Li, Jingge Wang, Miaomiao Tang, Yishan Wang, Jie Tang et Zhaogang Nie. 2017. « In situ measurement of the topological charge of a perfect vortex using the phase shift method ». *Optics Letters,* vol. 42, nº 1, p. 135-138.

Maione, TL, DD Sell et DH Wolaver. 1978. « Atlanta Fiber System Experiment: Practical 45-Mb/s Regenerator for Lightwave Transmission ». *Bell Labs Technical Journal,* vol. 57, nº 6, p. 1837-1856.

Martinez-Rios, A, D Monzon-Hernandez et I Torres-Gomez. 2010. « Highly sensitive cladding-etched arc-induced long-period fiber gratings for refractive index sensing ». *Optics Communications,* vol. 283, nº 6, p. 958-962.

Masri, Gilad, Shir Shahal, Avi Klein, Hamootal Duadi et Moti Fridman. 2016. « Polarization dependence of asymmetric off-resonance long period fiber gratings ». *Optics express,* vol. 24, nº 26, p. 29843-29851.

Maurer, Christian, Alexander Jesacher, Severin Fürhapter, Stefan Bernet et Monika Ritsch-Marte. 2007. « Tailoring of arbitrary optical vector beams ». *New Journal of Physics,* vol. 9, nº 3, p. 78.

Milione, Giovanni, Angela Dudley, Thien An Nguyen, Ougni Chakraborty, Ebrahim Karimi, Andrew Forbes et Robert R Alfano. 2014. « Experimental measurement of the self-healing of the spatially inhomogeneous states of polarization of radially and azimuthally polarized vector Bessel beams ». *arXiv preprint arXiv:1412.2722*.

Milione, Giovanni, Angela Dudley, Thien An Nguyen, Ougni Chakraborty, Ebrahim Karimi, Andrew Forbes et Robert R Alfano. 2015. « Measuring the self-healing of the

spatially inhomogeneous states of polarization of vector Bessel beams ». *Journal of Optics,* vol. 17, nº 3, p. 035617.

Minardo, Aldo, Romeo Bernini et Luigi Zeni. 2014. « Experimental and numerical study on stimulated Brillouin scattering in a graded-index multimode fiber ». *Optics express,* vol. 22, nº 14, p. 17480-17489.

Mizrahi, V, T Erdogan, DJ DiGiovanni, PJ Lemaire, WM MacDonald, SG Kosinski, S Cabot et JE Sipe. 1994. « Four channel fibre grating demultiplexer ». *Electronics letters,* vol. 30, nº 10, p. 780-781.

Mizuno, Takayuki, Takayuki Kobayashi, Hidehiko Takara, Akihide Sano, Hiroto Kawakami, Tadao Nakagawa, Yutaka Miyamoto, Yoshiteru Abe, Takashi Goh et Manabu Oguma. 2014. « 12-core x 3-mode dense space division multiplexed transmission over 40 km employing multi-carrier signals with parallel MIMO equalization ». In *Optical Fiber Communication Conference*. p. Th5B. 2. Optical Society of America.

Mizuno, Takayuki, Hidehiko Takara, Akihide Sano et Yutaka Miyamoto. 2015. « Dense Space Division Multiplexed Transmission Technology ». In *CLEO: 2015*. (San Jose, California, 2015/05/10), p. SW4M.1. Coll. « OSA Technical Digest (online) »: Optical Society of America.
< http://www.osapublishing.org/abstract.cfm?URI=CLEO_SI-2015-SW4M.1 >.

Mizuno, Takayuki, Hidehiko Takara, Akihide Sano et Yutaka Miyamoto. 2016. « Dense space-division multiplexed transmission systems using multi-core and multi-mode fiber ». *Journal of lightwave technology,* vol. 34, nº 2, p. 582-592.

Mizuno, Yosuke, Zuyuan He et Kazuo Hotate. 2009. « One-end-access high-speed distributed strain measurement with 13-mm spatial resolution based on Brillouin optical correlation-domain reflectometry ». *IEEE Photonics Technology Letters,* vol. 21, nº 7, p. 474-476.

Nejad, Reza Mirzaei, Karen Allahverdyan, Pravin Vaity, Siamak Amiralizadeh, Charles Brunet, Younès Messaddeq, Sophie LaRochelle et Leslie Ann Rusch. 2016. « Mode division multiplexing using orbital angular momentum modes over 1.4-km ring core fiber ». *Journal of Lightwave Technology,* vol. 34, nº 18, p. 4252-4258.

Nejad, Reza Mirzaei, Lixian Wang, Xun Guan, Sophie LaRochelle et Leslie A Rusch. 2018. « Four-Channel RoF Transmission over Polarization Maintaining Elliptical Ring Core Fiber ». In *Optical Fiber Communication Conference*. p. M4J. 6. Optical Society of America.

Nemova, Galina, et Raman Kashyap. 2008. « High-power long-period-grating-assisted erbium-doped fiber amplifier ». *JOSA B,* vol. 25, nº 8, p. 1322-1327.

Nguyen, Duc Minh, Stéphane Blin, Thanh Nam Nguyen, Sy Dat Le, Laurent Provino, Monique Thual et Thierry Chartier. 2012. « Modal decomposition technique for multimode fibers ». *Applied optics,* vol. 51, nº 4, p. 450-456.

Nicholson, Jeffrey W, S Ramachandran, S Ghalmi, E Monberg, F DiMarcello, M Yan, P Wisk et J Fleming. 2003a. « Characterization of dispersion in higher order mode fibers using electrical spectrum measurements ». In *Optical Fiber Communication Conference*. p. FK8. Optical Society of America.

Nicholson, JW, S Ramachandran, S Ghalmi, EA Monberg, FV DiMarcello, MF Yan, P Wisk et JW Fleming. 2003b. « Electrical spectrum measurements of dispersion in higher order mode fibers ». *IEEE Photonics technology letters,* vol. 15, nº 6, p. 831-833.

Niederriter, Robert, Mark E Siemens et Juliet Gopinath. 2015. « Fiber optic sensors based on orbital angular momentum ». In *CLEO: Science and Innovations*. p. SM1L. 5. Optical Society of America.

Nikles, Marc, Luc Thevenaz et Philippe A Robert. 1997. « Brillouin gain spectrum characterization in single-mode optical fibers ». *Journal of Lightwave Technology,* vol. 15, nº 10, p. 1842-1851.

Olsson, NA, et JP Van der Ziel. 1986. « Cancellation of fiber loss by semiconductor laser pumped Brillouin amplification at 1.5 μm ». *Applied physics letters,* vol. 48, nº 20, p. 1329-1330.

Ostrovsky, Andrey S, Carolina Rickenstorff-Parrao et Víctor Arrizón. 2013. « Generation of the "perfect" optical vortex using a liquid-crystal spatial light modulator ». *Optics letters,* vol. 38, nº 4, p. 534-536.

Pan, Zhongqi, Yi Weng et Junyi Wang. 2015. « Investigation of nonlinear effects in few-mode fibers ». *Photonic Network Communications*, p. 1-11.

Poole, CD, HM Presby et JP Meester. 1994. « Two-mode fibre spatial-mode converter using periodic core deformation ». *Electronics Letters,* vol. 30, nº 17, p. 1437-1438.

Porfirev, Alexey P, Andrey V Ustinov et Svetlana N Khonina. 2016. « Polarization conversion when focusing cylindrically polarized vortex beams ». *Scientific Reports,* vol. 6, nº 1, p. 6.

Pradhan, Prabin, Dipankar Sengupta, Haythem Rehouma, Véronique Francois, Christine Tremblay et Bora Ung. 2015. « Excitation of vector modes in few-mode fiber using wire-based mechanical long period fiber grating ». In *Photonics North, 2015*. p. 1-1. IEEE.

Pradhan, Prabin, Dipankar Sengupta, Lixian Wang, Christine Tremblay, Sophie LaRochelle et Bora Ung. 2017a. « The Brillouin gain of vector modes in a few-mode fiber ». *Scientific Reports,* vol. 7.

Pradhan, Prabin, Dipankar Sengupta, Lixian Wang, Christine Tremblay, Sophie LaRochelle et Bora Ung. 2017b. « The Brillouin gain of vector modes in a few-mode fiber ». *Scientific Reports,* vol. 7, nº 1, p. 1552.

Pradhan, Prabin, Manish Sharma et Bora Ung. 2018. « Generation of perfect cylindrical vector beams with complete control over the ring width and ring diameter ». *IEEE Photonics Journal,* vol. 10, nº 1, p. 1-10.

Qian, Dayou, Ezra Ip, Ming-Fang Huang, Ming-jun Li, Arthur Dogariu, Shaoliang Zhang, Yin Shao, Yue-Kai Huang, Yequn Zhang et Xilin Cheng. 2012. « 1.05 Pb/s transmission with 109b/s/Hz spectral efficiency using hybrid single-and few-mode cores ». In *Frontiers in Optics*. p. FW6C. 3. Optical Society of America.

Rademacher, Georg, Ruben S Luís, Benjamin J Puttnam, Tobias A Eriksson, Erik Agrell, Ryo Maruyama, Kazuhiko Aikawa, Hideaki Furukawa, Yoshinari Awaji et Naoya Wada. 2018a. « 159 Tbit/s C+ L Band Transmission over 1045 km 3-Mode Graded-Index Few-Mode Fiber ». In *Optical Fiber Communication Conference*. p. Th4C. 4. Optical Society of America.

Rademacher, Georg, Roland Ryf, Nicolas K Fontaine, Haoshuo Chen, René-Jean Essiambre, Benjamin J Puttnam, Ruben S Luís, Yoshinari Awaji, Naoya Wada et Simon Gross. 2018b. « Long-Haul Transmission Over Few-Mode Fibers With Space-Division Multiplexing ». *Journal of Lightwave Technology,* vol. 36, nº 6, p. 1382-1388.

Ramachandran, S, M Das, Z Wang, J Fleming et M Yan. 2002. « High extinction, broadband polarisers using long-period fibre gratings in few-mode fibres ». *Electronics Letters,* vol. 38, nº 22, p. 1327-1328.

Ramachandran, S, S Golowich, MF Yan, E Monberg, FV Dimarcello, J Fleming, S Ghalmi et P Wisk. 2005. « Lifting polarization degeneracy of modes by fiber design: a platform for polarization-insensitive microbend fiber gratings ». *Optics letters,* vol. 30, nº 21, p. 2864-2866.

Ramachandran, Siddharth, et Poul Kristensen. 2013. « Optical vortices in fiber ». *Nanophotonics,* vol. 2, nº 5-6, p. 455-474.

Ramachandran, Siddharth, Poul Kristensen et Man F Yan. 2009. « Generation and propagation of radially polarized beams in optical fibers ». *Optics letters,* vol. 34, nº 16, p. 2525-2527.

Rego, G, O Okhotnikov, E Dianov et V Sulimov. 2001. « High-temperature stability of long-period fiber gratings produced using an electric arc ». *Journal of Lightwave Technology,* vol. 19, nº 10, p. 1574.

Rego, Gaspar. 2016. « Arc-Induced Long Period Fiber Gratings ». *Journal of Sensors,* vol. 2016, p. 14.

Rego, Gaspar, et Oleg Ivanov. 2011. « Investigation of the mechanisms of formation of long-period gratings arc-induced in pure-silica-core fibres ». *Optics Communications,* vol. 284, nº 8, p. 2137-2140.

Rego, Gaspar, Oleg V Ivanov et Paulo VS Marques. 2006. « Demonstration of coupling to symmetric and antisymmetric cladding modes in arc-induced long-period fiber gratings ». *Optics Express,* vol. 14, nº 21, p. 9594-9599.

Rego, Gaspar, PVS Marques, JL Santos et HM Salgado. 2005. « Arc-induced long-period gratings ». *Fiber and Integrated Optics,* vol. 24, nº 3-4, p. 245-259.

Ren, Fang, Juhao Li, Zhongying Wu, Jinyi Yu, Qi Mo, Jianping Wang, Yongqi He, Zhangyuan Chen et Zhengbin Li. 2017. « All-fiber optical mode switching based on cascaded mode selective couplers for short-reach MDM networks ». *Optical Engineering,* vol. 56, nº 4, p. 046104.

Richardson, DJ, JM Fini et LE Nelson. 2013. « Space-division multiplexing in optical fibres ». *Nature Photonics,* vol. 7, nº 5, p. 354.

Ryf, Roland, H Chen, NK Fontaine, AM Velazquez-Benitez, Jose Antonio-Lopez, C Jin, B Huang, M Bigot-Astruc, D Molin et F Achten. 2015. « 10-mode mode-multiplexed transmission over 125-km single-span multimode fiber ». In *Optical Communication (ECOC), 2015 European Conference on*. p. 1-3. IEEE.

Ryf, Roland, Sebastian Randel, Nicolas K Fontaine, Marc Montoliu, Ellsworth Burrows, Sethumadhavan Chandrasekhar, Alan H Gnauck, Chongjin Xie, Rene-Jean Essiambre et Peter Winzer. 2013. « 32-bit/s/Hz spectral efficiency WDM transmission over 177-km few-mode fiber ». In *Optical fiber communication conference*. p. PDP5A. 1. Optical Society of America.

Ryf, Roland, Sebastian Randel, Alan H Gnauck, Cristian Bolle, Alberto Sierra, Sami Mumtaz, Mina Esmaeelpour, Ellsworth C Burrows, René-Jean Essiambre et Peter J Winzer. 2012. « Mode-Division Multiplexing Over 96 km of Few-Mode Fiber Using Coherent 6$\,\times\, $6 MIMO Processing ». *Journal of Lightwave technology,* vol. 30, nº 4, p. 521-531.

Sakaguchi, J, BJ Puttnam, W Klaus, Y Awaji, N Wada, A Kanno et T Kawanishi. 2012a. « SDM technology beyond 100 Tb/s ». In *Opto-Electronics and Communications Conference (OECC), 2012 17th*. p. 553-554. IEEE.

Sakaguchi, Jun, Benjamin J Puttnam, Werner Klaus, Yoshinari Awaji, Naoya Wada, Atsushi Kanno, Tetsuya Kawanishi, Katsunori Imamura, Harumi Inaba et Kazunori Mukasa. 2012b. « 19-core fiber transmission of 19x100x172-Gb/s SDM-WDM-PDM-QPSK signals at 305Tb/s ». In *Optical Fiber Communication Conference*. p. PDP5C. 1. Optical Society of America.

Salsi, Massimiliano, David Peyrot, Gabriel Charlet, Sébastien Bigo, Roland Ryf, Nicolas K Fontaine, Miquel A Mestre, Sebastian Randel, Xavi Palou et Cristion Bolle. 2012. « A six-mode erbium-doped fiber amplifier ». In *European Conference and Exhibition on Optical Communication*. p. Th. 3. A. 6. Optical Society of America.

Santagiustina, M, G Eisenstein, Luc Thévenaz, J Capmany, J Mork, JP Reithmaier, A De Rossi, S Sales, Kresten Yvind et S Combrie. 2012. « Slow light devices and their applications to microwaves and photonics ». *IEEE Photonics Society Newsletter,* vol. 26, nº EPFL-REVIEW-174930, p. 5-12.

Savin, S, MJF Digonnet, GS Kino et HJ Shaw. 2000. « Tunable mechanically induced long-period fiber gratings ». *Optics letters,* vol. 25, nº 10, p. 710-712.

Shibahara, Kohki, Takayuki Mizuno, Doohwan Lee et Yutaka Miyamoto. 2018. « Advanced MIMO Signal Processing Techniques Enabling Long-Haul Dense SDM Transmissions ». *Journal of Lightwave Technology,* vol. 36, nº 2, p. 336-348.

Sillard, Pierre, Marianne Astruc, David Boivin, Hélène Maerten et Lionel Provost. 2011. « Few-mode fiber for uncoupled mode-division multiplexing transmissions ». In *European Conference and Exposition on Optical Communications*. p. Tu. 5. LeCervin. 7. Optical Society of America.

Sleiffer, VAJM, Yongmin Jung, Vladimir Veljanovski, RGH Van Uden, Maxim Kuschnerov, H Chen, B Inan, L Grüner Nielsen, Y Sun et David J Richardson. 2012. « 73.7 Tb/s (96 x 3 x 256-Gb/s) mode-division-multiplexed DP-16QAM transmission with inline MM-EDFA ». *Optics Express,* vol. 20, nº 26, p. B428-B438.

Smietana, M, WJ Bock et P Mikulic. 2010. « Comparative study of long-period gratings written in a boron co-doped fiber by an electric arc and UV irradiation ». *Measurement Science and Technology,* vol. 21, nº 2, p. 025309.

Smietana, M, WJ Bock, P Mikulic et J Chen. 2010. « Increasing sensitivity of arc-induced long-period gratings—pushing the fabrication technique toward its limits ». *Measurement Science and Technology,* vol. 22, nº 1, p. 015201.

Snyder, Allan W, et John Love. 2012. *Optical waveguide theory*. Springer Science & Business Media.

Soma, Daiki, Shohei Beppu, Yuta Wakayama, Koji Igarashi, Takehiro Tsuritani, Itsuro Morita et Masatoshi Suzuki White Box GE. 2018a. « 257-Tbit/s Weakly-coupled 10-Mode C+ L-band WDM Transmission ». *Journal of Lightwave Technology*.

Soma, Daiki, Yuta Wakayama, Shohei Beppu, Seiya Sumita, Takehiro Tsuritani, Tetsuya Hayashi, Takuji Nagashima, Masato Suzuki, Masato Yoshida et Keisuke Kasai. 2018b. « 10.16-Peta-B/s Dense SDM/WDM Transmission Over 6-Mode 19-Core Fiber Across the C+ L Band ». *Journal of Lightwave Technology,* vol. 36, nº 6, p. 1362-1368.

Song, Kwang-Yong, Kwanil Lee, Hyuk-Jin Yoon et Sang Bae Lee. 2009. « Tunable optical delays based on Brillouin dynamic grating in a polarization maintaining fiber ». In *20th International Conference on Optical Fibre Sensors*. Vol. 7503, p. 75037L. International Society for Optics and Photonics.

Song, Kwang Yong. 2011. « Operation of Brillouin dynamic grating in single-mode optical fibers ». *Optics letters,* vol. 36, nº 23, p. 4686-4688.

Song, Kwang Yong, et Yong Hyun Kim. 2013. « Characterization of stimulated Brillouin scattering in a few-mode fiber ». *Optics letters,* vol. 38, nº 22, p. 4841-4844.

Song, Kwang Yong, Yong Hyun Kim et Byoung Yoon Kim. 2013. « Intermodal stimulated Brillouin scattering in two-mode fibers ». *Optics letters,* vol. 38, nº 11, p. 1805-1807.

Song, Kwang Yong, et Hyuk Jin Yoon. 2010. « High-resolution Brillouin optical time domain analysis based on Brillouin dynamic grating ». *Optics letters,* vol. 35, nº 1, p. 52-54.

Song, Kwang Yong, Weiwen Zou, Zuyuan He et Kazuo Hotate. 2008. « All-optical dynamic grating generation based on Brillouin scattering in polarization-maintaining fiber ». *Optics letters,* vol. 33, nº 9, p. 926-928.

Takara, Hidehiko, Akihide Sano, Takayuki Kobayashi, Hirokazu Kubota, Hiroto Kawakami, Akihiko Matsuura, Yutaka Miyamoto, Yoshiteru Abe, Hirotaka Ono et Kota Shikama. 2012. « 1.01-Pb/s (12 SDM/222 WDM/456 Gb/s) crosstalk-managed transmission with 91.4-b/s/Hz aggregate spectral efficiency ». In *European Conference and Exhibition on Optical Communication*. p. Th. 3. C. 1. Optical Society of America.

Teng, Lei, Peilin Tong, Taofei Jiang, Hongying Zhang, Zhiwei Lu, Liang Chen, Xiaoyi Bao et Yongkang Dong. 2015. « High-sensitive distributed transverse load sensing based

on Brillouin dynamic gratings ». In *24th International Conference on Optical Fibre Sensors*. Vol. 9634, p. 96346M. International Society for Optics and Photonics.

Thévenaz, Luc, Avi Zadok, Avishay Eyal et Moshe Tur. 2008. « All-optical polarization control through Brillouin amplification ». In *Optical Fiber communication/National Fiber Optic Engineers Conference, 2008. OFC/NFOEC 2008. Conference on*. p. 1-3. IEEE.

Tkach, RW, AR Chraplyvy et RM Derosier. 1986. « Spontaneous Brillouin scattering for single-mode optical-fibre characterisation ». *Electronics Letters,* vol. 22, nº 19, p. 1011-1013.

Török, P, et PRT Munro. 2004. « The use of Gauss-Laguerre vector beams in STED microscopy ». *Optics express,* vol. 12, nº 15, p. 3605-3617.

Ung, B, P Vaity, L Wang, Y Messaddeq, LA Rusch et S LaRochelle. 2014. « Few-mode fiber with inverse-parabolic graded-index profile for transmission of OAM-carrying modes ». *Optics express,* vol. 22, nº 15, p. 18044-18055.

Vaity, Pravin, Charles Brunet, Younès Messaddeq, Sophie LaRochelle et Leslie A Rusch. 2014. « Exciting OAM modes in annular-core fibers via perfect OAM beams ». In *Optical Communication (ECOC), 2014 European Conference on*. p. 1-3. IEEE.

Vaity, Pravin, et Leslie Rusch. 2015. « Perfect vortex beam: Fourier transformation of a Bessel beam ». *Optics letters,* vol. 40, nº 4, p. 597-600.

Van Deventer, M Oskar, et Andre J Boot. 1994. « Polarization properties of stimulated Brillouin scattering in single-mode fibers ». *Journal of Lightwave Technology,* vol. 12, nº 4, p. 585-590.

Van Uden, RGH, R Amezcua Correa, E Antonio Lopez, FM Huijskens, Cen Xia, G Li, A Schülzgen, H De Waardt, AMJ Koonen et CM Okonkwo. 2014. « Ultra-high-density spatial division multiplexing with a few-mode multicore fibre ». *Nature Photonics,* vol. 8, nº 11, p. 865.

Vengsarkar, Ashish M, Paul J Lemaire, Justin B Judkins, Vikram Bhatia, Turan Erdogan et John E Sipe. 1996a. « Long-period fiber gratings as band-rejection filters ». *Journal of lightwave technology,* vol. 14, nº 1, p. 58-65.

Vengsarkar, Ashish M, J Renee Pedrazzani, Justin B Judkins, Paul J Lemaire, Neal S Bergano et Carl R Davidson. 1996b. « Long-period fiber-grating-based gain equalizers ». *Optics Letters,* vol. 21, nº 5, p. 336-338.

Villafranca, Asier, José A Lázaro, Íñigo Salinas et Ignacio Garcés. 2005. « Stimulated Brillouin scattering gain profile characterization by interaction between two narrow-linewidth optical sources ». *Optics express,* vol. 13, nº 19, p. 7336-7341.

Villar, Ignacio Del, Jose Luis Cruz, Abian Bentor Socorro, Silvia Diaz, Jesus Maria Corres, Francisco Javier Arregui et Ignacio Raul Matias. 2017. « Monitoring the Etching Process in LPFGs towards Development of Highly Sensitive Sensors ». In *Multidisciplinary Digital Publishing Institute Proceedings*. Vol. 1, p. 331.

Volpe, G, et D Petrov. 2004. « Generation of cylindrical vector beams with few-mode fibers excited by Laguerre–Gaussian beams ». *Optics communications,* vol. 237, nº 1-3, p. 89-95.

Wang, Biao, Weigang Zhang, Zhiyong Bai, Li Wang, Liyu Zhang, Quan Zhou, Lei Chen et Tieyi Yan. 2015. « CO 2-laser-induced long period fiber gratings in few mode fibers ». *IEEE Photonics Technology Letters,* vol. 27, nº 2, p. 145-148.

Wang, Jian, Shuhui Li, Ming Luo, Jun Liu, Long Zhu, Chao Li, Dequan Xie, Qi Yang, Shaohua Yu et Junqiang Sun. 2014a. « N-dimentional multiplexing link with 1.036-Pbit/s transmission capacity and 112.6-bit/s/Hz spectral efficiency using OFDM-8QAM signals over 368 WDM pol-muxed 26 OAM modes ». In *Optical Communication (ECOC), 2014 European Conference on*. p. 1-3. IEEE.

Wang, Jian, Jeng-Yuan Yang, Irfan M Fazal, Nisar Ahmed, Yan Yan, Hao Huang, Yongxiong Ren, Yang Yue, Samuel Dolinar et Moshe Tur. 2012. « Terabit free-space data transmission employing orbital angular momentum multiplexing ». *Nature photonics,* vol. 6, nº 7, p. 488.

Wang, L, P Vaity, B Ung, Y Messaddeq, LA Rusch et S LaRochelle. 2014b. « Characterization of OAM fibers using fiber Bragg gratings ». *Optics express,* vol. 22, nº 13, p. 15653-15661.

Wang, Lixian, Cang Jin, Younès Messaddeq et Sophie LaRochelle. 2014c. « Microwave interferometric technique for characterizing few mode fibers ». *IEEE Photonics Technology Letters,* vol. 26, nº 17, p. 1695-1698.

Wang, Lixian, Reza Mirzaei Nejad, Alessandro Corsi, Jiachuan Lin, Younès Messaddeq, Leslie A Rusch et Sophie LaRochelle. 2017a. « MIMO-free transmission over six vector modes in a polarization maintaining elliptical ring core fiber ». In *Optical Fiber Communications Conference and Exhibition (OFC), 2017*. p. 1-3. IEEE.

Wang, Lixian, Reza Mirzaei Nejad, Alessandro Corsi, Jiachuan Lin, Younès Messaddeq, Leslie Rusch et Sophie LaRochelle. 2017b. « Linearly polarized vector modes: enabling MIMO-free mode-division multiplexing ». *Optics express,* vol. 25, nº 10, p. 11736-11749.

Wang, Lixian, Pravin Vaity, Stéphane Chatigny, Younès Messaddeq, Leslie Ann Rusch et Sophie LaRochelle. 2016. « Orbital-angular-momentum polarization mode dispersion in optical fibers ». *Journal of Lightwave Technology,* vol. 34, nº 8, p. 1661-1671.

Wang, Rugang, Liuying Zhou et Xuping Zhang. 2014. « Performance of Brillouin optical time domain reflectometer with erbium doped fiber amplifier ». *Optik-International Journal for Light and Electron Optics,* vol. 125, nº 17, p. 4864-4867.

Wang, Teng, Feng Wang, Fan Shi, Fufei Pang, Sujuan Huang, Tingyun Wang et Xianglong Zeng. 2017c. « Generation of femtosecond optical vortex beams in all-fiber mode-locked fiber laser using mode selective coupler ». *Journal of Lightwave Technology,* vol. 35, nº 11, p. 2161-2166.

Wang, Tonglu, Shiyao Fu, Feng He et Chunqing Gao. 2017d. « Generation of perfect polarization vortices using combined gratings in a single spatial light modulator ». *Applied optics,* vol. 56, nº 27, p. 7567-7571.

Weerdenburg, JV, R Ryf, JC Alvarado-Zacarias, RA Alvarez-Aguirre, NK Fontaine, H Chen, R Amezcua-Correa, T Koonen et C Okonkwo. 2017. « 138 Tbit/s Transmission over 650 km Graded-Index 6-Mode Fiber ». *ECOC, Th. PDP. A,* vol. 4.

Weng, Yi, Ezra Ip, Zhongqi Pan et Ting Wang. 2015a. « Few-mode distributed optical fiber sensors ». In *Optical Sensors*. p. SeS3C. 3. Optical Society of America.

Weng, Yi, Ezra Ip, Zhongqi Pan et Ting Wang. 2015b. « Single-end simultaneous temperature and strain sensing techniques based on Brillouin optical time domain reflectometry in few-mode fibers ». *Optics express,* vol. 23, nº 7, p. 9024-9039.

Willner, Alan E, Hao Huang, Yan Yan, Yongxiong Ren, Nisar Ahmed, Goudong Xie, Changjing Bao, L Li, Y Cao et Z Zhao. 2015. « Optical communications using orbital angular momentum beams ». *Advances in Optics and Photonics,* vol. 7, nº 1, p. 66-106.

Winzer, Peter J. 2014. « Making spatial multiplexing a reality ». *Nature Photonics,* vol. 8, nº 5, p. 345.

Winzer, Peter J, et Gerard J Foschini. 2011. « MIMO capacities and outage probabilities in spatially multiplexed optical transport systems ». *Optics Express,* vol. 19, nº 17, p. 16680-16696.

Wonko, R, P Marć et LR Jaroszewicz. 2017. « Fabrication of tapered long period fiber gratings for sensors application by filament heating ». In *Optical Fibers and Their Applications 2017*. Vol. 10325, p. 1032507. International Society for Optics and Photonics.

Wu, Chuang, Zhengyong Liu, Kit Man Chung, Ming-Leung Vincent Tse, Florence YM Chan, Alan Pak Tao Lau, Chao Lu et Haw-Yaw Tam. 2012. « Strong $\hbox {LP} _ {01} $ and $\hbox {LP} _ {11} $ Mutual Coupling Conversion in a Two-Mode Fiber Bragg Grating ». *IEEE Photonics Journal,* vol. 4, nº 4, p. 1080-1086.

Wu, Hang, Shecheng Gao, Bingsen Huang, Yuanhua Feng, Xincheng Huang, Weiping Liu et Zhaohui Li. 2017. « All-fiber second-order optical vortex generation based on strong modulated long-period grating in a four-mode fiber ». *Optics letters,* vol. 42, nº 24, p. 5210-5213.

Xinlei, Zhou, Yu Qingxu et Peng Wei. 2012. « Simultaneous measurement of down-hole pressure and distributed temperature with a single fiber ». *Measurement Science and Technology,* vol. 23, nº 8, p. 085102.

Xu, Yanping, Meiqi Ren, Yang Lu, Ping Lu, Xiaoyi Bao, Lixian Wang, Younès Messaddeq et Sophie LaRochelle. 2016. « Multi-parameter sensor based on stimulated Brillouin scattering in inverse-parabolic graded-index fiber ». *Optics letters,* vol. 41, nº 6, p. 1138-1141.

Yaman, Fatih, Neng Bai, Benyuan Zhu, Ting Wang et Guifang Li. 2010. « Long distance transmission in few-mode fibers ». *Optics Express,* vol. 18, nº 12, p. 13250-13257.

Yeniay, Aydin, Jean-Marc Delavaux et Jean Toulouse. 2002. « Spontaneous and stimulated Brillouin scattering gain spectra in optical fibers ». *Journal of lightwave technology,* vol. 20, nº 8, p. 1425.

Yin, Guolu, Jian Tang, Changrui Liao et Yiping Wang. 2016. « Automatic arc discharge technology for inscribing long period fiber gratings ». *Applied optics,* vol. 55, nº 14, p. 3873-3878.

You, Bei, Hongzhi Jia et Liao Wang. 2016. « A novel mode add/drop multiplexer based on two parallel combinative long period fiber gratings ». *Optical and Quantum Electronics,* vol. 48, nº 7, p. 359.

Youngquist, RC, JL Brooks et Herbert J Shaw. 1984. « Two-mode fiber modal coupler ». *Optics letters,* vol. 9, nº 5, p. 177-179.

Youngworth, Kathleen S, et Thomas G Brown. 2000. « Focusing of high numerical aperture cylindrical-vector beams ». *Optics Express,* vol. 7, nº 2, p. 77-87.

Yu, Wentao, Ziheng Ji, Dashan Dong, Xusan Yang, Yunfeng Xiao, Qihuang Gong, Peng Xi et Kebin Shi. 2016. « Super-resolution deep imaging with hollow Bessel beam STED microscopy ». *Laser & Photonics Reviews,* vol. 10, nº 1, p. 147-152.

Zhan, Qiwen. 2009. « Cylindrical vector beams: from mathematical concepts to applications ». *Advances in Optics and Photonics,* vol. 1, nº 1, p. 1-57.

Zhang, Xiaohui, Yange Liu, Zhi Wang, Jie Yu et Hongwei Zhang. 2018. « LP 01-LP 11a mode converters based on long-period fiber gratings in a two-mode polarization-maintaining photonic crystal fiber ». *Optics express,* vol. 26, nº 6, p. 7013-7021.

Zhao, Yunhe, Yunqi Liu, Chenyi Zhang, Liang Zhang, Guangjun Zheng, Chengbo Mou, Jianxiang Wen et Tingyun Wang. 2017. « All-fiber mode converter based on long-period fiber gratings written in few-mode fiber ». *Optics letters,* vol. 42, nº 22, p. 4708-4711.

Zhao, Yunhe, Yunqi Liu, Liang Zhang, Chenyi Zhang, Jianxiang Wen et Tingyun Wang. 2016. « Mode converter based on the long-period fiber gratings written in the two-mode fiber ». *Optics express,* vol. 24, nº 6, p. 6186-6195.

Zhou, Xiang, Lynn E Nelson, Peter Magill, Rejoy Isaac, Benyuan Zhu, David W Peckham, Peter I Borel et Kenneth Carlson. 2013. « High spectral efficiency 400 Gb/s transmission using PDM time-domain hybrid 32–64 QAM and training-assisted carrier recovery ». *Journal of Lightwave Technology,* vol. 31, nº 7, p. 999-1005.

Zhou, Xiaojun, Shenghui Shi, Zhiyao Zhang, Jun Zou et Yong Liu. 2011. « Mechanically-induced π-shifted long-period fiber gratings ». *Optics Express,* vol. 19, nº 7, p. 6253-6259.

Zhou, Zhi, Jianping He, Genda Chen et Jinping Ou. 2009. « A new kind of smart cable with functionality of full scale monitoring using BOTDR technique ». In *Proc. of SPIE Vol*. Vol. 7293, p. 72930L-1.

Zhou, Zhi, Jianping He, Kai Yan et Jinping Ou. 2007. « Large scale distribution monitoring of FRP-OF based on BOTDR Technique for Infrastructures ». In *Proc. SPIE*. Vol. 6530, p. 653006-653006.

Zhu, B, TF Taunay, M Fishteyn, X Liu, S Chandrasekhar, MF Yan, JM Fini, EM Monberg et FV Dimarcello. 2011. « 112-Tb/s space-division multiplexed DWDM transmission with 14-b/s/Hz aggregate spectral efficiency over a 76.8-km seven-core fiber ». *Optics Express,* vol. 19, nº 17, p. 16665-16671.

Zhu, Long, Andong Wang, Shi Chen, Jun Liu et Jian Wang. 2018. « Orbital angular momentum mode multiplexed transmission in heterogeneous few-mode and multi-mode fiber network ». *Optics letters,* vol. 43, nº 8, p. 1894-1897.

Zhu, Long, Chen Yang, Dequan Xie et Jian Wang. 2017. « Demonstration of km-scale orbital angular momentum multiplexing transmission using 4-level pulse-amplitude modulation signals ». *Optics letters,* vol. 42, nº 4, p. 763-766.

Zou, Weiwen, Zuyuan He et Kazuo Hotate. 2009. « Complete discrimination of strain and temperature using Brillouin frequency shift and birefringence in a polarization-maintaining fiber ». *Optics express,* vol. 17, nº 3, p. 1248-1255.